To the Graduate Council:

I am submitting herewith a thesis written by Yujie Meng entitled "**Methods for characterizing mechanical properties of wood cell walls via nanoindentation.**" I have examined the final electronic copy of this thesis for form and content and recommend that it be accepted in partial fulfillment of the requirements for the degree of Master of Science, with a major in Forestry.

Siqun Wang

Major Professor

We have read this thesis and recommend its acceptance:

Richard Bennett

Timothy M. Young

Zhiyong Cai

Accepted for the Council:

Carolyn R. Hodges

Vice Provost and Dean

of the Graduate School

(Original signatures are on file with official student records.)

Methods for Characterizing Mechanical Properties of Wood Cell Walls via Nanoindentation

A Thesis

Presented for the

Master of Science Degree

The University of Tennessee, Knoxville

Yujie Meng

August 2010

Copyright © 2010 by Yujie Meng

All rights reserved

ACKNOWLEDGMENTS

The encouragement and support of many people have gotten me through the writing of my thesis and I am grateful to them. Special thanks to my advisor, Dr. Siqun Wang, for the advice and teaching he provided throughout this research. I am very grateful for the opportunities he afforded me to help me study at University of Tennessee. I would also like to thank my committee members, Drs. Richard Bennett, Zhiyong Cai and Timothy M. Young, for their kind help, advice, and time spent on this research. All of the above have proved to be valuable mentors.

I would like to thank the office of the United States Department of Agriculture (USDA), whose funding provided financial support in the forms of the Wood Utilization Grant and the McIntire-Stennis Forestry Grant. In addition, I am grateful to Dr. Benhao Jiang and Dr. Zhaoyang Xu, who provided many ideas and insight during my research. Dr. John Dunlap kindly helped train me in the sample preparation method, and Dr. Shuangxi Song and Dr. Changli Wang were especially helpful and provided many useful tricks and tips for nanoindentation experiments. Thanks also go to Dr. Joseph E. Jakes for sharing his nanoindentation knowledge with me. I would also like to thank Dr. Zengqian Shi, Dr. Omid Hosseinaei, and Mr. Sandeep Sudhakaran Nair, who worked with me throughout the past two years and made the work both pleasanter and easier. Special thanks to Miss Amanda and Mr. Chris Helton, my good friends and mentors, who helped me understand more about American culture. I am also grateful to Mr. Caijun Su for his company, help, and encouragement.

The most important part of my life is my family. I would never have been able to accomplish any of my goals without the support of my mother, Jingping Guo, and my father, Jianping Meng, far away from me but always in my heart. I thank them for their understanding and trust and love them with all my heart.

The accomplishment of my master's degree thesis is not only a milestone in my life but also a starting point from which I can fly higher in the future.

ABSTRACT

Nanoindentation is a method of contacting a material whose mechanical properties are unknown with another material whose properties are known. Nanoindentation has the advantage of being able to probe a material's microstructure while being sensitive enough to detect variations in mechanical properties. However, nanoindentation has some limitations as a testing technique due to the specific formation and structure of some biomaterials. The main objective of this research is to identify any factors that influence the nanoindentation measurement of wood cell walls (a typical biomaterial).

The function of the embedding media in describing the properties of wood cells is poorly understood. This research demonstrated that Spurr's resin, when diffused into wood cell wall during the embedding process, enhanced both the Young's modulus and hardness of the cell walls. A substitute sample preparation method was developed to avoid this resin penetration into cell wall and was determined to be both effective and easy to perform.

The nanoindentation procedure involves the application of a monitor and an analysis of the load-displacement behavior and the response in the material. It can be anticipated that various ways of loading, including the maximum force, the loading time, and others, will cause a variety of mechanical properties. Thus, our second aim was to study the effect of load function on nanoindentation measurement in wood. It was discovered that a fast loading rate contributed to greater contact depth and lower hardness. Increasing the holding time decreased measured values for both Young's

modulus and hardness. However, no significant difference of Young's modulus and hardness among three loading functions with different unloading rates.

The final part of the research was to study the effect of moisture content on the micromechanical properties of wood material. Several nanoindentations were performed on the wood cell wall while varying the moisture content of wood. Results indicated that both the Young's modulus and hardness decreased significantly with an increase of moisture content. A rheology model was developed to describe the nanoindentation behaviors of wood cell walls at different moisture contents. Five parameters were extracted from Burger's model, and the relationships among those five parameters were quantified.

TABLE OF CONTENTS

CHAPTER 1. INTRODUCTION 1
1.1 Project description 2
1.2 Rationale and significance 4
1.3 Project goal and technical objectives 4
CHAPTER 2. LITERATURE REVIEW 6
2.1 Introduction and problem formulation 7
2.2 Structure of wood fiber 7
2.2.1 Wood structure 7
2.2.2 Wood cell wall's structure 9
2.3 Nanoindentation 13
2.3.1 Brief introduction to nanoindentation 13
2.3.2 Nanoindentation in biomaterials 16
2.3.3 Specimen preparation 19
2.3.4 Viscoelasticity 20
2.4 Moisture content and its effect on mechanical properties of the wood cell wall 23
2.4.1 Water in the cell wall 23
2.4.2 Effect of water inside the cell wall on its mechanical properties 24
2.5 Summaries 26
References 28
CHAPTER 3. EFFECT OF EPOXY EMBEDDING MEDIUM ON THE MEASUREMENT OF MECHANICAL PROPERTIES OF LIGNOCELLULOSIC MATERIALS 33
3.1 Abstract 34
3.2 Introduction 35
3.3 Materials and Methods 37
3.3.1 Material collection and sample preparation 37
3.3.2 Nanoindentation 42

3.3.3 Measurements of wood cell wall hardness and Young's modulus by nanoindentation 43
3.4 Results and Discussion 44
3.4.1 Influence of embedding medium on the Young's modulus and hardness of wood cell wall 44
3.4.2 Roughness of sample 48
3.4.3 Scanning Electron Microscopy (SEM) and Energy Dispersive Spectroscopy (EDS) analysis 49
3.4.4 Effect of vacuum time on the Young's modulus and hardness of wood cell wall 52
3.5 Conclusions 55
References 56
CHAPTER 4. EFFECT OF LOAD FUNCTION ON THE NANOINDENTATION MEASUREMENT OF WOOD CELL WALL 59
4.1 Abstract 60
4.2 Introduction 61
4.3 Materials and Methods 63
4.3.1 Materials 63
4.3.2 Specimen preparation 64
4.3.3 Nanoindentation 65
4.3.4 Load function of nanoindentation 66
4.4 Results and Discussion 72
4.4.1 Effect of loading rate on the Young's modulus and hardness from nanoindentation 72
4.4.2 Effect of holding time on the Young's modulus and hardness in nanoindentation testing 76
4.4.3 Effect of unloading rate on the Young's modulus and hardness from nanoindentation 78
4.4.4 Indentation size effect and edge effect 81
4.5 Conclusions 90
References 91

CHAPTER 5. EFFECT OF MOISTURE CONTENT ON THE MECHANICAL MEASUREMENT OF WOOD CELL WALL BY NANOINDENTATION 93

5.1 Abstract 94

5.2 Introduction 94

5.3 Materials and Methods 96

5.3.1 Material and sample preparation 96

5.3.2 Humidity generation 97

5.3.3 Nanoindentation 98

5.4 Rheological models 100

5.4.1 Burger's model and creep compliance 100

5.5 Results and Discussion 104

5.5.1 Cell-wall swelling 104

5.5.2 Effect of moisture content on Young's modulus and hardness 106

5.5.3 Investigation of nanoindentation creep 113

5.5.4 Water absorption and its relationship with cell wall ultrastructure 117

5.5.5 Short-term creep of wood cell wall by nanoindentation 121

5.5.6 Simulated results using Burger's model 124

5.6 Conclusions 129

References 130

CHAPTER 6. CONCLUSIONS AND FUTURE WORKS 136

6.1 Conclusions 137

6.1.1 Effect of epoxy embedding medium on the measurement of mechanical properties of lignocellulosic materials 137

6.1.2 Effect of load function on the nanoindentation measurement of wood cell wall 137

6.1.3 Effect of moisture content on the mechanical measurement of wood cell wall by nanoindentation 138

6.2 Future Works 139

6.2.1 Temperature-dependent properties of wood cell wall via nanoindentation 139

6.2.2 Dynamic mechanical properties analysis (Nano DMA) of wood cell wall at small scale and modulus mapping technique 139

Vita 141

LIST OF FIGURES

Figure 2.1 Cross section of tree trunk (A)bark, (B)cambium,(C)sapwood,(D)heartwood,(E)pith,(F)phloem,(G)wood ray,(H)annual ring (adopted from http://visual.merriam-webster.com/plants-gardening/plants/tree/cross-section-trunk.php) 8
Figure 2.2 The early wood and latewood transition (Haygreen and Bowyer, 1996)..... 9
Figure 2.3 Sketch map of cell wall's structure (Fengel and G.Wegener, 1984) ML: middle lamella 10
Figure 2.4 Illustration of indentation geometry at maximum force..... 13
Figure 2.5 Schematic sample plot of load vs. displacement for Nanoindentation..... 14
Figure 2.6 Schematic diagram of load-displacement curve during loading and..... 21
Figure 3.1 Specimen preparation procedure for wood block embedded in epoxy resin. (a) Small wood block of loblolly pine; (b) Small wood block of loblolly pine embedded in epoxy resin ; (c) Microscopic picture of embedded loblolly pine cell wall 39
Figure 3.2 Specimen preparation procedure for wood block without epoxy resin (a)Red oak disk; (b)Red oak block with four sides pyramid shape; (c) Microscopic picture of unembedded red oak cell wall 40
Figure 3.3 Specimen preparation procedure for wood block isolated by thin film (a)Loblolly pine's small wood block sealed by thin film; (b)Loblolly pine small wood block with sealed film embedded in epoxy resin ; (c) Interference microscopic picture of loblolly pine cell wall isolated by thin film 41
Figure 3.4 Comparison between Young's modulus measurements for embedded and unembedded samples of loblolly pine and red oak by nanoindentation..... 46
Figure 3.5 Comparison between hardness measurements for embedded and unembedded samples of loblolly pine and red oak by nanoindentation 47
Figure 3.6 Young's modulus and hardness of isolated and embedding loblolly pine by nanoindentation 48
Figure 3.7 AFM topographic image of single indent for loblolly pine cell wall..... 49

Figure 3.8 SEM image of loblolly pine cell wall 50
Figure 3.9 SEM image of loblolly pine cell wall embedded in Spurr's resin 51
Figure 3.10 Dependence of vacuum time on Young's modulus and hardness of wood cell wall 54
Figure 4.1 Typical load–displacement curves for multiload indents 62
Figure 4.2 Polarized light microscopy (PLM) image of yellow pine's cell wall 65
Figure 4.3 Indentation load versus time curve for 0.1s loading time 66
Figure 4.4 Indentation load versus time curve for 1s loading time 67
Figure 4.5 Indentation load versus time curve for 50s loading time 67
Figure 4.6 Indentation load vs time curve for 0.1s holding time 68
Figure 4.7 Indentation load vs time curve for 1s holding time 68
Figure 4.8 Indentation load vs time curve for 50s holding time 69
Figure 4.9 Indentation load vs time curve for 0.2s unloading time 70
Figure 4.10 Indentation load vs time curve for 1s unloading time 70
Figure 4.11 Indentation load vs time curve for 50s unloading time 71
Figure 4.12 Indentation load vs time curve for 5s loading, 5s holding and 5s unloading 71
Figure 4.13 Comparison of the load-displacement curves for different loading rate under the maximum load 200 μN with holding time 5s 74
Figure 4.14 Hardness of yellow pine under different load functions 75
Figure 4.15 Young's modulus of yellow pine under different load functions 75
Figure 4.16 Comparison of the load-displacement curves for different holding time under the maximum load 200 μN 77
Figure 4.17 Comparison of displacement rate for different holding time under the maximum load 200 μN 78
Figure 4.18 Comparison of the load-displacement curves for different unloading rate under the maximum load 200 μN with holding time 5s 80
Figure 4.19 Comparison of the load-displacement curves for different load force with 5s loading time and 5s holding time 81
Figure 4.20 Relationships between the maximum displacement and the Young's modulus and the hardness at a loading time of 5 second with a 5-s hold period 82

Figure 4.21 AFM pictures of residual indent mark under different loading force A: 150 μN, ... 84
Figure 4.22Relationships between the applied load and the machine-calculated contact area..... 84
Figure 4.23 Sketch map of elastic heterogeneities as an interface with a dissimilar material like epoxy resin..... 88
Figure 4.24 Sketch image of indentation edge effect 90
Figure 5.1 Schematic image of cell fluid tip..... 99
Figure 5.2 Schematic image of four-element Burgers model..... 103
Figure 5.3 Interference microscopic picture of loblolly pine cell wall under air-dry condition..... 105
Figure 5.4 Interference microscopic picture of loblolly pine cell wall after immersed in to water for 2 hours..... 105
Figure 5.5 Comparison of cell wall profile before and after absorbing water..... 106
Figure 5.6 Young's modulus of cell wall without embedding under different moisture content 107
Figure 5.7 Hardness of wood cell wall without embedding under different moisture content 108
Figure 5.8 Typical indentation curves at different moisture contents with fluid cell indenter loading with a peak load of 250 μN. Five seconds holding time at maximum load for creep..... 109
Figure 5.9 Atomic force microscope image of wood cell wall after indentation under different moisture content..... 109
Figure 5.10 Young's modulus of embedded cell wall under different moisture content 111
Figure 5.11 Hardness of embedded cell wall under different moisture content..... 111
Figure 5.12 Young's modulus of wood cell wall with small MFA under different moisture content 112
Figure 5.13 Hardness of wood cell wall with small MFA under different moisture content 113

Figure 5.14 Relationship between displacement and time in the creep procedure of sample B under different moisture content 115
Figure 5.15 Effect of moisture content on the creep ratio of wood cell wall 116
Figure 5.16 Schematic diagram of a single repeat unit of the cellulose molecule..... 118
Figure 5.17 Schematic diagram of a single repeat unit of the cellulose molecule reacting with water 119
Figure 5.18 Schematic diagram of a single repeat unit of the hemicellulose molecule (galactoglucomannans) 120
Figure 5.19 Schematic diagram of a single repeat unit of the hemicelluloses molecule (galactoglucomannans) reacting with water 121
Figure 5.20 Creep Compliance J(t) of wood cell wall under oven-dry condition and Burgers model fit 122
Figure 5.21 Creep Compliance J(t) of wood cell wall under air-dry condition and Burgers model fit 123
Figure 5.22 Creep Compliance J(t) of wood cell wall under 6% moisture content and Burgers model fit 123
Figure 5.23 Creep Compliance J(t) of wood cell wall fully immersed into water and Burgers model fit 124
Figure 5.24 Effect of moisture content on the parameter Ee in Burger's model 126
Figure 5.25 Effect of moisture content on the parameter Ed in Burger's model 126
Figure 5.26 Effect of moisture content on the parameter η1 in Burger's model 127
Figure 5.27 Effect of moisture content on the parameter η2 in Burger's model 127
Figure 5.28 Effect of moisture content on the parameter τ_0 in Burger's model 128

LIST OF TABLES

Table 3.1 Components of Spurr's epoxy resin..... 38
Table 3.2 Comparison of carbon/oxygen content among pure Spurr's resin, resin embedded cell wall, and reference cell wall..... 51
Table 3.3 Young's modulus of loblolly pine under different vacuum time..... 53
Table 4.1 δ and n values obtained from power-law fits to the nanoindentation loading curve of six different materials along with the correlation coefficients..... 86
Table 4.2 Indices for indentation size effects 87
Table 5.1 Summary table of parameters for moisture content control during test 98
Table 5.2 Burgers model parameters with respect to different moisture content 125

CHAPTER 1. INTRODUCTION

1.1 Project description

Nanoindentation is a powerful technique that has been used in biomaterials research. Using nanoindentation, researchers have successfully characterized the mechanical properties of cell walls (Konnerth and Gindl, 2006; Lee et al., 2007; Wu et al., 2009). However, many view the data obtained with skepticism because they do not understand how those data are obtained.

Because a wood cell has a complex multi-component structure, its structural arrangement is one of the important factors that affect its mechanical properties. So far, a great deal of research has focused on the structure of wood cell wall, leading to some commonly held conclusions (Eder et al., 2009; Fengel and G.Wegener, 1984; Holmberg et al., 1999; Salmen and Burgert, 2009; Salmen and Olsson, 1998). It is known that a cell wall is made up of a primary wall, a secondary wall and a middle lamella. Typically, the structure of the secondary wall includes a narrow outer layer called the S1 layer, a very thin and narrow inner layer called the S3 layer, and a middle layer called the S2 layer.

For biomaterials like bone, wood, or plant stems, the sample preparation procedure for nanoindentation is time-consuming, requiring meticulous care due to each material's specific structure and character. Although some progress has been made in this area, at least two major obstacles must be overcome. The first problem is the effect of embedding medium on the obtaining of exact value of the materials. The most common sample preparation method is to immerse the wood specimen into Spurr's resin, which supports the sample during microtome cutting, and then to vacuum the sample to remove air bubbles. However, the embedding medium may diffuse into the wood cell wall,

altering the cell-wall properties and rendering the results unreliable. Thus, the first challenge is to detect the effect of the embedding medium and try to remove any artificial error caused by sample preparation.

Even apart from embedding media difficulties, it is challenging to obtain true values by nanoindentation because nanoindentation tests typically involve several other problems as well, all of which are related to load function. The load function varies with different indentation equipment, test objectives, and researchers. In particular, sample surface roughness, size effect, edge effect, loading rate, and creep have not been either well understood or able to be eliminated. Thus, there is a need to understand how load function determines and affects the final data. Generally, a common load function for wood, which is a viscoelastic material, is made up of three stages: loading, holding and unloading. The essential relationship between the measured load function and the Young's modulus or hardness of wood cell walls has not been reported in detail.

Wood is a hydrophilic (water-attracting) and hygroscopic (water-absorbing) material. Moisture content has been proved to affect such macro-scale physical properties of wood as elastic modulus, shrinkage, and heat conductivity (Hernandez, 2007; Koponen et al., 1989; Koponen et al., 1991; Nakano, 2008). The interaction between wood and water has been discussed widely from a variety of viewpoints, and a number of models regarding the effect of moisture content on the wood cell wall have been developed. It is now necessary to verify these new techniques and test methods. In this study, nanoindentation is tested as a new technique capable of characterizing the cell wall's mechanical properties in nanoscale. As an effective experimental method, it can help

verify other theoretical simulations as well, such as the rheology model and assumptions about cell-wall structures, among others.

1.2 Rationale and significance

Wood bonding, coupling agent, moisture content and other factors make bio-composite characterization more complicated. This research has the potential to improve the existing test methodology for nanoindentation tests on wood materials used in the creation of bio-composites. This study first gauges the influence of the embedding medium on the mechanical property measurement of wood cell walls, which have a complex structure and components. Then, a new sample preparation method is developed to prevent epoxy resin from penetrating into the cell wall.

Since biomaterials are sensitive to the test environment, how to compare nanoindentation data among different research groups becomes an important issue. This study improves understanding of the essential relationship between load function and the mechanical properties of wood cell wall. Secondly, bio-energy and bio-products are becoming important. Fiber's size reduction always is the first step for those processes. To identify the optimal manufacturing condition is another important issue, so exploring the moisture-dependent properties of wood cell wall makes it possible to better guide the manufacture of bio-products. In brief, this research knowledge has the potential to provide insight into the development of new nanoindentation test methods on wood materials.

1.3 Project goal and technical objectives

The main objective of this project is to investigate the effect of embedding medium, moisture content, and loading function on the nanoindentation measurement of wood cell walls. Specifically, its goals are three:

1. To investigate the influence of the embedding medium on the nanoindentation of wood cell wall and develop a new sample preparation method to avoid potential influence of the embedding medium on the test results.

2. To understand the essential principle of nanoindentation load function and the corresponding response of the wood material and to propose an appropriate load function.

3. To explore the effect of moisture content on the mechanical properties of wood cell wall and the short-term creep phenomenon as one of the ways to characterize viscoelastic material.

CHAPTER 2. LITERATURE REVIEW

2.1 Introduction and problem formulation

Current literature on the use of nanoindentation to characterize the cell walls of biomaterials was reviewed, concentrating on four areas: 1) wood cell-wall structures and mechanical properties; 2) the use of nanoindentation as the main instrument to investigate small-scale mechanical properties, as well as a description of the technique and its limitations; 3) the application of nanoindentation to the study of the rheological properties of viscoelastic materials and experimental methods and data analysis for probing and characterizing time-dependent phenomena; and 4) the influence of any important environmental factors, such as water or humidity, on material properties.

2.2 Structure of wood fiber

2.2.1 Wood structure

Cross section of a tree trunk is shown in Figure 2.1. Basically, wood can be divided into several parts according to its structure and natural characters. The bark, including an outer corky dead part and inner thin living part which took on to carry food from root; The cambium layer, which is located inside of inner bark, has the ability to form bark cell. Phloem is the innermost layer of the bark which obtained live tissue to carry organic nutrients. Wood parts could be assorted as sapwood, heartwood and pith, which located in the center of the tree. Figure 2.2 shows the early wood and latewood transition. The annual ring seen in the horizontal cross section could be a sign to reveal the change in growth speed through the seasons of the years. Inner portion of the annual ring is formed early in the season, when wood has a rapid growth period, which is also

known as early wood. By contrast, the outer portion of the annual ring named as later wood reveals a slow growth period. It is denser, cells range closely, cell wall is thick and the shape of lumen is approximately rectangular slit-shaped for late wood while early wood characterized as cells with larger cavities and extremely thin wall. Annual rings are more obvious to read in species with sharp transition from early wood to latewood.

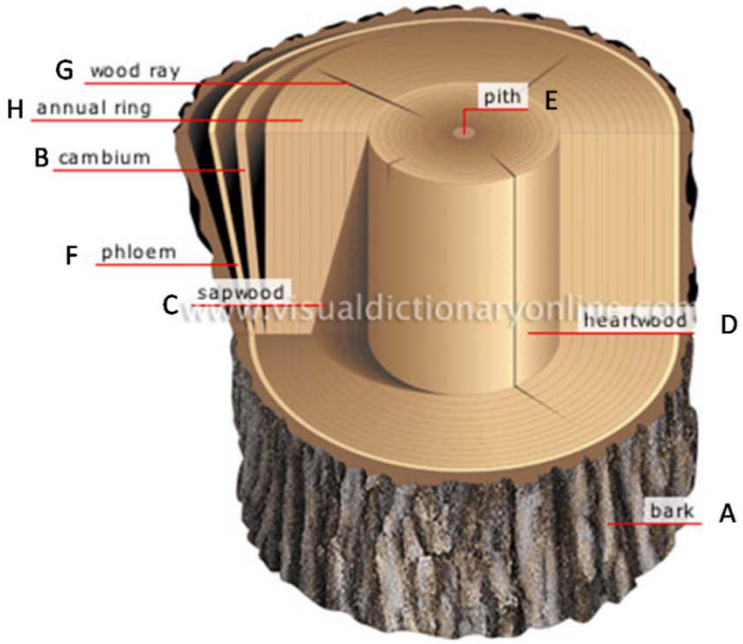

Figure 2.1 Cross section of tree trunk (A)bark, (B)cambium,(C)sapwood,(D)heartwood,(E)pith,(F)phloem,(G)wood ray,(H)annual ring (adopted from http://visual.merriam-webster.com/plants-gardening/plants/tree/cross-section-trunk.php)

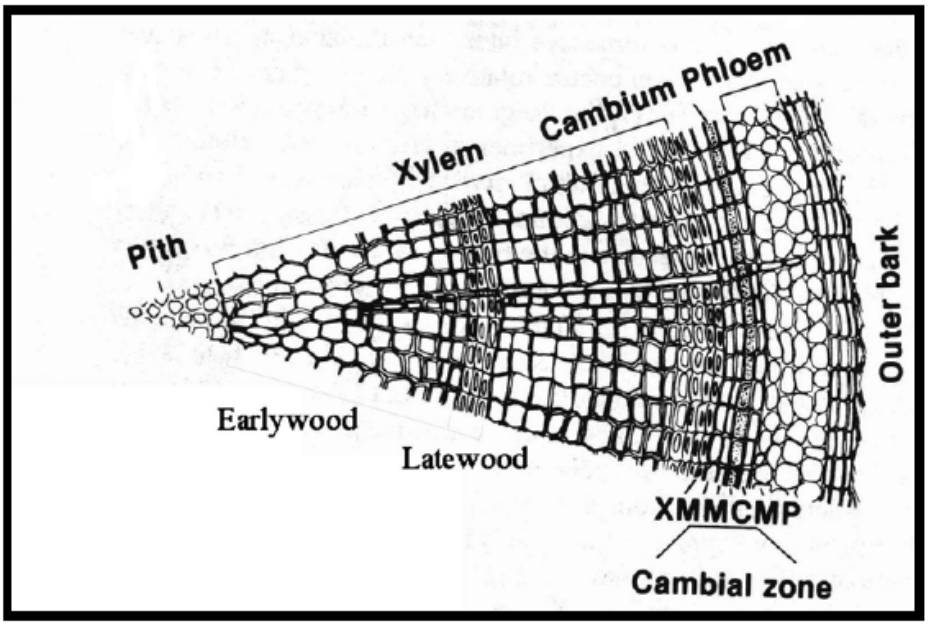

Figure 2.2 The early wood and latewood transition (Haygreen and Bowyer, 1996)

2.2.2 Wood cell wall's structure

Wood has evolved as a complex multi-component structure in order to adapt to the diverse environmental demands of trees' various habitats. Usually, the cell wall is made up of a primary wall, a secondary wall, and a middle lamella. The primary wall is formed in the period when the cell wall is growing. It is composed of cellulose at the initial stage and is lignified (i.e., it develops into wood) with the accretion of the cell wall. The secondary cell wall is developed later and is formed inside of the primary wall. It composes more than 80% (by weight) and 95% (by thickness) of the fiber wall. The main components of the secondary cell wall are cellulose, hemi-cellulose, and lignin; its structure includes a narrow outer layer called the S1 layer; a very thin and narrow inner layer called the S3 layer; and a middle layer called the S2 layer. The parallel-distributed cellulose fibrils are slanted toward the cell axis, which generates the micro fibril angle

(MFA) and the three layers can be easily distinguished by the different inclinations of the microfibrils. As Figure 2.3 shows, the middle layer is the thickest of the three layers, and it plays the dominant role in the determination of the cell wall's physical and mechanical properties (Yamamoto, Kojima 2002).

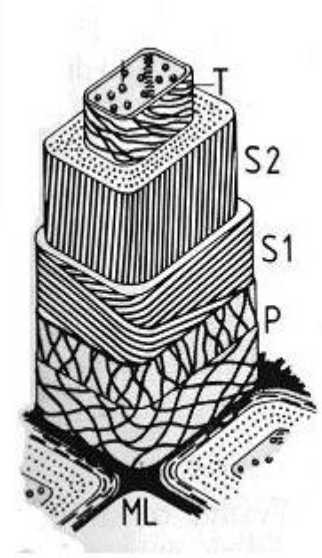

Figure 2.3 Sketch map of cell wall's structure (Fengel and G.Wegener, 1984) ML: middle lamella P primary wall; S_1 secondary wall1; S_2 secondary wall2; T or S_3 tertiary wall or secondary wall3

Cellulose microfibrils are helically arranged and oriented toward the long axis of the cell in the S2 layer, which makes the MFA change from 10 to 30 degrees. There is a strong belief that the microfibril angle of the S2 layer is a crucial factor in the determination of mechanical behaviors of wood (Megraw, 1986). The S1 layer contains a few microfibrils spiraled around the cell interior, with the long axis of the microfibrils nearly perpendicular to the long axis of cell wall, usually ranging from 50 to 70 degrees. Similarly, the S3 layer has fibrils oriented from 60 to 90 degrees from the cell axis.

To further study the cell-wall structure, atomic force microscopy (AFM) was used to investigate the orientation of the lamellar structure of the wood cell wall in cross section by fracturing and tensile testing. AFM showed concentric lamellae in the fracture zone and no structural connection to the splinters in the radial direction, which would be a consequence of energy released during fracture of the wood (Fahlen and Salmen, 2002). Raman spectroscopy was used to probe the wood and paper fiber's cellwall structure during tensile deformation by detecting the shift of wave numbers. This has been proved to be an effective and valuable method for understanding the micromechanism of deformation in cellulose materials (Eichhorn et al., 2001). The cell geometry, cell-wall fraction, and MFA were investigated by light microscopy, scanning electron microscopy (SEM), and wide-angle X-ray diffraction. Micro-tensile tests on the single tracheid have revealed that there is significant difference in tensile stiffness between early wood and later wood (Eder et al., 2009). The interaction among the three components has also been discussed by Lennart Salmen (Salmen and Burgert, 2009), who found that the bonding of hemicelluloses to the cellulose fibril was not based on the covalent bonds but mainly on

the hydrogen bonds. However, lignin covalently bonded to hemicelluloses. This result helped to enrich the understanding of the cell wall‘s structure as a highly dynamic network formation of the lignin on the surface of hemicelluloses, thus leading to a strengthening of the bonding in the sides of cell walls.

Several models were proposed from the standpoint of the cell wall‘s composite structure. Barber and Meylan firstly brought forward the wood fiber model, which shows the S1 layer located between the compound middle lamella (I+P) and the S2 layer. Each layer contains CMF bundles as the framework and the isotropic lignin-hemicelluloses skeleton as the matrix (Barber.N.F and Meylan, 1964). Based on Barber and Meylan‘s reinforced-matrix hypothesis, Yamamoto et al. (Yamamoto and Kojima, 2002) analyzed a multi-layered circular cylinder as a model of lingo-cellulosic fiber containing CML, S1 and S2 layers. The advantage of this model is that it not only took the structural factor but also the environmental conditions into consideration. Later on, Cave (1978) gave a more detailed formulation model especially for cell-wall shrinkage which described a “basic cell-wall element” as consisting of a planar array of parallel cellulose microfibrils embedded in a hemicelluloses matrix. Bergander investigated the influence of the elastic constants of three wood polymers on the Young’s modulus of wood cell wall and came out with the result that cellulose was the main factor in the determination of cell-wall properties. However, he also suggested lowering the assumed elastic constant value of hemicelluloses for the purpose of reducing the discrepancy between experimental data and model values for the elastic modulus of wood cell wall (Bergander and Salmen, 2002) .

2.3 Nanoindentation

2.3.1 Brief introduction to nanoindentation

As a powerful and effective tool for investigating the mechanical properties of materials on a small scale, the nanoindentation technique has gained popularity in recent years. This method is derived from traditional indentation tests in macro or micro indentation. Basically, it is a relatively new method for the mechanical testing of hardness. Nanoindentation, also called instrumental indentation, uses high-resolution equipment to measure the load-displacement response (Fischer-Cripps, 2004). The procedure of indentation involves a specially designed tip that penetrates into material and records the load and the corresponding displacement. Figure 2.4 is a schematic of the indentation process for an indenter. When the indenter is driven into the material, both elastic and plastic deformations occur, generating an impression in the material that follows the geometric shape of the indenter and produces a contact depth referred to as hc.

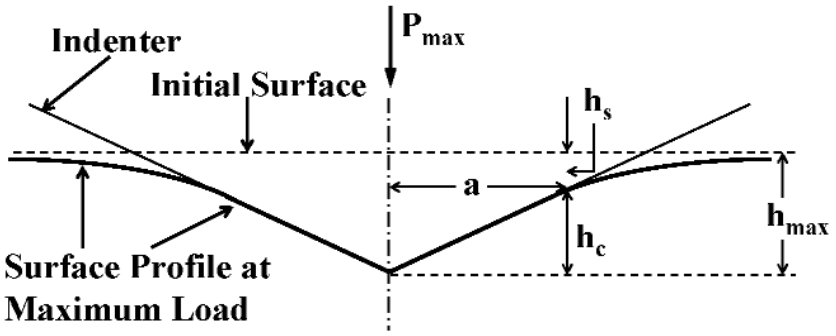

Figure 2.4 Illustration of indentation geometry at maximum force

The test system will record some important quantities, such as peak load (Pmax), maximum depth (hmax), residual depth after unloading (hf), and the slope of the upper portion of the unloading curve($S = dP/dh$). Young's modulus and the hardness can be obtained by analyzing the load-displacement curve, as shown in Figure 2.5.

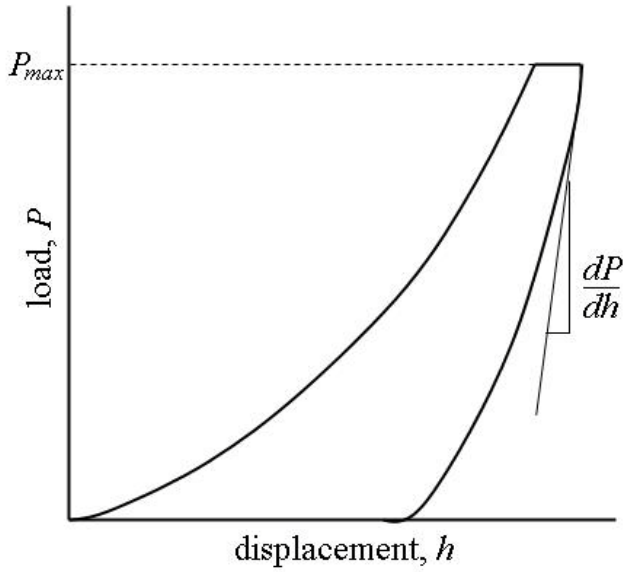

Figure 2.5 Schematic sample plot of load vs. displacement for Nanoindentation

So far, the most commonly used method for analyzing nanoindentation load-displacement data is the Oliver-Pharr method (Oliver and Pharr, 1992), which expands on ideas developed by Loubet et al. and Doerner and Nix (Doerner and Nix, 1986). The fundamental relationship between hardness and Young's modulus is defined as:

$$H = P_{\max} / A \qquad \text{Equation 2-1}$$

where H is hardness, P_{max} is the peak load and A_{hc} is the project contact area at peak load

$$E_r = \frac{\sqrt{\pi}(dP/dh)_{unloading}}{2\beta\sqrt{A_{hc}}} \qquad \text{Equation 2-2}$$

and where the reduced modulus E_r can be gained by the contact stiffness and project contact area A_{hc}. β is the constant corresponding to the geometry of the indenter.

$$\frac{1}{E_r} = \frac{1-\nu^2}{E} + \frac{1-\nu_i^2}{E_i} \qquad \text{Equation 2-3}$$

The reduced modulus is the sum of both samples, and the indenter's modulus ν is Poisson's ratio

For the diamond indenter, E_i equals to 1141GPa and ν_i equals to 0.07. In order to calculate a sample's modulus, its Poisson ratio must be given. Even if there is only a rough estimate of the material's Poisson ratio around 0.25±0.1, there still exists a 5% uncertainty in the calculated value of E for the material (Hay and Pharr, 2000) .

Nanoindentation has been used for the characterization of metals for many decades (Bobji et al., 1997; Lim and Chaudhri, 2001). However, it is still a new application tool in the field of biomaterials, such as bone, tooth, soft tissue, crop stalks,

wood, bamboo, Lyocell fiber, lignocelluloses and others. Because of its geometry-known tip size, nanoindentation makes it possible to investigate the mechanical properties of thin, small and heterogeneous materials in small volume. This enables the testing of target material of interest that often have dimensions of only a few micrometers; testing of such materials cannot be achieved by traditional method directly. In wood material, this technique allows us to actually detect the properties of different locations within the microstructure of wood cell walls.

2.3.2 Nanoindentation in biomaterials

The physical and mechanical properties of three main phases of bone, a heterogeneous material, were tested by nanoindentation (Kinney et al., 2003). Most biological materials are naturally hydrated, but in the very beginning, many of the early studies on nanoindentation were performed on dehydrated samples embedded in epoxy resin, which can potentially modify the sample. Later on, the effects of preservation and processing on bone were explored by means of nanoindentation (Bushby, 2003). In this study, bone was reported to have its highest modulus value when embedded in polymethyl methacrylate (PMMA), followed by the value obtained when samples dehydrated in ethanol; the lowest value was found with samples immersed in water. This work proposed a potential future study on the effect of water on mechanical behavior inside bone. Other scientists found similar trends and reported that bone samples were found by nanoindentation to have increased moduli after dehydration. Since there is no uniform test method existing in this research area, some of the work focused on the study of the effects of embedding materials, rate and depth of indentation, sample storage time

and so forth. These factors may or may not strongly influence the final data, depending on the material's response (Mittra et al., 2006).

Nanoindentation on cellulose fibers is another important topic that has recently come under intensive investigation. A large proportion of current nanoindentation literature focuses on the measurement of hardness and Young's modulus in cellulose fibers. Earlier research on this topic goes back to 1995, when Wimmer measured the longitudinal hardness and Young's modulus of a spruce tracheid S2 layer by using nanoindentation, reporting that both the hardness and the Young's modulus of latewood was higher than those of early wood. It was the first time the nanoindentation technique had been applied to a single tracheid cell wall to make a direct comparison with the ultrastructure. Later on, Gindl also performed experiments on spruce cell-wall structures, finding out that only the elastic modulus rather than hardness is significantly dependent on the MFA (Gindl et al., 2004).

Wu et al. (2010) reported the value of nanoindentation in the characterization of agricultural biomaterials such as crop stalks, cotton stalk, soybean stalk, cassava stalk, rice straw, and wheat straw. Meanwhile, the cell walls of ten different species of hardwood were investigated by nanoindentation, with the result that there was no significant difference among the 10 species in hardness, whereas the elastic moduli showed distinct differences (Wu et al., 2009). In other research, the nanoscale structure and mechanical characterization of bamboo cell walls were analyzed, and it was found that bamboo fibers are somewhat ductile ((Zou et al., 2009). Yu et al. (2007) conducted

nanoindentation on bamboo fibers in both the longitudinal and transverse directions and the results showed different deformation mechanisms between the directions.

The mechanical properties of individual wood fibers by using continuous nanoindentation measurement were studied (Tze et al., 2007). They calculated the size-effect index and proved that size effect is considerably small on the wood cell wall. Jakes conducted more detailed experimental research, and his results agree well with Tze's prediction (Jakes et al., 2007). The consensus is that there is a strong relationship between the microfibril angles and the hardness or stiffness of wood cell wall (Tze et al., 2007). Similar conclusions were drawn in Konnerth's experiment (Konnerth, 2009).

The nanoindentation technique can also be used to evaluate the interphase; Lee et al. investigated the hardness and Young's modulus of the interphase region between cellulose fiber and the polypropylene matrix. An approximate interphase width of less than 1 μm was gained by monitoring the change of stiffness and hardness. 3D finite element analysis verified and agreed very well with experimental measurement (Lee et al., 2007). Konnerth et al. (2007) conducted a mapping experiment of a wood/phenol-resorcinol-formaldehyde adhesive bond by nanoindentation and found a clear trend of decreasing hardness with increasing distance from the bond line. The most often-used resin for modifying wood, melamine–formaldehyde resin penetrated into cell wall, has the potential to improve mechanical properties. This has been confirmed by Gindl's research using nanoindentation (Gindl and Gupta, 2002). In more detailed research on the application of the Oliver-Pharr method to wood material, Jakes et al. focused on the material's structural compliance during nanoindentation data analysis. He observed that

not only the mechanical compliance, which could be calculated by the testing system automatically, but also the structural compliance needs to be considered. Moreover, it has been proved that structural compliance can vary as a function of position within the specimen and can be isolated and removed (Jakes et al., 2008).

2.3.3 Specimen preparation

Because biomaterials usually have a complicated microstructure, environmental changes can have a considerable impact on their properties. It has been verified that drying bone increases its modulus of elasticity, tensile strength, and bending strength, and will reduce the fracture toughness. Many nanoindentation studies on biomaterials such as wood, bone and teeth need a special sample preparation. The most commonly used preparation method for metal and polymer is polishing. A metal specimen is held in contact with a rotating polishing wheel. The wheel is placed upon a mat that has been impregnated with a polishing compound (Fischer-Cripps, 2004). A smooth surface will be generated by progressively decreasing the grit size. However, this method is not suitable for biomaterials because polishing will damage the microstructure as well as the surface of the material. Another specimen preparation method commonly used is microtoming, which is often used to thin-slice biological specimens, typically for SEM or TEM testing. It is usually necessary to embed material after dehydration so that the specimen will be easy to slice.

In most of the studies on wood indentation in the literature, specimens were embedded in Spurr's epoxy resin first (Gindl et al., 2004; Lee et al., 2007; Spurr, 1969; Tze et al., 2007; Wimmer et al., 1997; Wu et al., 2009; Wu et al., 2010; Xing et al., 2009)

to support the cell-wall structure. However, this procedure may influence the mechanical properties or cause some undesired chemical modifications of the wood cell wall. Resin penetration into cell wall is another important issue; even limited studies have showed that the penetration of epoxy resin into plant cell wall will increase the stiffness of fiber composites (Hepworth et al., 2000). Recently, Jakes et al. developed a new sample preparation without resin embedding to avoid this potential artifact. It consisted of generating a gently sloping pyramid-shaped surface and cutting the apex of sample with glass and diamond knives.

2.3.4 Viscoelasticity

The value of nanoindentation in determining the rheology properties of polymeric materials has recently attracted attention. The most common effects of viscoelasticity observed have been creep and stress relaxation, which was measured by pressing the tip into the sample at a constant load and controlling the displacement of the tip's sinking into the sample, respectively (Liu et al., 2006). More recently, many studies have showed that creep does occur during nanoindentation unloading for viscoelastic materials such as polymer (Liu et al., 2006; Oyen and Cook, 2003), wood and so forth. This creep phenomenon will eventually lead to an overestimation of Young's modulus due to Oliver and Pharr's method and calculation, which is based on the assumption that there is only elasticity existing in the unloading part. The creep phenomenon can be easily observed by analyzing the displacement at constant load during indentation. Many studies on viscoelastic materials have mentioned a "nose" (shown in Figure 2.6) appearing in the most extreme cases of viscoelasticity. Liu et al. (2006) have proposed that when the

"nose" appears, the overall displacement is the sum of the elastic displacement, the viscous displacement, and the plastic displacement. The "nose" shape will make the contact stiffness seem larger than it actually is and sometimes even negative, thus causing an overestimation of the Young's modulus. To get a more accurate hardness and Young's modulus in the indentation, a common method suggested has been to create sufficient creep time at peak load to eliminate the creep effect during unloading (Ngan and Tang, 2002).

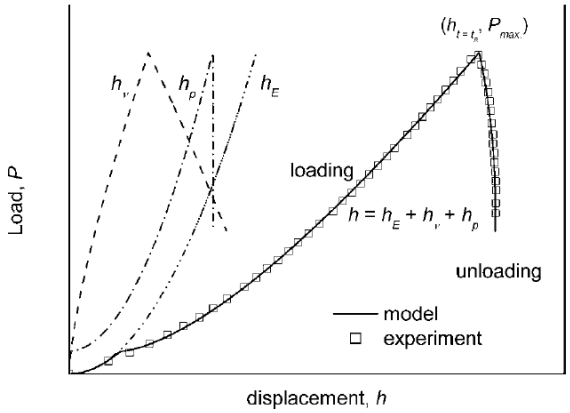

Figure 2.6 Schematic diagram of load-displacement curve during loading and unloading for viscoelastic material

There are several rheology models that could be applied to describe observed relaxation and creep. Those models all consist of springs and dashpots, which represent the elastic and viscous properties of the material, respectively. Different materials' rheology properties were explained by combining the springs and dashpots in a number of different ways. One of the most popular models was Burger's model, which consisted of a liner combination of a Maxwell and a Kelvin model. Other models, such as the generalized Maxwell and Kelvin model, the logarithmic model, and the power model could be used to analyze the creep phenomenon as well. Schiffmann et al. summarized the creep and relaxation tests of polycarbonate by using four different models to fit the data. His work involved creep and stress relaxation tests using feedback-controlled nanoindentation with varying loads and indentation depths, data-fitting using different models and comparing among them, and the computation of the relaxation modulus and creep compliance (Schiffmann, 2006). Li conducted creep experiments on bulk metallic glasses to investigate time-dependent properties, and was able to describe those properties using a generalized Kelvin model (Li et al., 2008). Ma et al. (2008) tested Ni thin films under different holding times to investigate the creep behavior, finding a decrease of the Young's modulus with an increase of holding time. Bembey performed nanoindentation creep tests on bone under three different conditions (ethanol, acetone and methanol) and found a dramatically greater creep for the sample bone immersed in acetone. Creep compliance was used as a creep parameter to make the comparison (Bembey et al., 2006). Olesiak proposed a viscous-elastic-plastic (VEP) indentation model to analyze the creep data obtained from three polymers and five bones. The

simulated data by using VEP solution matched both polymer and bone experimental data very well (Olesiak et al., 2010).

As wood is a viscoelastic material, the time-dependent properties associated with water content should be taken into consideration. Kojima proposed a simulation of the creep behavior of the secondary wall as affected by the microfibril angle (MFA) and investigated the moisture content's contribution to the tensile creep behavior. His discussion was based on the point of view of the composite structure of the cell wall, and his conclusion was that tensile creep behavior was highly dependent on both the moisture content and the MFA (Kojima and Yamamoto, 2004; Kojima and Yamamoto, 2005). Mukudai et al. (1987) proposed a viscoelastic bending model to interpret the characteristics of viscoelastic wood under moisture change cycles and based on the assumption that there is a slippage of S1 and S2 during the drying. The accelerated creep was monitored in a tensile creep experiment by putting a single fiber in variable relative humidity.

2.4 Moisture content and its effect on mechanical properties of the wood cell wall

2.4.1 Water in the cell wall

Moisture content is one of the most important factors in the wood material. The absolute moisture content of wood in defined in the following equation:

$$W = (G_s - G_{go}) / G_{go} \times 100\% \qquad \textbf{Equation 2-4}$$

where G_s is the green wood's weight and G_{go} is the weight of the oven-dried wood

Moisture content can vary within and among wood species, ranging from about 30% up to more than 200% of the weight. There are two different types of water exist in wood: the liquid water or water vapor, defined as “free” water and the water chemically held in the cell wall which is termed “bound” water. Free water usually exists in the cell lumen and bound water exists in between micro fibrils, serving as a part of the cell wall. The maximum moisture content is reached when both the cell wall and lumen are completely saturated with water. The free water in the lumen is first to vaporize when the wood is dried. A point called the Fiber Saturation Point (FSP) is the most important sign to show the form of the moisture content in wood. The fiber saturation point can be defined as the point at which only the cell walls are completely saturated (i.e., all bounded water) but no water exists in the cell’s lumens (Dietenberger, 1999).

2.4.2 Effect of water inside the cell wall on its mechanical properties

The behavior of wood is strongly influenced by moisture content. A wide range of studies regarding the moisture content-related properties of wood at the macro scale have well established the mechanical parameters and moisture content (Skaar, 1988). Many physical properties, such as the elastic modulus, shrinkage, and heat conductivity, are affected by moisture content. Stiffness and strength of wood typically decrease with increasing moisture content. It has been shown that moisture content plays important roles in the bending strength and stiffness and that an increase in moisture content will definitely decrease both properties (Arnold, 2010).

Currently, a great deal of research has been focused on the relationship between moisture content and the mechanical properties of a single component in the wood cell

wall from the viewpoint of the composite structure of the wood cell wall. Cousins (1976) conducted a measurement of the Young's and shear moduli for isolated lignin at different moisture contents and found that both the Young's and shear moduli were dependent on the moisture content of lignin; also, there was a linearly decrease of the Young's modulus and shear modulus as the moisture content of lignin increased from 3.6% to 12%. Cousins also investigated the effect of moisture content on the Young's modulus of hemicelluloses and proved that hemicelluloses are more sensitive to moisture content than cellulose and lignin. The same trend was observed as with lignin, that increasing the moisture content of the extracted hemicelluloses will strongly decrease the Young's modulus and shear modulus. These observations contribute to the explanation of models of the mechanical behavior of wood cell walls as a whole (Cousins, 1978). Several remaining questions are associated with this issue, however: for instance, what is the interaction among the different components when are absorbing water? How does the wood cell wall respond with water based on its complicated structure? Luckily, research associated with the paper industry on paper pulp and paper fiber helps us better understand these questions. In 1992, the elastic moduli of cell-walls of pulp fibers were calculated with relationship to the pulp yield by measuring the degrees of swelling (Scallan and Tigerstrom, 1992). A theoretical explanation of the hydrogen-bond, dominance were employed to predict how increasing the water content lowers the fiber's modulus (Zauscher et al., 1996).

Apart from experimental methods, other scientists have worked setting up a model on this issue from the perspective of the cell wall's shrinkage. A number of

models regarding the influence of moisture content on the wood cell wall have been developed. A computational 3D model for the analysis of the cell wall's micromechanical hydro elastic properties and shrinkage was established by Qing to investigate the influence of moisture on the stiffness properties (Qing and Mishnaevsky, 2009). Cave et al. (1976.1978) brought forward a theoretical model to predict the longitudinal shrinkage and Young's modulus with various moisture contents. The swelling of the cell wall and its contribution to the cell-wall ultrastructure was considered by Koponen et al. (Koponen et al., 1989). Potential chemical changes due to the restrained swelling have been proved to be proportional to the moisture content (Nakano, 2003; Nakano et al., 2006). Finally, the direction of cell-wall swelling has been predicted and determined by a cylindrical model (Nakano, 2008) .

2.5 Summaries

Nanoindentation, also called instrumental indentation, has proved itself to be a powerful technique in the measurement of the mechanical properties of diverse biomaterials. It has the advantage of probing the materials' unclear microstructure at a very fine scale and is extremely sensitive to the slight changes within the material's structure. More importantly, the application of nanoindentation to the characterization of bio-materials makes possible the quantitative assessment of mechanical properties in materials that were previously unattainable. As one of the most effective experimental methods, it can verify many theoretical simulations such as rheology models, cell-wall structure models and so forth. Traditionally, small scale mechanical properties of cellulose fiber were only obtainable with different treatments such as sample preparation,

storage method, bonding, relative humidity change and resin treatments. Nanoindentation has proved to be a dynamic, growing area of exploration in the biomaterial research area from which many new developments can be expected. However, many new methods and analysis will be required for future study. We expect many more big developments in the use of nanoindentation techniques as we probe the microstructures of cellulose fiber materials in future.

References

Arnold, M., 2010. Effect of moisture on the bending properties of thermally modified beech and spruce. Journal of Materials Science, 45, 669-680.

Barber.N.F, Meylan, B.A., 1964. The anisotropic shrinkage of wood.A theoretical model. Holzforschung, 18.

Bembey, A.K., Oyen, M.L., Bushby, A.J., Boyde, A., 2006. Viscoelastic properties of bone as a function of hydration state determined by nanoindentation. Philosophical Magazine, 86, 5691 - 5703.

Bergander, A., Salmen, L., 2002. Cell wall properties and their effects on the mechanical properties of fibers. Journal of Materials Science, 37, 151-156.

Bobji, M.S., Biswas, S.K., Pethica, J.B., 1997. Effect of roughness on the measurement of nanohardness - a computer simulation study. Applied Physics Letters, 71, 1059-1061.

Bushby, A.J., 2003. Nanoindentation of bone: Comparison of specimens tested in liquid and embedded in polymethylmethacrylate. J.Mater.Res,, 19.

Cave, I.D., 1976. Modelling the structure of the softwood cell wall for computation of mechanical properties. Wood Science and Technology, 10, 10-28.

Cave, I.D., 1978. Modeling moisture-related mechanical-properties of wood .1.properties of wood constituents

Wood Science and Technology, 12, 75-86.

Cave, I.D., 1978. Modelling moisture-related mechanical properties of wood Part II: Computation of properties of a model of wood and comparison with experimental data. Wood Science and Technology, 12, 127-139.

Cousins, W.J., 1976. Elastic modulus of lignin as related to moisture content. Wood Science and Technology, 10, 9-17.

Cousins, W.J., 1978. Youngs modulus of hemicelluloses as related to moisture-content. Wood Science and Technology, 12, 161-167.

Dietenberger, G., Kretschmann, Hernandez, Highley, Ibach, Liu, McDonald, Miller, Moody, Rowell, Simpson, Soltis, TenWolde, Wolfe, Vick, White, Williams, Williams, Winandy, Youngquist, 1999. Wood handbook : wood as an engineering material. Madison. in: F.P.L. USDA Forest Service (Ed.).

Doerner, M.F., Nix, W.D., 1986. A method for interpreting the data from depth-sensing indentation instruments. Journal of Materials Research,, 1.

Eder, M., Jungnikl, K., Burgert, I., 2009. A close-up view of wood structure and properties across a growth ring of Norway spruce (Picea abies [L] Karst.). Trees - Structure and Function, 23, 79-84.

Eichhorn, S.J., Sirichaisit, J., Young, R.J., 2001. Deformation mechanisms in cellulose fibres, paper and wood. Journal of Materials Science, 36, 3129-3135.

Fahlen, J., Salmen, L., 2002. On the lamellar structure of the tracheid cell wall. Plant Biology, 4, 339-345.

Fengel, D., G.Wegener, 1984. Wood: chemistry,ultrastructure,reactions. Walter de Gruyter

Fischer-Cripps, A.C., 2004. Nanoindentation. New York : Springer, New York.

Gindl, W., Gupta, H.S., 2002. Cell-wall hardness and Young's modulus of melamine-modified spruce wood by nano-indentation. Composites Part A: Applied Science and Manufacturing, 33, 1141-1145.

Gindl, W., Gupta, H.S., Schoberl, T., Lichtenegger, H.C., Fratzl, P., 2004. Mechanical properties of spruce wood cell walls by nanoindentation. Applied Physics a-Materials Science & Processing, 79, 2069-2073.

Hay, J.L., Pharr, G.M., 2000. Instrumented indentation testing. ASM Handbook 8, 232-243.

Haygreen, J.G., Bowyer, J.L., 1996. Forest products and wood science:An introduction. Iowa State University Press, Ames,Iowa,USA.

Hepworth, D.G., Vincent, J.F.V., Jeronimidis, G., Bruce, D.M., 2000. The penetration of epoxy resin into plant fibre cell walls increases the stiffness of plant fibre composites. Composites Part A: Applied Science and Manufacturing, 31, 599-601.

Jakes, J.E., Frihart, C.R., Beecher, J.F., Moon, R.J., Stone, D.S., 2008. Experimental method to account for structural compliance in nanoindentation measurements. Journal of Materials Research, 23, 1113-1127.

Jakes, J.E., Stone, D.S., Frihart, C.R., 2007. Nanoindentation size effect in wood 30th Annual Meeting of The adhesion Society, Inc. , pp. 15-17.

Kinney, J.H., Marshall, S.J., Marshall, G.W., 2003. The mechanical properties of human dentin: A critical review and re-evaluation of the dental literature. Critical Reviews in Oral Biology & Medicine, 14, 13-29.

Kojima, Y., Yamamoto, H., 2004. Properties of the cell wall constituents in relation to the longitudinal elasticity of wood - Part 2: Origin of the moisture dependency of the longitudinal elasticity of wood. Wood Science and Technology, 37, 427-434.

Kojima, Y., Yamamoto, H., 2005. Effect of moisture content on the longitudinal tensile creep behavior of wood. Journal of Wood Science, 51, 462-467.

Konnerth, J., 2009. Actual versus apparent within cell wall variability of nanoindentation results from wood cell walls related to cellulose microfibril angle. J Mater Sci, 44.

Konnerth, J., Valla, A., Gindl, W., 2007. Nanoindentation mapping of a wood-adhesive bond. Applied Physics a-Materials Science & Processing, 88, 371-375.

Koponen, S., Toratti, T., Kanerva, P., 1989. Modeling longitudinal elastic and shrinkage properties of wood

Wood Science and Technology, 23, 55-63.

Lee, S.H., Wang, S.Q., Pharr, G.M., Xu, H.T., 2007. Evaluation of interphase properties in a cellulose fiber-reinforced polypropylene composite by nanoindentation and finite element analysis. Composites Part a-Applied Science and Manufacturing, 38, 1517-1524.

Li, W.H., Shin, K., Lee, C.G., Wei, B.C., Zhang, T.H., He, Y.Z., 2008. The characterization of creep and time-dependent properties of bulk metallic glasses using nanoindentation. Materials Science and Engineering: A, 478, 371-375.

Lim, Y.Y., Chaudhri, M.M., 2001. Do residual nano indentations in metals and ceramics relax with time? Journal of Physics D-Applied Physics, 34, L70-L78.

Liu, C.K., Lee, S., Sung, L.P., Nguyen, T., 2006. Load-displacement relations for nanoindentation of viscoelastic materials. Journal of Applied Physics, 100, 9.

Ma, Z., Long, S., Pan, Y., Zhou, Y., 2008. Loading rate sensitivity of nanoindentation creep in polycrystalline Ni films. Journal of Materials Science, 43, 5952-5955.

Megraw, R.A., 1986. Wood quality factors in loblolly pine

Mittra, E., Akella, S., Qin, Y.-x., 2006. The effects of embedding material, loading rate and magnitude, and penetration depth in nanoindentation of trabecular bone. Journal of Biomedical Materials Research Part A, 79.

Mukudai, J., Yata, S., 1987. Further modeling and simulation of viscoelastic behavior (bending deflection) of wood under moisture change. Wood Science and Technology, 21, 49-63.

Nakano, T., 2003. Effects of cell structure on water sorption for wood. Holzforschung, 57, 213-218.

Nakano, T., 2008. Analysis of cell wall swelling on the basis of a cylindrical model. Holzforschung, 62, 352-356.

Nakano, T., Yamamoto, S., Norimoto, M., Nakai, T., Ishikura, Y., 2006. Effects of ultrastructure on water adsorption of bamboo. Mokuzai Gakkaishi, 52, 352-357.

Ngan, A.H.W., Tang, B., 2002. Viscoelastic effects during unloading in depth-sensing indentation. Journal of Materials Research, 17, 2604-2610.

Olesiak, S., Oyen, M., Ferguson, V., 2010. Viscous-elastic-plastic behavior of bone using Berkovich nanoindentation. Mechanics of Time-Dependent Materials, 14, 111-124.

Oliver, W.C., Pharr, G.M., 1992. An Improved technique for determining hardness and elastic-modulus using load and displacement sensing indentation experiments

Journal of Materials Research, 7, 1564-1583.

Oyen, M.L., Cook, R.F., 2003. Load-displacement behavior during sharp indentation of viscous-elastic-plastic materials. Journal of Materials Research, 18, 139-150.

Qing, H., Mishnaevsky, L., 2009. Moisture-related mechanical properties of softwood: 3D micromechanical modeling. Computational Materials Science, 46, 310-320.

Salmen, L., Burgert, I., 2009. Cell wall features with regard to mechanical performance. A review COST Action E35 2004-2008: Wood machining - micromechanics and fracture. Holzforschung, 63, 121-129.

Scallan, A.M., Tigerstrom, A.C., 1992. Swelling and elasticity of the cell-walls of pulp fibers

Journal of Pulp and Paper Science, 18, J188-J193.

Schiffmann, K.I., 2006. Nanoindentation creep and stress relaxation tests of polycarbonate: Analysis of viscoelastic properties by different rheological models. International Journal of Materials Research, 97, 1199-1211.

Skaar, C., 1988. Wood-water relations

Spurr, A.R., 1969. A low-viscosity epoxy resin embedding medium for electron microscopy. Journal of Ultrastructure Research, 26, 31-43.

Tze, W.T.Y., Wang, S., Rials, T.G., Pharr, G.M., Kelley, S.S., 2007. Nanoindentation of wood cell walls: Continuous stiffness and hardness measurements. Composites Part A: Applied Science and Manufacturing, 38, 945-953.

Wimmer, R., Lucas, B.N., Oliver, W.C., Tsui, T.Y., 1997. Longitudinal hardness and Young's modulus of spruce tracheid secondary walls using nanoindentation technique. Wood Science and Technology, 31, 131-141.

Wu, Y., Wang, S., Zhou, D., Xing, C., Zhang, Y., 2009. Use of nanoindentation and silviscan to determine the mechanical properties of 10 hardwood species

Wood and Fiber Science, 41, 64-73.

Wu, Y., Wang, S., Zhou, D., Xing, C., Zhang, Y., Cai, Z., 2010. Evaluation of elastic modulus and hardness of crop stalks cell walls by nano-indentation. Bioresource Technology, 101, 2867-2871.

Xing, C., Wang, S., Pharr, G., 2009. Nanoindentation of juvenile and mature loblolly pine (Pinus taeda L.) wood fibers as affected by thermomechanical refining pressure. Wood Science and Technology, 43, 615-625.

Yamamoto, H., Kojima, Y., 2002. Properties of cell wall constituents in relation to longitudinal elasticity of wood. Wood Science and Technology, 36, 55-74.

Yu, Y., Fei, B., Zhang, B., Yu, X., 2007. Cell-wall mechanical properties of bamboo investigated by in-situ imaging nanoindentation. Wood and Fiber Science, 39, 527-535.

Zauscher, S., Caulfield, D.F., Nissan, A.H., 1996. The influence of water on the elastic modulus of paper .1. Extension of the H-bond theory. Tappi Journal, 79, 178-182.

Zou, L., Jin, H., Lu, W.-Y., Li, X., 2009. Nanoscale structural and mechanical characterization of the cell wall of bamboo fibers. Materials Science and Engineering: C, 29, 1375-1379.

CHAPTER 3. EFFECT OF EPOXY EMBEDDING MEDIUM ON THE MEASUREMENT OF MECHANICAL PROPERTIES OF LIGNOCELLULOSIC MATERIALS

3.1 Abstract

In recent decades, modulus and hardness testing by nanoindentation has been widely used to characterize the small-scale mechanical properties of a number of materials. The ability of nanoindentation technology to measure the force and displacement on the nanometer scale makes it possible to investigate the mechanical properties of the microstructures of lignocellulosic materials as well. However, there are still some testing limitations because of the specific conformation and structure of biomaterial. To improve the utilization of nanoindentation technology, more detailed knowledge regarding sample preparation is needed. Thus, in this chapter, the effect of the embedding medium on the nanoindentation measurement of wood material was investigated both experimentally and theoretically. Significant differences in Young's modulus and hardness between reference wood cell walls and epoxy resin embedded cell wall were found. Scanning Electric Microscope (SEM) and Energy Dispersive Spectroscopy (EDS) analysis were used to verify resin penetration into wood cell walls. Further investigation detected the influence of different vacuum times during the embedding procedure on the Young's modulus and hardness. Regression analysis showed that vacuum times had no significant impact on either the Young's modulus or the hardness of a wood cell wall. It was concluded that penetration of epoxy resin during a sample's preparation for nanoindentation increases both the Young's modulus and hardness. A cautious assumption was made in this thesis based on previous cell-wall structure research, i.e., that resin penetration leads to structural and chemical changes in the wood cell-wall constituents that may significantly alter the material properties as

compared to non-embedded wood. A novel sample preparation especially for use with single fibers or small wood blocks was set up to avoid the influence of the embedding medium on the measurements.

3.2 Introduction

Nanoindentation is a tool for the exploration of the mechanical properties of small-scale, small-volume, and microstructure features; it is becoming more popular in the area of biomaterial research. This technique has been successfully used to probe the micro mechanical properties of many biomaterials, such as bone (Bushby, 2003), tooth (Xie et al., 2009), soft tissue (Franke et al., 2008), crop stalks (Wu et al., 2010), wood (Xing et al., 2009), bamboo (Zou et al., 2009), Lyocell fiber (Lee et al., 2007), lignocelluloses (Lee et al., 2007) and others.

Since nanoindentation tests are all performed at the nano-scale, one of the most important factors in nanoindentation measurement is the roughness of sample. In order to get a sample's surface smooth enough to perform indentation, most biomass materials, need to be embedded in an embedding medium, typically Spurr's epoxy resin, in order to support the cell wall both in microtoming (Spurr, 1969) and in performing indentation. The embedding approach appears to be simple and straightforward; however, the reliability of absolute values has been questioned due to the influence of the embedding medium. Some caveats regarding this issue including the following. First, previous research has not paid much attention to the embedding medium penetration, possibly causing researchers to miss any effects of the resin's effect as an additive (Gindl and Gupta, 2002). Secondly, the wood structure is complicated, especially in regard to its

porosity, its multiple layers, and the arrangement of its microfibrils; these require further consideration in research (Konnerth, 2009).

The micro-mechanics of a wood cell wall are often dominated by its complex multi-component structures and the arrangement of its sublayers. As a native porous and anisotropic material, considerable research efforts are being directed at the effects of the added adhesive and the penetration on the mechanical properties of the cell wall (Xing et al., 2005). Adhesive penetration is known to be a factor in the cell wall mechanical properties for wood bond lines (Konnerth et al., 2007). Johannes Konnerth has observed that embedding wood specimens in epoxy resin for nanoindentation may affect measurements (Konnerth et al., 2007).

Earlier research has revealed that adhesive penetration of wood cell usually takes place along three paths, namely through cell lumens, pits, and by nano-penetration in the cell wall (Kamke and Lee, 2007). However, there are only limited studies showing that the penetration of epoxy resin into plant cell wall will increase the stiffness of fiber composites (Hepworth et al., 2000).

The primary purpose of this chapter is to investigate the effect of the embedding medium on the measurement of the micro–mechanical properties of wood cell wall as a representative woody biomass material. In this investigation, we examined in detail the epoxy resin penetration as affected by the vacuum and curing time, i.e., to explore the influence of resin penetration on the data. This may result in the development of an

efficient testing method for improved precision of metrics from nanoindentation experimentation.

3.3 Materials and Methods

3.3.1 Material collection and sample preparation

Two different wood species were chosen, loblolly pine (Pinus taeda L.) and red oak (Quercus rubra). A loblolly pine disk was cut 0.3m above the ground from a tree. The 32nd annual ring was cut into a block with a dimension of 8mm x 8mm x 15mm in radial, tangential, and longitudinal directions, respectively (Tze et al., 2007). The late wood portion of the 32nd annual ring with a micro fibril angle value of 31° was chosen and cut to a small block with dimensions of 1mm x 1mm x 5mm. A red oak disk was cut 0.5m above the ground from a tree. The 38th annual ring was cut into a block with the same dimensions as above. Latewood cells with a micro fibril angle of 11.9° were chosen as the target location. Three different specimen preparation methods were used.

3.3.1.1 Small wood block embedded into epoxy resin

In this study, the latewood portion of the 32th growth ring of the loblolly pine sample was cut into small pieces; this was followed by dehydration at 40°C for 30 minutes. Each piece was embedded in low viscosity epoxy resin. Spurr resin[1] is one of the easily prepared embedding materials for research of biomaterial's microstructure research. The components of Spurr's resin are given in Table 3.1. The embedded specimens were treated with a vacuum-pressure system for several minutes to remove air bubbles inside the cell wall lumen, which resulted in the resin's diffusion into the

[1] Spurr's resin has very low viscosity. It is a common embedding medium that enables specimen to be successfully embedded.

specimen. The specimens were then cured at 70°C in an oven for eight hours. The cured specimens were mounted on holders ready for microtoming. Trapezoids shapes were cut in epoxy embedded specimens and tiny flat surfaces were obtained with a glass knife and refined with a diamond knife. Figure 3.1 shows the sample preparation procedure in detail. In the end, a smooth surface with roughness of less than 5 nm was obtained for nanoindentation. Six different vacuum time treatments were performed on the specimens with the same growth ring and fibril angles: 0 min, 10 min, 20 min, 30min, 50 min and 120min.

Table 3.1 Components of Spurr's epoxy resin

Name	**ERL-4221**	**ERL-4221DER-736**	**NSA**	**DAME**
Proportion	**5**	**3**	**13**	**0.2**
Weight	**2.5**	**1.5**	**6.5**	**0.1**

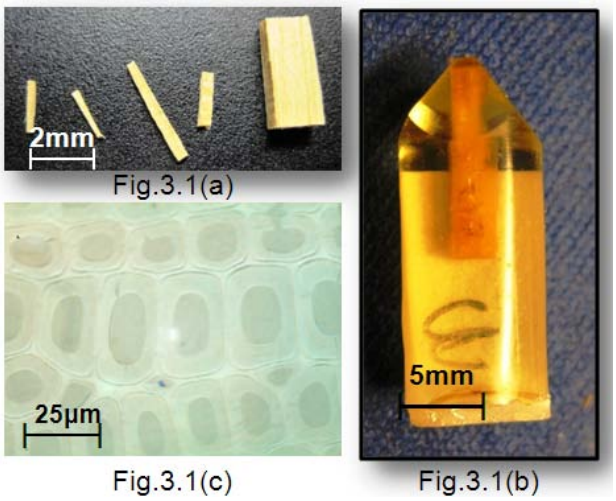

Figure 3.1 Specimen preparation procedure for wood block embedded in epoxy resin. (a) Small wood block of loblolly pine; (b) Small wood block of loblolly pine embedded in epoxy resin ; (c) Microscopic picture of embedded loblolly pine cell wall

3.3.1.2 Wood blocks without embedding

Samples were cut into a block with the size of 8mm × 8mm × 10mm to ensure that the bottom and top were parallel to each other and exactly perpendicular to the cell wall longitudinal axis. The transverse surface was made into a pyramid shape with the latewood located at the apex. Figure 3.2 shows the detailed procedure. An ultramicrotome equipped with a glass knife was chosen to cut the apex to make a small flat surface. Finally, a diamond knife was used to cut the apex and generate a smooth surface of area 1mm2. The best surface was obtained when the cutting angle was set at 4°. The typical progression involved cutting multiple sections off at one um, 500nm, 250nm, 100nm and then 50nm. A thin slice with purple color was a good indication of an ideal cutting. The sample surface was ready for indentation or AFM test when intact cell wall structure and shining sample surface were obtained under the optical microscope.

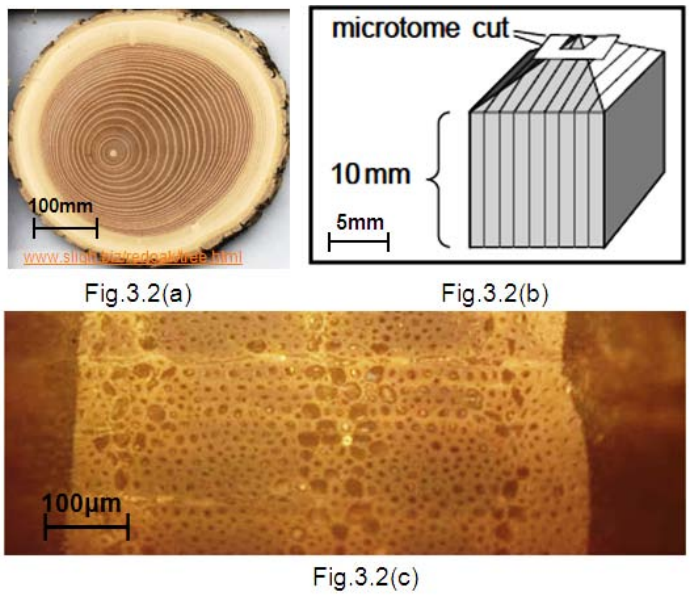

Figure 3.2 Specimen preparation procedure for wood block without epoxy resin (a)Red oak disk; (b)Red oak block with four sides pyramid shape; (c) Microscopic picture of unembedded red oak cell wall

3.3.1.3 Small wood blocks without resin penetration

A novel method for sample preparation suitable for wood chips or signal fiber without resin diffusion was developed using plastic sealing and embedding. Specimens were cut into small pieces and sealed by FoodSaver® polymer film as shown in Figure 3.3(a). A small wood block was placed between two films and pressed by the electric iron with temperature set at 160°C. The pre-sealed samples were then embedded in epoxy resin using the aforementioned procedure; see Figure 3.3(b). As observed in Konnerth's research (Konnerth, 2009), misalignment between the longitudinal cell axis and the indentation direction will introduce a test value bias caused by the artificial change of the microfibril angle. This pre-sealed thin film for the wood chip makes it easy to mount inside the embedding mold parallel to the longitudinal axis of the wood cell wall. The

sample was mounted onto a metal sample holder specially designed for ultra-microtoming, and cell walls with empty lumens were obtained by diamond knife cutting. Figure 3.3(c) illustrates the interference microscopic picture taken after the ultramicrotome cut. Although there is some polymer penetration in between the bond line of the wood cell wall and the thin film used for isolating, the majority of the cell walls were protected well enough for the indentation test to be performed.

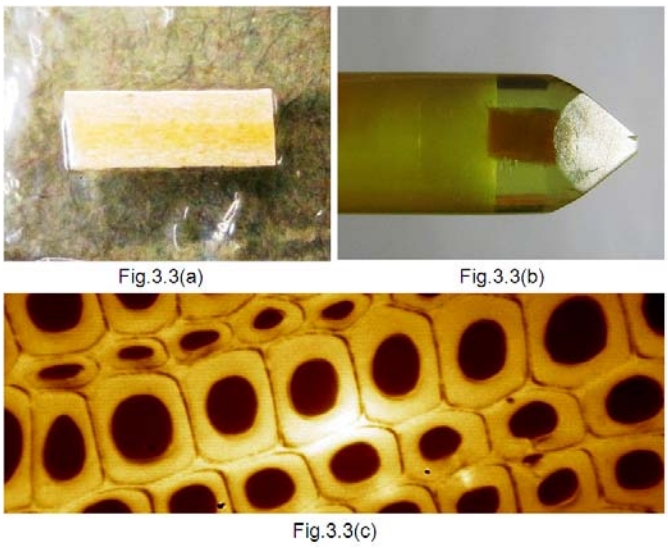

Figure 3.3 Specimen preparation procedure for wood block isolated by thin film (a)Loblolly pine's small wood block sealed by thin film; (b)Loblolly pine small wood block with sealed film embedded in epoxy resin ; (c) Interference microscopic picture of loblolly pine cell wall isolated by thin film

3.3.2 Nanoindentation

The nanoindentation test was performed under Triboindentor in conjunction with scanning probe microscopy (SPM) at a room temperature of 20°C and relative humidity of 25±4%. All the samples were put into the Triboindentor chamber at least 24 hours before indentations were performed. This procedure is critical because thermal expansion or contraction of the sample during the indentation test will significantly affect the accuracy of the final results (Fischer-Cripps, 2004).

3.3.2.1 Theory of nanoindentation

On the basis of the theory of nanoindentation, the reduced modulus, Er (the composite modulus for indenter and sample combination), can be evaluated from the nanoindentation measurements by employing the following equation 2-2 (Oliver and Pharr, 1992). The Meyer hardness (H) can be obtained from the following equation 2-1,

The specimen Young's modulus (E_s) was then calculated by equation 2-3 (Oliver and Pharr, 1992)

$$E_s = \left(1-\nu_s^2\right)\left(\frac{1}{E_r}-\frac{1-\nu_i^2}{E_i}\right)^{-1} \qquad \text{Equation 3-1}$$

where ν_s and ν_i (0.07) are the Poisson's ratios of the specimen and indenter, respectively, whereas E_i is the modulus of the diamond indenter (1141GPa). The sample's Poisson's ratio ν_s for the cell walls in all calculation was assumed to be 0.25, to achieve a consensus with Wu's results (Wu et al., 2009).

3.3.2.2 Morphological Analysis

Topographies of the sample after indentation were obtained by an atomic force microscopy (AFM) (XE-100, PSIA CORP., Sang-Daewon-dong, Korea), operated in contact mode. With a rigidly mounting in the AFM stage, samples were scanned at a 0.5 Hz rate and a set point of 1.0 μN.

3.3.3 Measurements of wood cell wall hardness and Young's modulus by nanoindentation

A TriboIndenter® system manufactured by Hysitron, Inc. was used for all the indentation tests. A Berkovich indenter with a three-sided pyramidal shape and with an area-to-depth function was loaded for all experiments (Oliver and Pharr, 1992). All experiments were conducted with a closed-loop feedback control aimed at providing precise control of the nanoindentation probe in load-controlled modes. Drift monitor time for 40 seconds was set up to measure the drift of the system before any test. The single indentation procedure included four parts: first, there was a 2 μN set point force between the probe and sample surface. The indentation test did not start until the 2 μN pro-load force was detected by the transducer. Second, the peak load was achieved at a loading rate of 30 μN/s. Third, at this peak load, the loading was held for 5 seconds to avoid the effect of creep occurring in viscous material during the unloading (Liu et al., 2006). Finally, the unloading was executed at the same loading rate as those for the loading, 5 seconds. The scanning probe microscopy (SPM) assembly in the Triboindentor system is capable of accurately positioning the wood cell walls' S2 layer. With a scanning size of 40μm×40μm, interesting indent positions were marked on the SPM image and

indentations were implemented and checked by rescanning the image. Only indentations in the middle of the cell wall's S2 layer were selected as valid data. Indentations performed in the embedding epoxy or at the border of the cell walls were all expunged.

The experiment procedure for vacuum impregnation was as follows: The specimen was immersed into low viscosity resin, the specimens and epoxy resin were placed into a vacuum oven, a vacuum-pressure was then applied on the sample, and the resin diffused in voids inside of the wood cell wall and the lumen. Different vacuum times were used ranging from zero min to 120 min for the purpose of observing the amount of penetration. Later, all specimens were cured at 70°C in an oven for eight hours. Certain numbers of indentations were performed on the different cell walls in the same sample. Indentations performed on five different cell walls within the same sample under certain vacuum times were defined as statistical replications, and different vacuum times were referred to as one treatment with six different levels.

3.4 Results and Discussion

3.4.1 Influence of embedding medium on the Young's modulus and hardness of wood cell wall

Figures 3.4 and 3.5 show the results of the indentation experiments. The mean value of the elastic moduli of unembedded loblolly pine was 13.4±1.50 GPa and the mean value of the hardness was 0.44±0.07 GPa. According to the definition of Meyer hardness, hardness was determined at peak load. Thus, the hardness value was dependent not only on the plastic but also the elastic deformation, which could be expressed by the ratio between the Young's modulus and the yield strength σy. Since yield strength σy

cannot be measured directly by nanoindentation, for most of the materials, the constraint factor, given as the ratio of $H/\sigma y$, should be around 3. However, for the cell corner middle lamellae (CCML), the constraint factor usually comes to 1.5, as proposed by Gindl (Gindl et al., 2004). Thus, for a wood cell wall's S_2 layer in this case, when applying these values to the E/H ratio, the $E/\sigma y$ should be somewhere between 45 to 90. Sink-in behavior was expected due to the small $E/\sigma y$ ratio and could be observed in the topographic image obtained by AFM, as shown in Figure 3.5. In contrast, the mean value of the Young's modulus (15.3±1.94 GPa) and the hardness (0.58±0.05 GPa) of loblolly pine treated with epoxy resin was significantly greater than of the reference cells which were not embedded. A good agreement with Lee's report (Lee et al., 2007) was achieved considering that the relative humidity was 25% in this research and 60% in Lee's experiment, which resulted in the increase of both hardness and elastic modulus. This indicates that the moisture content of wood cell wall is such an important factor that it will affect the mechanical properties.

It is also possible that this increase might be accounted for by the differences in some parameters of the setup, such as the upper and lower fit of the unloading curve, in the different experimental facilities. Similarly, the Young's modulus of unembedded red oak was 17.9±2.70 GPa, and the hardness was 0.53±0.05 GPa, compared to embedded red oak, which were 20.7±1.35 GPa and 0.59±0.04 GPa separately. The data from the epoxy resin-embedded sample obtained a good agreement with Yan's results (Wu et al., 2009), considering the pure error existing among typical samples, such as microfibril angles and cell wall density.

The effect of the embedding medium on wood cell wall properties was studied with nonparametric analysis at the confidence level of 95%. Wilcoxon rank sum test results show that the Z value was 5.57, and the P value stood at 0.0001, which is less than 0.05 and therefore significant. Thus we reject the null hypothesis and conclude at confidence level of 95% that there is a significant difference between the measurement of elastic moduli of the embedded loblolly pine sample and the un-embedded one. In brief, there was a 14.2% increase of Young's modulus and a 32% increase of hardness for loblolly pine treated with of epoxy resin at a confidence level of 95%. Analogously, there was a 15.6% increase of the Young's modulus and 11.3% increase of the hardness for epoxy-resin-treated red oak at the confidence level of 95%.

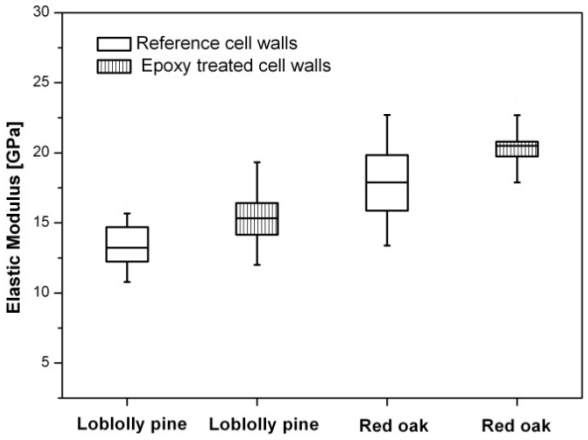

Figure 3.4 Comparison between Young's modulus measurements for embedded and unembedded samples of loblolly pine and red oak by nanoindentation

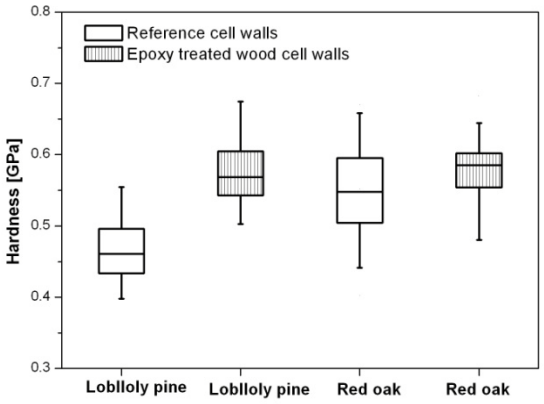

Figure 3.5 Comparison between hardness measurements for embedded and unembedded samples of loblolly pine and red oak by nanoindentation

Figure 3.6 shows the results a comparison of the Young's modulus and hardness measurements of isolated sample and embedded sample. To avoid other affecting factors like cell wall variability, cell inclination, microfibril angle variance, and so forth, the experiments were performed by using the same sample, even the same tree ring. The mean value of Young's modulus of isolated pine is 14.8 ±2.17 GPa compared with 17.8 ±2.20 Gpa after embedding. Nonparametric analysis results show that the P value equals to 0.0001 which is small than 0.05, so there is a significant difference between un-embedded and embedded samples. The mean value of the hardness of isolated pine is 0.53±0.04 GPa while it is 0.55±0.05 Gpa after the sample is embedded in to epoxy resin. Nonparametric analysis results show that the P value equals to 0.02 which is smaller than 0.05, so there is a significant difference in the hardness value between the embedded sample and the unembedded one. This result validates the novel embedding method and strengthens the enhancement function of epoxy resin.

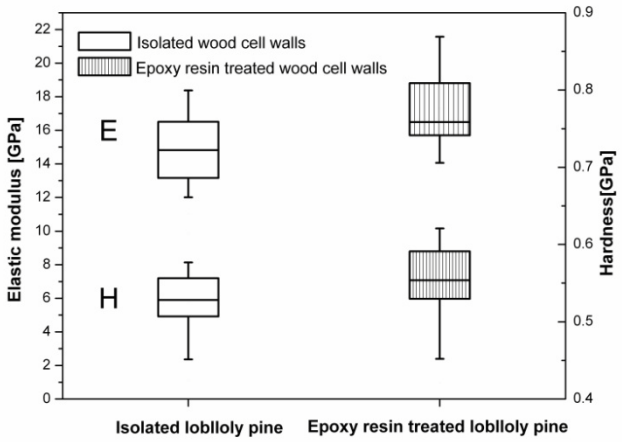

Figure 3.6 Young's modulus and hardness of isolated and embedding loblolly pine by nanoindentation

3.4.2 Roughness of sample

The sample roughness is an important factor that influences the final value. It can cause errors in the determination of sample surface during indentations. The varying indentation depth caused by the roughness can result in a high standard deviation for the final data (Bobji et al., 1997). Since the performed indentation depths on wood cells were just 100 nm, in order to eliminate the effect of sample surface roughness, all the test surface were cut by a diamond knife to make the sample's average roughness less than 5 nm (Fischer-Cripps, 2004). This made it possible to control surface roughness to less than 10% of the total penetration depth, providing relatively accurate results. Figure 3.7 shows AFM topographic of the residual indents performed in the cross section of the cell wall's S2 layer. The scan size is 5μm x 5μm and the sample surface has a vertical range of 60nm with root mean square surface roughness amplitude of 2.5 nm.

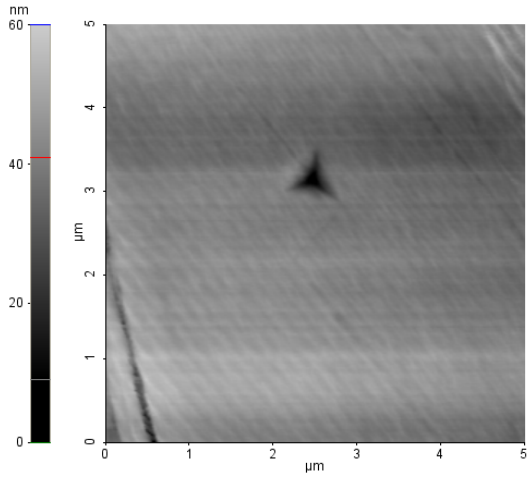

Figure 3.7 AFM topographic image of single indent for loblolly pine cell wall

3.4.3 Scanning Electron Microscopy (SEM) and Energy Dispersive Spectroscopy (EDS) analysis

From the indentation results mentioned above, a question arose about the possibility of resin penetration procedure and reasons for an increase of modulus and hardness. Figure 3.8 and 3.9 show SEM images of wood cell wall. Several important characteristics of the SEM images are worthy of note. First, the cell wall lumen was fully diffused by epoxy resin in Figure 3.9 compared to Figure 3.8. This observation suggests that epoxy resin has already occupied the cell wall lumen after curing in the oven. However, it is insufficient to prove cell wall penetration. Hence, whether the resin penetrated into cell wall or not could not be directly confirmed by SEM images. Further investigation by Energy Dispersive X-ray Spectroscopy (EDS) experimentation needed to be executed. This technology is based on the interaction between the primary beam and

the atoms in the sample; it causes shell transitions and results in the emission of an X-ray (Larnøy et al., 2010). Interesting locations such as cell wall A, cell wall B and epoxy resin were chosen as shown in Figures 3.8 and 3.9. The major elements in Spurr's resin are carbon and oxygen, which are the same as the elements in cell walls. EDS element analysis was made and proved for resin penetration by observation of the carbon and oxygen content. Table 3.2 shows the element analysis results. The carbon content of cell wall B, embedded by epoxy resin, was more than that of the epoxy resins and less than that of the reference cell wall. In contrast, the oxygen content of cell wall B was lower than that of the reference and higher than that of the epoxy resin. This could be an indication of resin penetration into cell wall, which changes the content ratio.

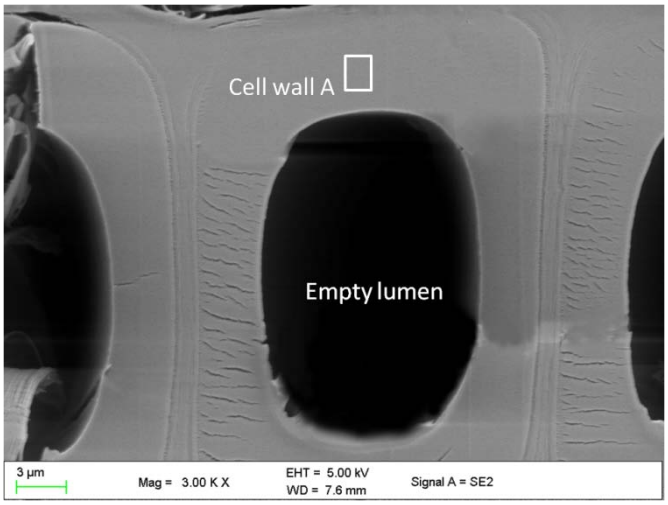

Figure 3.8 SEM image of loblolly pine cell wall

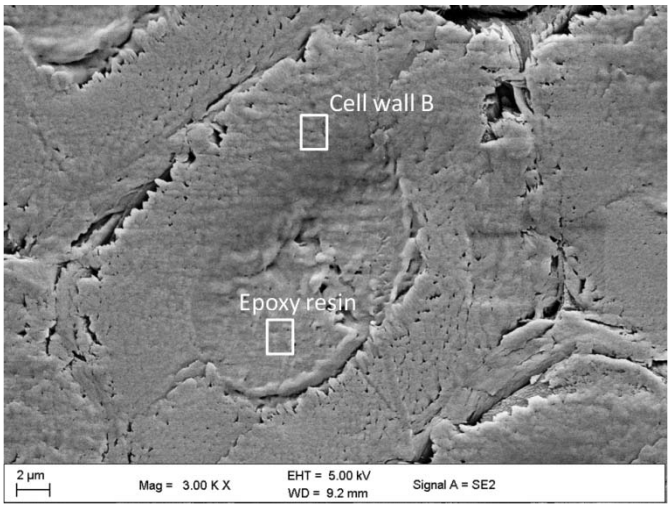

Figure 3.9 SEM image of loblolly pine cell wall embedded in Spurr's resin

Table 3.2 Comparison of carbon/oxygen content among pure Spurr's resin, resin embedded cell wall, and reference cell wall

	Carbon Content [%]	**Oxygen Content [%]**
Epoxy resin	81.7± 1.84	18.3±1.84
Reference cell wall A	72.2± 1.42	27.8±1.42
Epoxy resin treated cell wall B	75.2± 1.71	24.8±1.71

Note: Values given were mean±SD with units of percentage and were averaged from the four different areas in 3 samples each.

Embedding medium that has penetrated into the cell wall has increased both the Young's modulus and hardness. This was caused by the wood cell wall's texture and the properties of the cell-wall components. Lennart Salmen observed that the interactions between the constituents of cell wall occur on an extremely intermixed level (Salmen and Burgert, 2009). The S2 layer of wood cell wall should be considered as natural, unidirectional fiber-reinforced composite: the cellulose made up of cellulose microfibrils plays the role of the frame substance, where hemicelluloses and carbohydrate serve as a

matrix substance to support the stiffness of the cell wall. Moreover, the lignin diffused in the texture considered as encrusting substance, which will greatly increase the hardness of cell wall. Although all indentation and EDS element measurements give indirect evidence of where and how exactly the epoxy resin located within cell wall, it can be cautiously assumed that polymer chains of Spurr's resin penetrate into the cell wall through the pit, the lumen and nano-penetration due to the low-viscosity properties. Spaces in the cellulose–hemicelluloses structure are filled with resin (Gindl et al., 2002) and then occupy the void spaces among the cellulose microfibrils. The mainly hydrogen bonds between hemicelluloses and cellulose enable a strong but relative flexible connection, indicating a possible interaction between the C=O bond in the epoxy and the –OH bond in the cellulose. This enables the effective bonding between the Spurr's resin and the microfibrils. Furthermore, the cell-wall density was increased by the resin filling. All the factors mentioned above could account for the increase of both Young's modulus and hardness.

3.4.4 Effect of vacuum time on the Young's modulus and hardness of wood cell wall

To analyze all the data taken by the indentations at different vacuum times, Complete Randomized Design (CRD) with replication and repeated measurements were taken based on the obtained data. All those definitions were based on the assumption that each sample is homogeneous, considering the pure error between different cell walls. Previous experiments performed by Tze et al. on five adjacent tracheids detected no significant differences in either hardness or modulus values among five tracheids of the same growth ring (Tze et al., 2007). Wimmer's results also confirmed this (Wimmer et

al., 1997). Linear regression was used to determine whether a relationship existed between the elastic modulus/hardness and the vacuum time, and the data were collected and grouped by individual cell wall. All the indentations were performed under at a relative humidity of 25% and a temperature of 70oF. Table 3.3 shows a series of the mean values of Young's modulus and hardness of wood cell wall S2 layers obtained by single indentation with 150 μN peak load. Basically, the pooled data obey normal distribution. One-way analysis of variance (ANOVA) analysis results show that Prob $>|t|$ equals to 0.8878 for vacuum time, which is larger than 0.05, indicating that the regression coefficient is not significantly different from zero.

Table 3.3 Young's modulus of loblolly pine under different vacuum time

Vacuum time (min)	Number of valid data	Young's modulus (GPa)	Hardness (GPa)
0	**47**	**17.0(4.76)**	**0.65(3.39)**
10	**46**	**16.0(5.31)**	**0.63(3.58)**
20	**39**	**15.7(7.16)**	**0.63(2.30)**
30	**38**	**16.6(10.1)**	**0.65(5.03)**
50	**35**	**16.5(4.59)**	**0.61(3.86)**
120	**40**	**16.4(8.79)**	**0.630(5.15)**

Note: Young's modulus and hardness values represents the mean value of indents on 5 cell walls in each sample. The coefficient of variation (CV, in bracket; units in percentage) represents the variability of the Young's modulus and hardness.

Figure 3.10 reveals that the Young's modulus and hardness of wood cell wall at different vacuum times are nearly constant from 0min vacuum time to 120min. Even though the regression coefficient shows a small negative value, R-Square equals to 0.000723 indicating that the vacuum time during embedding procedure does not have significant impact on Young's modulus or hardness when tested at the 0.05 level of significance. This result implies that the progress of the embedding medium's penetration is fast and not affected by the vacuum time, although the vacuum procedure will help and ensure the fully diffusion. Epoxy resin will more easily penetrate the wood cell wall and lumen due to the low viscosity of the resin itself.

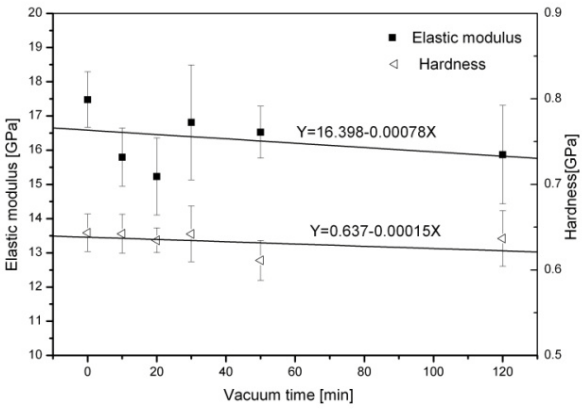

Figure 3.10 Dependence of vacuum time on Young's modulus and hardness of wood cell wall

3.5 Conclusions

Nanoindentation has proved itself to be a valuable tool for characterizing the mechanical properties of cell wall in recent years. However, this technique is still not been fully matured due facility and sample preparation limitations. Many efforts have been made to improve the estimation of cell wall properties by nanoindentation. A better understanding of the effect of the role of the embedding medium is crucial for insight into the interaction between epoxy resin and cell wall structure. A series of contrast experiments was made to verify that embedding medium enhanced both the Young's modulus and the hardness of the wood cell wall. Typically, the modulus of loblolly pine embedded in epoxy resin increased by 14% and the hardness by 32% compared to unembedded wood cell, at a confidence level of 95%. Similarly, there was a 15.5% increase for the Young's modulus and 11.3% for the hardness of red oak at the confidence level of 95%. Moreover, vacuum time affects neither reduced modulus nor the hardness of wood cell wall, which indicates that resin penetration is a fast procedure and occurs through several avenues, including pits, lumen, and nano-penetration. Finally, a new embedding method was developed to prevent resin from penetrating into wood cell wall. This method is reasonable for small specimens, such as a single fiber, wood chip, wood remains, and so forth.

References

Bobji, M.S., Biswas, S.K., Pethica, J.B., 1997. Effect of roughness on the measurement of nanohardness - a computer simulation study. Applied Physics Letters, 71, 1059-1061.

Bushby, A.J., 2003. Nanoindentation of bone: Comparison of specimens tested in liquid and embedded in polymethylmethacrylate. J.Mater.Res,, 19.

Fischer-Cripps, A.C., 2004. Nanoindentation. New York : Springer, New York.

Franke, O., Göken, M., Hodge, A., 2008. The nanoindentation of soft tissue: Current and developing approaches. JOM Journal of the Minerals, Metals and Materials Society, 60, 49-53.

Gindl, W., Gupta, H.S., 2002. Cell-wall hardness and Young's modulus of melamine-modified spruce wood by nano-indentation. Composites Part A: Applied Science and Manufacturing, 33, 1141-1145.

Gindl, W., Gupta, H.S., Grunwald, C., 2002. Lignification of spruce tracheid secondary cell walls related to longitudinal hardness and modulus of elasticity using nano-indentation. Canadian Journal of Botany-Revue Canadienne De Botanique, 80, 1029-1033.

Gindl, W., Gupta, H.S., Schoberl, T., Lichtenegger, H.C., Fratzl, P., 2004. Mechanical properties of spruce wood cell walls by nanoindentation. Applied Physics a-Materials Science & Processing, 79, 2069-2073.

Hepworth, D.G., Vincent, J.F.V., Jeronimidis, G., Bruce, D.M., 2000. The penetration of epoxy resin into plant fibre cell walls increases the stiffness of plant fibre composites. Composites Part A: Applied Science and Manufacturing, 31, 599-601.

Kamke, F., Lee, J., 2007. Adhesive Penetration in Wood—a Review. Wood and Fiber Science, 39, 205-220.

Konnerth, J., 2009. Actual versus apparent within cell wall variability of nanoindentation results from wood cell walls related to cellulose microfibril angle. J Mater Sci, 44.

Konnerth, J., Harper, D., Lee, S.-H., Rials, T.G., Gindl, W., 2007. Adhesive penetration of wood cell walls investigated by scanning thermal microscopy (SThM). Holzforschung, 62, 91-98.

Konnerth, J., Valla, A., Gindl, W., 2007. Nanoindentation mapping of a wood-adhesive bond. Applied Physics a-Materials Science & Processing, 88, 371-375.

Larnøy, E., Eikenes, M., Militz, H., 2010. Detection of chlorine-labelled chitosan in Scots pine by energy-dispersive X-ray spectroscopy. Wood Science and Technology.

Lee, S.H., Wang, S.Q., Pharr, G.M., Kant, M., Penumadu, D., 2007. Mechanical properties and creep behavior of lyocell fibers by nanoindentation and nano-tensile testing. Holzforschung, 61, 254-260.

Lee, S.H., Wang, S.Q., Pharr, G.M., Xu, H.T., 2007. Evaluation of interphase properties in a cellulose fiber-reinforced polypropylene composite by nanoindentation and finite element analysis. Composites Part a-Applied Science and Manufacturing, 38, 1517-1524.

Liu, C.K., Lee, S., Sung, L.P., Nguyen, T., 2006. Load-displacement relations for nanoindentation of viscoelastic materials. Journal of Applied Physics, 100, 9.

Oliver, W.C., Pharr, G.M., 1992. An Improved technique for determining hardness and elastic-modulus using load and displacement sensing indentation experiments

Journal of Materials Research, 7, 1564-1583.

Salmen, L., Burgert, I., 2009. Cell wall features with regard to mechanical performance. A review COST Action E35 2004-2008: Wood machining - micromechanics and fracture. Holzforschung, 63, 121-129.

Spurr, A.R., 1969. A low-viscosity epoxy resin embedding medium for electron microscopy. Journal of Ultrastructure Research, 26, 31-43.

Tze, W.T.Y., Wang, S., Rials, T.G., Pharr, G.M., Kelley, S.S., 2007. Nanoindentation of wood cell walls: Continuous stiffness and hardness measurements. Composites Part A: Applied Science and Manufacturing, 38, 945-953.

Wimmer, R., Lucas, B.N., Oliver, W.C., Tsui, T.Y., 1997. Longitudinal hardness and Young's modulus of spruce tracheid secondary walls using nanoindentation technique. Wood Science and Technology, 31, 131-141.

Wu, Y., Wang, S., Zhou, D., Xing, C., Zhang, Y., 2009. Use of nanoindentation and silviscan to determine the mechanical properties of 10 hardwood species

Wood and Fiber Science, 41, 64-73.

Wu, Y., Wang, S., Zhou, D., Xing, C., Zhang, Y., Cai, Z., 2010. Evaluation of elastic modulus and hardness of crop stalks cell walls by nano-indentation. Bioresource Technology, 101, 2867-2871.

Xie, Z.H., Swain, M.V., Swadener, G., Munroe, P., Hoffman, M., 2009. Effect of microstructure upon elastic behaviour of human tooth enamel. Journal of Biomechanics, 42, 1075-1080.

Xing, C., Riedl, B., Cloutier, A., Shaler, S., 2005. Characterization of urea–formaldehyde resin penetration into medium density fiberboard fibers. Wood Science and Technology, 39, 374-384.

Xing, C., Wang, S., Pharr, G., 2009. Nanoindentation of juvenile and mature loblolly pine (Pinus taeda L.) wood fibers as affected by thermomechanical refining pressure. Wood Science and Technology, 43, 615-625.

Zou, L., Jin, H., Lu, W.-Y., Li, X., 2009. Nanoscale structural and mechanical characterization of the cell wall of bamboo fibers. Materials Science and Engineering: C, 29, 1375-1379.

CHAPTER 4. EFFECT OF LOAD FUNCTION ON THE NANOINDENTATION MEASUREMENT OF WOOD CELL WALL

4.1 Abstract

Nanoindentation, also well known as depth-sensing indentation, is a technique to measure the Young's modulus and the hardness of metals, polymers, and biomaterials. Nanoindentation improves the ability to evaluate a material on a small scale because of the small probe size. The indentation procedure involves an application to monitor and analyze the load-displacement behavior of a material. When a controlled load is applied to the sample surface by an indentation tip of small size, a displacement occurs inside the material. It can be anticipated that the maximum force, the loading time, and other different load behaviors will result in the measurement of a variety of mechanical properties

Thus, this portion of the thesis considers the effect of load function on nanoindentation measurement in biomaterials such as wood. A series of load functions were run to investigate the response of Southern yellow pine (Pinus spp) by varying loading rates, holding times, and unloading rates. Displacement rate was used to observe and estimate the load-displacement relationship and the creep effect during the indentation procedure. Size and edge effects, which are considered important factors affecting the precision of final data, were also examined.

A very low loading rate was tested first and found to result in primary creep in the holding segment of the sample of wood material. This contributed to a larger contact depth and a lower hardness measurement. However, a fast loading rate made the tip over-extend into the material's surface, generating a huge impact force and decreased hardness values. Second, increasing the holding time made the creep more concentrated in the

holding segment but decreased both the Young's modulus and hardness. Third, there was no significant difference in Young's modulus and hardness among the three loading functions with different unloading rates. The size effect of yellow pine was not significant under low peak load, while edge effect is the main contribution at high peak load, such as 450 μN and 600 μN.

4.2 Introduction

Nanoindentation experiments performed on wood material are more complicated than with other materials because of its viscoelastic properties. Wood belongs to polymer and its mechanical properties of cell wall expect more detailed exploration regarding the different load function setups. Besides, the load function varies with different indentation equipment and systems. For some research and experiments using the Nano Indenter II (MTS Systems Corp. Oak Ridge, TN), the load function usually included four parts: a fast approach procedure at a rate of 10 nm s-1, a loading procedure at a constant strain rate until the designated indentation depth reach, a holding segment for the purpose of eliminating the creep effect on viscoelastic material, and finally, an unloading part at a constant displacement rate to remove 90% of the maximum load (Xing et al., 2009). Others have used the continuous stiffness measurement (CSM) to test, which involves cycles of indentation, each of which consists of incremental loading and partial unloading. The CSM method was performed at constant displacement rate to drive the tip reach to a penetration depth and then the peak load was held for a certain number of seconds. Unloading was then performed at constant rate until 90% of the load was removed (Tze et al., 2007). For experiments under the Triboindentor (Hysitron, Inc.,

Minneapolis, MN), some of the studies were done under a load function which consists of a 5-s loading segment followed by 5-s holding at maximum load and 5-s unloading (Jakes et al., 2007). A multiload indents method has also been employed in wood material research. It consists of 1s loading segments ,15s holding at partial loads, 5s unloading segments and 5s holds at the partial unloads (Jakes et al., 2008). Figure 4.1 illustrates a typical load-displacement curve for multiload indents.

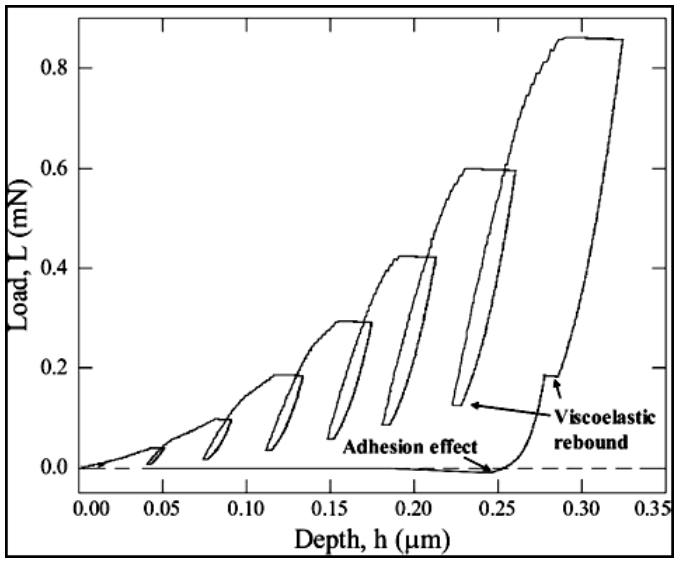

Figure 4.1 Typical load–displacement curves for multiload indents

Several loading segments with different percentages of the final maximum load were loaded on the sample. The final partial unload was held for 60s to calculated thermal drift. Last was the complete unloading. Many studies on polymer material have suggested that a certain holding time is necessary because this segment will help to avoid a “nose” shape appearing in the unloading curve due to the viscoelastic properties of the polymer material. This will lead to an overestimation of Young’s modulus and sometimes even a negative value (Ngan and Tang, 2002).It has been found that the indentation load-displacement curve is highly dependent on the loading rate (Oyen and Cook, 2003).The loading methods vary among different research groups with different loading rates, holding times, unloading rates and even peak loads. Will the load function affect final data? Why and how do different researchers choose the load function values? What is the effect of the loading rate, the holding time and the unloading rate on the Young’s modulus and hardness measurement due to the response of different materials? In this chapter, research will focus on the effect of the loading rate, the holding time, and the unloading rate on the nanoindentation measurement of the wood cell wall; we will see whether there is any size effect or edge effect during the experiment.

4.3 Materials and Methods

4.3.1 Materials

For the load function experiment, Southern yellow pine (Pinus spp) was chosen for all experiments in this chapter. For the experiments investigating the size and edge effects, loblolly pine (Pinus taedaL.) was used. A loblolly pine disk was cut 0.3m above the ground. The 32nd annual ring was cut to a block of dimensions 8mm x 8mm x

15mmm in radial, tangential, and longitudinal directions, respectively. The sample we used was the same as in Tze's research (Tze et al., 2007). A latewood portion of the 32nd annual ring with a microfibril angle value of 31° was chosen and cut down to a small block of 1mm x 1mm x 5mm in three dimensions. The 35th annual ring of Southern yellow pine, obtained from Georgia, was chosen, with the latewood located in the apex of the block. The microfibril angle value was 15°.

Nanoindentation tests were performed under the Triboindentor in conjunction with scanning probe microscopy at a room temperature of 20℃ and a relative humidity of 25±4%. All the samples were put into the Triboindentor's chamber at least 24 hours before the indentations were performed. This procedure is critical because thermal expansion or contraction of the sample during the indentation test will significantly affect the accuracy of the final results (Fischer-Cripps, 2004).

4.3.2 Specimen preparation

4.3.2.1 Yellow pine small wood blocks without resin penetration

A novel method for sample preparation-most suitable for wood chips or single fiber without resin diffusion-was developed in the course of this study. Yellow pine was embedded without resin penetration. For more detailed information, see the sample preparation procedure described in Chapter 3. Figure 4.2 gives a clear view of the polarized light microscopy (PLM) image for yellow pine prepared using pre-sealed thin film. With this preparation method, no epoxy resin penetrates into the cell wall or lumen; the sample surface is flattened first with a glass knife and then smoothed with a diamond knife.

Figure 4.2 Polarized light microscopy (PLM) image of yellow pine's cell wall

4.3.2.1 Loblolly pine small wood blocks embedded into epoxy resin

The embedding procedure for loblolly pine into epoxy resin is the same as used in Chapter three. Thus sample could be prepared by referring to the procedure used in Chapter three.

4.3.3 Nanoindentation

A three-side pyramidal Berkovich diamond indenter with an area-to-depth function was used for all experiments (Oliver and Pharr, 1992). All experiments were conducted with a closed loop feedback control aimed at providing precise control of the nanoindentation probe in load-controlled modes. A drift monitor time of 40s was set up for measuring the drift of the system before any test. The test methodology follows ISO145777 standards. The calculation and theoretical basis of TriboIndenter system from

Hysitron conformed to the most common method, Oliver and Pharr's method, which refines the Doerner and Nix model to account for a nonlinear unloading curve in the calculation of contact stiffness. All of the calculation equations are presented in Chapter 3.

4.3.4 Load function of nanoindentation

The indentation procedure consisted of three parts: loading, holding and unloading respectively. To explore the effect of the loading rate on the nanoindentation measurement of wood cell wall, with the same peak load, three loading times were employed to generate different loading rates ranging from 2 mN/s(t=0.1s) to 0.004 mN/s (t=50s). Load functions are shown in Figures 4.3, 4.4 and 4.5.

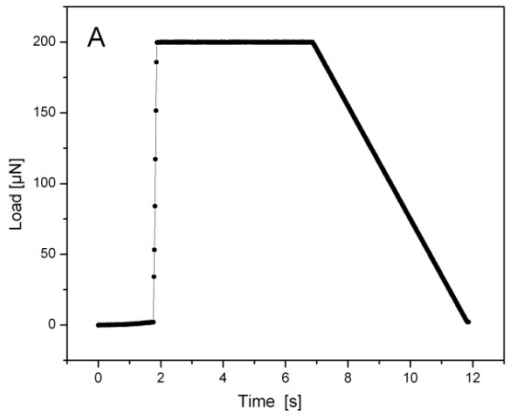

Figure 4.3 Indentation load versus time curve for 0.1s loading time

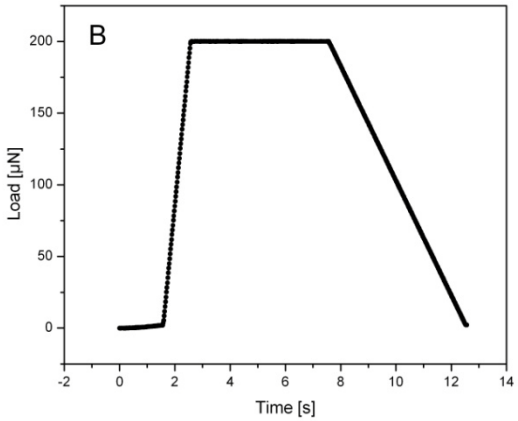

Figure 4.4 Indentation load versus time curve for 1s loading time

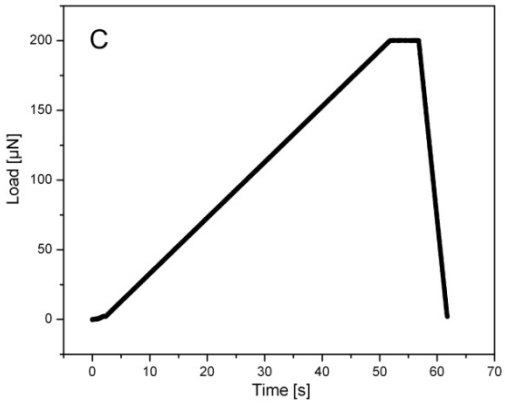

Figure 4.5 Indentation load versus time curve for 50s loading time

Similarly, load functions for the detection of creep effect by performing different holding times were set up. They involved a 0.1-s holding time, a 1-s holding time and a 50-s holding time. Load vs time curves in Figure 4.6 to 4.8 clearly show the relationship between time and load.

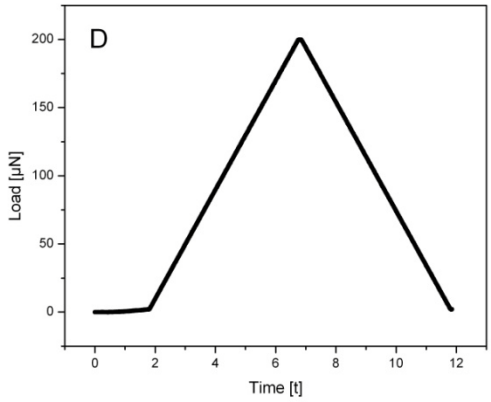

Figure 4.6 Indentation load vs time curve for 0.1s holding time

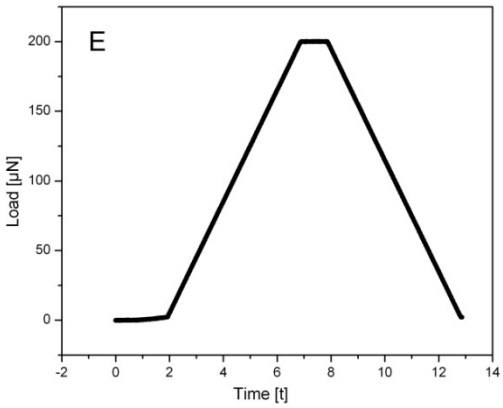

Figure 4.7 Indentation load vs time curve for 1s holding time

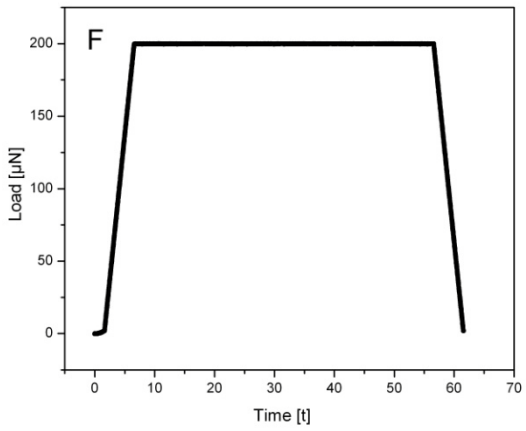

Figure 4.8 Indentation load vs time curve for 50s holding time

In order to investigate the effect of the unloading rate on the Young's modulus and hardness for yellow pine cell wall, another three load functions were set up with unloading rates ranging from 0.004mN/s to 1mN/s. Figures 4.9 to 4.11 illustrate the whole indentation procedure. The amount of data obtained in a short time was not worthy. Because of the feedback control model employed in all the experiments, data were acquired at a rate of 60 points per second. However, for shorter-time indents, the maximum number of data points will be limited. As a reference, Figure 4.12 is the normal load function commonly used for single indents.

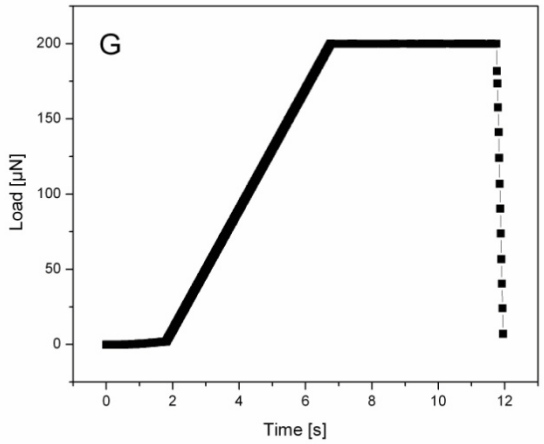

Figure 4.9 Indentation load vs time curve for 0.2s unloading time

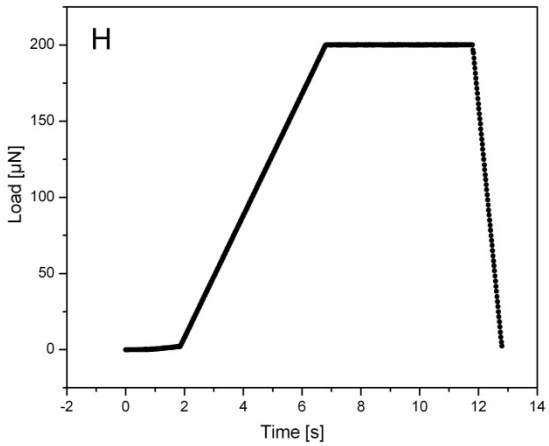

Figure 4.10 Indentation load vs time curve for 1s unloading time

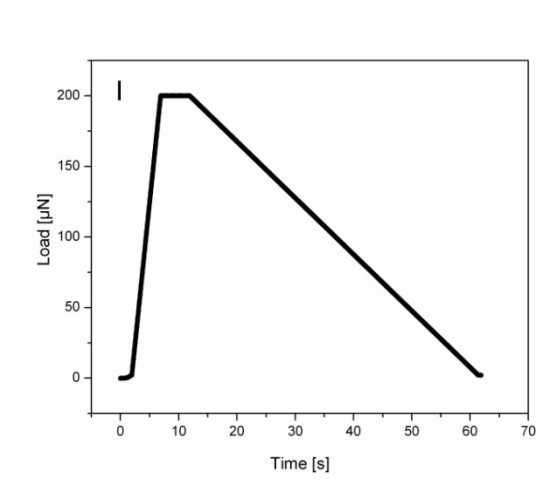

Figure 4.11 Indentation load vs time curve for 50s unloading time

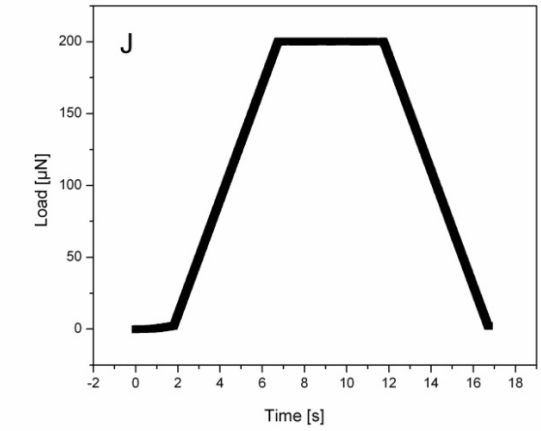

Figure 4.12 Indentation load vs time curve for 5s loading, 5s holding and 5s unloading

In the experiment to investigate the size effect and edge effect on wood material, a series of indentations at varying peak loads was placed on the tracheid. The load was first raised to 150 μN in 5s with a 5-s static hold period at this peak load, and then it was unloaded at the same rate as the loading had been. All other indentations followed the load function as described above except for the different peak loads. All the indents were all maintained in the middle of the S_2 layer, which was keep the same distance from the edge of the lumen.

4.4 Results and Discussion

4.4.1 Effect of loading rate on the Young's modulus and hardness from nanoindentation

The indentation responses of the yellow pine were investigated as a function of the loading rate. Nanoindentations performed on yellow pine cell wall generated three different loading rates (2, 0.2, and 0.004 mN/s), corresponding to the loading segment rise times of 0.1s, 1s and 50s, as shown in Figure 4.13. The load-displacement curves show markedly different shapes, with essentially, greater peak displacements for gradually slower loading rates. Oyen observed distinct maximum displacement (h_{max}) values targeted at the unloading curve rather than at peak load, which shows a "nose" shape in the load-displacement curve (Oyen and Cook, 2003). Liu has summarized the total displacement h in viscoelastic material as the summation of the elastic displacement h_E, the viscous displacement h_v, and the plastic displacement h_p during loading (Liu et al., 2006). However, there is no obvious "nose" shape existing in the load displacement curve in this experiment due to the fact that the tests were all performed with a five -second

holding time, which partly eliminates the effect of creep in the viscoelastic material. Because of the relation between hardness and contact depth, $h_c = h_{\max} - \varepsilon \frac{P_{\max}}{dP / dh}$, hardness can be estimated from the equation 2-1, which means that hardness is proportional to $1/h^2$. From the plot of the load-displacement curve, load function A (0.1s-5s-5s) has the largest maximum depth ($h_{\max}$), followed by load functions B and C. Statistical analysis with a one-way ANOVA on all of the values of the Young's modulus in three different load functions was conducted, resulting in the conclusion that there is no significant difference of Young's modulus among the three different load functions (P=0.8636). However, the hardness at load function A shows a significant difference from that of load function C, which is indicated by a t value equal to 1.99, which is larger than 1.711. Based on all these preconditions, we expect the lowest hardness value to be at load function A, which has the largest maximum depth, while there will be a higher hardness value at load function C, which has the smallest maximum depth when the indentation is performed. This assumption has been verified by the statistical data analysis of the hardness, as shown in Figure 4.14. The phenomenon for curve A, which has the largest maximum depth, may be attributed to the fast loading rate. There will be an overshoot of peak load at the end of the loading procedure due to the high impact on the material's surface in such a short time. Besides, the feedback system of the test machine results in a lack of ability to gain as many data points within 0.1s. A large displacement may have already been generated due to the ram caused by the large loading rate but without the testing machine's making a record of it. All the above-mentioned could account for the large maximum depth, which leads to a low hardness

measurement. The maximum depth of curve B is smaller than that of curve C, as can be seen in Figure 4.13. To explain this, the creep rate should be taken into consideration. The difference between load function B and C is the loading time. There will be enough time for primary creep to occur during the 50-second loading procedure, resulting to a larger maximum displacement. However, those differences are not distinct and statistical analysis shows no difference of Young's modulus among the three loading rates. In summary, load function A, which has a fast loading rate, is not adequate for obtaining true and stable data.

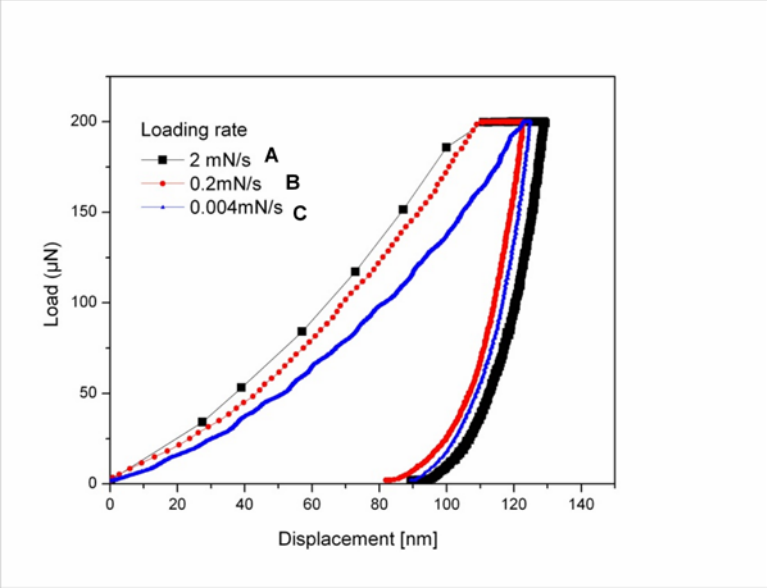

Figure 4.13 Comparison of the load-displacement curves for different loading rate under the maximum load 200 μN with holding time 5s

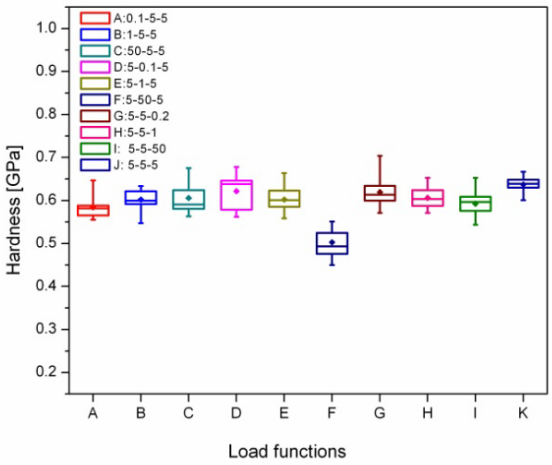

Figure 4.14 Hardness of yellow pine under different load functions

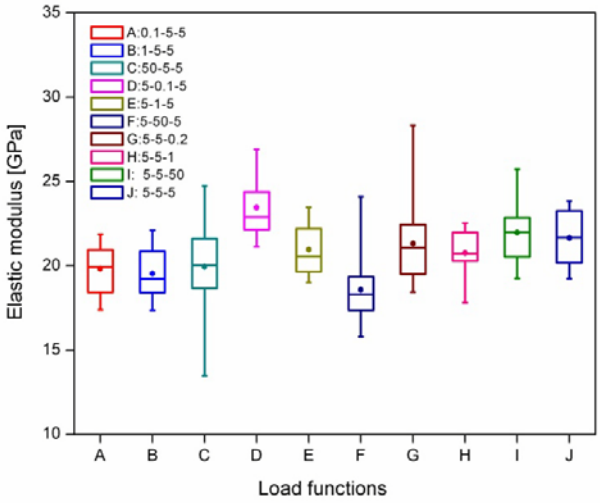

Figure 4.15 Young's modulus of yellow pine under different load functions

4.4.2 Effect of holding time on the Young's modulus and hardness in nanoindentation testing

Typical load-displacement curves obtained from nanoindentation creep test on yellow pine latewood cell wall is shown in Figure 4.16. The loading sections of three load-displacements show a very good overlap, which indicates a similar response of yellow pine under constant loading rate. The indentation displacement increases during the load holding segment. Moreover, displacement increases as the holding time is increased. A total displacement of 145nm is generated after 50s holding time. This result indicates that at room temperature, the creep effect on southern yellow pine cell wall is appreciable. Creep phenomenon observed in Figure 4.17 will lead to a significant decrease of both Young's modulus and hardness, according to Oliver and Pharr's equation. For the curve showing load function D, a "nose" segment in the unloading curve is expected, with a large contact stiffness, 15.7 μN /nm, which leads to an overestimate of the elastic modulus. In contrast, a long holding time will cause a larger contact depth as well as a smaller contact stiffness (13.86 μN /nm), ending with a very low elastic modulus. The effect of holding time on the measurement of the mechanical properties of Southern Yellow Pine was studied with a one-way ANOVA; results show that the measured hardness and Young's modulus of the Southern Yellow Pine were significantly different at different holding rates (creep) ($P=0.0001$). Of all of the Young's modulus values, load function F with the 50-second holding time was the lowest.

To more completely understand the effect of the holding procedure, the displacement rate during holding was investigated. Figure 4.17 shows a comparison of

the displacement rate for different holding times under the peak load of 200 μN and it describes the creep phenomenon in the material during loading. There is only one data point shown in the displacement rate curve for 0.1s holding time. The displacement rate was around 12mN/s, which indicates that it was still in the primary creep region. Similarly, the 1s holding time caused the displacement rate to decrease dramatically from 15mN/s to 2.5mN/s. Last, the displacement rate curve for a 50-s holding time covered both the primary creep region and the steady-state creep region. It reaches to the steady state creep region after three to five second's holding time on wood material. Based on these observations, we believe that five seconds holding time is long enough to eliminate creep effects in obtaining the Young's modulus and hardness. Thus, holding time should be chosen with caution because of the different responses of different materials undergoing nanoindentation.

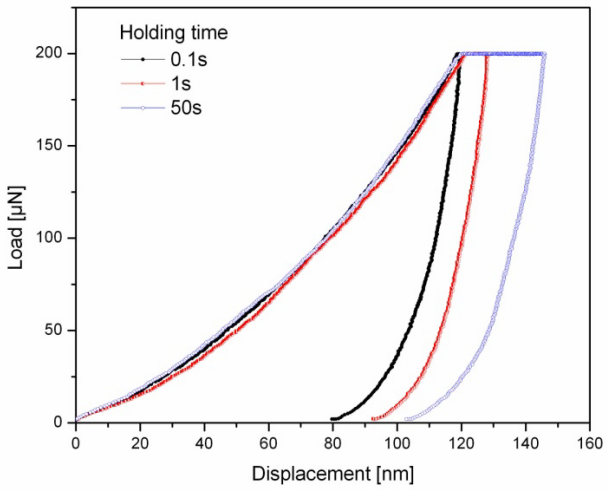

Figure 4.16 Comparison of the load-displacement curves for different holding time under the maximum load 200 μN

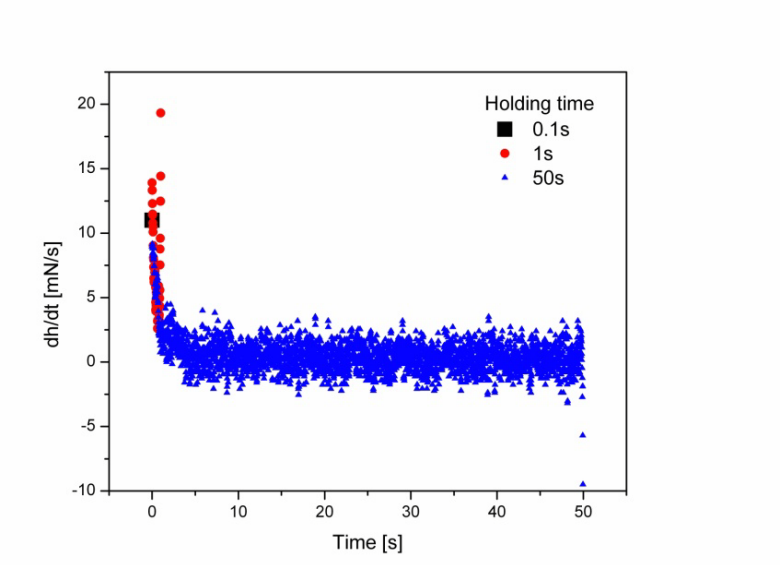

Figure 4.17 Comparison of displacement rate for different holding time under the maximum load 200 μN

4.4.3 Effect of unloading rate on the Young's modulus and hardness from nanoindentation

Figure 4.18 illustrates load-displacement curves under different unloading rates, namely 1mN/s, 0.2mN/s, and 0.004mN/s. As Oliver and Pharr mentioned in their research (Oliver and Pharr, 2004), in order to measure the hardness and Young's modulus of material from nanoindentation, there are three important quantities that must be measured from the P-h curve: elastic unloading stiffness $S = dP/dh$, contact depth, and peak load. There is a good superposition for all three curves in the loading and holding segments, indicating the same material response in this situation. The only difference among the three curves occurs in the unloading part. It can be observed that for curve J,

which possessed the lowest unloading rate, the unloading curve had the smallest final depth h_f, which means that the permanent depth of penetration after a fully unloaded was the smallest. This phenomenon also reveals that the material is subjected to both elastic and viscous recovery due to the viscoelastic properties of wood material, which leads to a smaller contact depth under a long unloading period (Hay and Pharr, 2000). Hay proposed that the Oliver and Pharr method should only be applied to a material that has purely elastic property during unloading. However, for most of the polymer materials, including wood, the indentation deformation is time-dependent. Time-dependent viscoelastic deformation will cause the indentation displacement to increase even during the unloading segment.

Thus, another important issue in the data analysis procedure is upper and lower fits. Once a load-displacement curve is generated for time-dependent material, more attention should be paid to the fitting percentage of the unloading part. The ideal fitting range should be at the very beginning of the unloading curve. However, it was always easily affected by error signals and could not be used for fitting. In order to get a relatively precise Young's modulus value, the fitting range should be chosen that best describes the fully elastic coverage during unloading. In this case, the contact stiffness was obtained from the fitting of the unloading curve in the range between 70% lower fit part and 90% upper fit part. Therefore, in this experiment, the contact stiffness obtained from the slope of 70% to 90% of the unloading curve will be the same, according to the Oliver and Pharr method. Statistical analysis performed with a one-way ANOVA on the values of Young's modulus and hardness under different load functions with the three

different unloading rates was conducted, leading to the conclusion that there is no significant difference of Young's modulus and hardness among three different load functions (Prob>F= 0.3909 for Young's modulus and Prob>F=0.1270 for hardness). This statistical result agrees with the prediction from a single indentation curve.

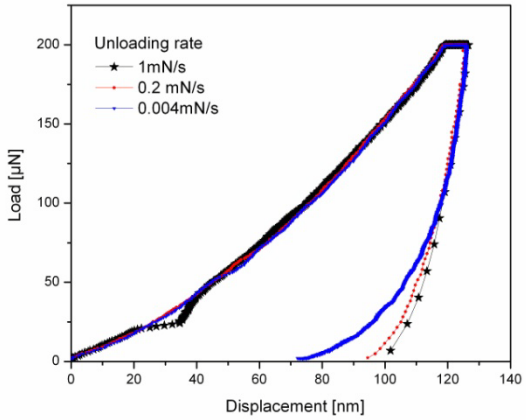

Figure 4.18 Comparison of the load-displacement curves for different unloading rate under the maximum load 200 μN with holding time 5s

4.4.4 Indentation size effect and edge effect

The nanoindentation size effect was studied by performing indentations on the wood cell wall with different peak loads. The load and displacement curves shown in Figure 4.19 were analyzed by the built-in software, which is based on Oliver and Pharr's equation. The increase of displacement during the loading parts is due to the increase of loading rate as well as the peak load.

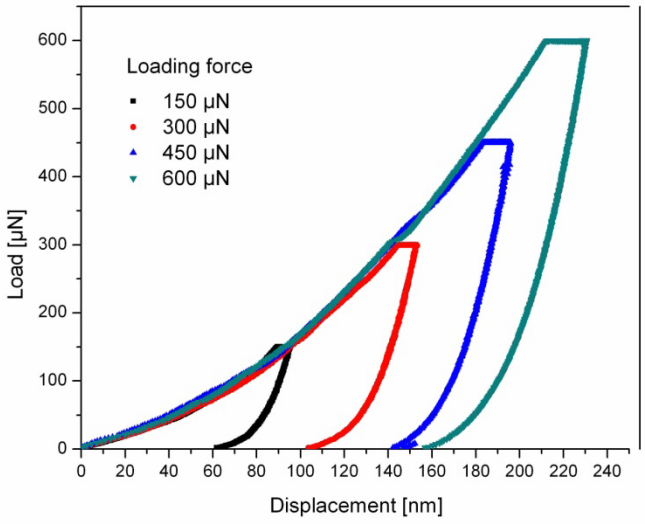

Figure 4.19 Comparison of the load-displacement curves for different load force with 5s loading time and 5s holding time

Indentation size effect has been put forward as one of the main factors affecting the test data. Particular attention was paid to the errors associated with the area function of the indenter during the indentation procedure, especially for shallow indentation. Figure 4.20 shows the relationship between maximum depth and hardness/elastic modulus. The results showed that both Young's modulus and hardness tend to decrease with an increase of the maximum depth.

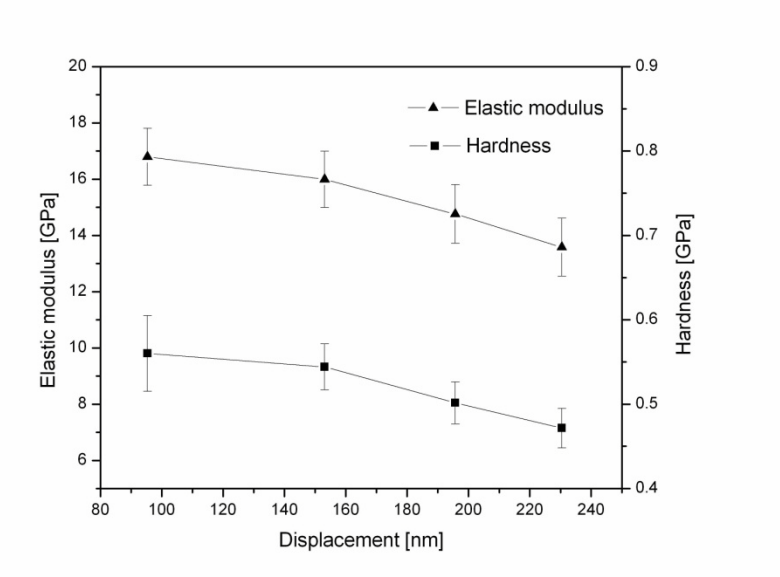

Figure 4.20 Relationships between the maximum displacement and the Young's modulus and the hardness at a loading time of 5 second with a 5-s hold period

Figure 4.21 is an AFM image revealing residual indentation marks under different peak loads ranging from 150 μN to 600 μN. The smallest residual mark observed in the image was generated under a 150 μN peak load, while the indentation marks enlarged with the increase of the peak load. The biggest residual mark was obtained at a 600 μN peak load. This observation can also be interpreted by the indentation contact area, as shown in Figure 4.22. Based on a material's response and the contact area calculation function, a larger peak load causes a greater indentation penetration depth, which leads to a larger contact area. Thus, a larger stress field beneath the indenter would be expected. However, for the shallow indentation, the machine could not easily detect sample surface, meaning that there may be a bias in the calculated area as a function of depth. Jakes et al. (Jakes et al., 2007) observed hardness and reduced modulus as calculated using area function. His research shows that both hardness and reduced modulus have higher values at low peak load compared to improved analysis by using AFM to measure the area. This was caused by the artifacts introduced by the machine calculation method. However, both hardness and reduced modulus decrease as the peak load increases at small depth and remain constant at large depth. Our research results agree with the findings of Jakes et al. (2007); i.e., an increase at low peak loads results from the artifacts due to several facility-related reasons.

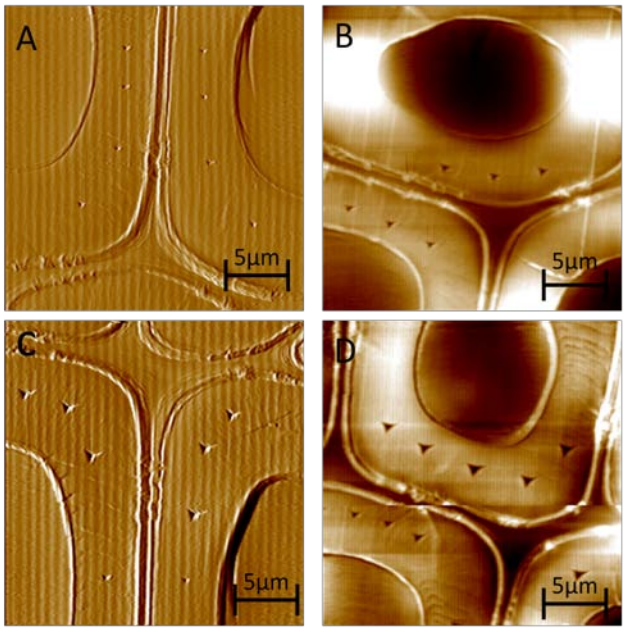

Figure 4.21 AFM pictures of residual indent mark under different loading force A: 150 µN, B: 300 µN, C: 450 µN and D: 600 µN

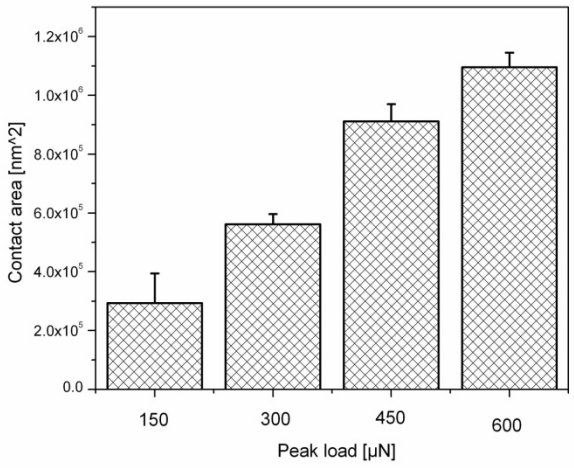

Figure 4.22Relationships between the applied load and the machine-calculated contact area

Fischer-Cripps (2004) mentioned some of the reasons that effect final values of Young's modulus and hardness, such as a) the presence of residual stresses and strain hardening arising from the specimen preparation, b) the presence of friction between the indenter and specimen, c) the errors associated with the area function of the indenter; the latter was considered to be the most common reason. The residual indentation mark was generated by the plastic deformation during nanoindentation. It is true that for pure elastic-plastic material like metals and ceramic, residual nanoindentation in these material, which are normally free from extensive cracking, change of temperature, or environmental attack, do not show any measurable relaxation over time (Lim and Chaudhri, 2001). However, there will be a distinct area recovery in viscoelastic materials like wood and polymers because of the time-dependent relaxation effect. A power-law equation can be used to explain the influence of the size effect:

$$P = \delta h^n \qquad \textbf{Equation 4-1}$$

Here, δ is a constant and n is the size-effect index (Hainsworth et al., 1996)

Theoretical calculation of factor n is expected to be close to 2 if there is no indentation size effect. Materials with size effect factors closer to 2 are least likely subject to the size effect. Hainsworth et al. listed the size-effect indices of six different materials fitted from the power-law equation, as shown in Table 4.1, and concluded that the power-law relationship holds well for a Berkovich indenter (Hainsworth et al., 1996).

Table 4.1 δ and n values obtained from power-law fits to the nanoindentation loading curve of six different materials along with the correlation coefficients

Material	δ	*n*	*R*
Copper	0.00047	1.59	0.99831
Phosphor bronze	0.00019	1.75	0.99982
Sapphire	0.00336	1.65	0.99835
Silicon	0.00040	1.85	0.99979
Soft iron	0.00093	1.57	0.99983
Steel	0.00178	1.66	0.99643

Tze et al. (2007) provided the size-effect index values of loblolly pine, which range from 1.74 to 1.86; neither Young's modulus nor hardness at 100nm penetration depth show a big difference between 200nm (over 200nm) depth, indicating that the penetration size effect is quite small for wood cell walls, considering the presence of the viscoelastic effects.

Table 4.2 Indices for indentation size effects

Peak load[μN]	δ	n	R^2
150	0.086±0.005	1.648±0.014	0.989
300	0.099± 0.002	1.607±0.008	0.999
450	0.137±0.003	1.553±0.004	0.999
600	0.078±0.008	1.665±0.004	0.998

Note: Values were averaged from 10 curves under same load function; the ± sign indicates the 95% confidence interval of the respective data sets.

The size-effect factor, n, and the constant, δ, are obtained by fitting load-displacement curves. Power-law fit to the loading curve data for yellow pine appears to show a good fit based on the correlation coefficients, which are all very close to 1.The n values we got in this experiment ranged from 1.55 to 1.66, as shown in Table 4.2, a value which is relatively lower compared to Tze's report (Tze et al., 2007). Thus, it is hard to judge the extent of the contribution of the size effect in Southern Yellow Pine, considering viscoelastic effects like creep and stress relaxation, which will cause a higher deviation of n from the ideal value of 2. Jakes et al. (2008) investigated the size effect and edge effect in tracheid wall from the perspective of the sample's structural compliance. He observed constant values of hardness calculated for a wide range of maximum loads based on the experimental design, in which all the indentations were maintained at about the same distance from the free edge. This phenomenon revealed that H is independent of load and verified that there is little indentation size effect in wood material. From the observation of the indentation hardness values at peak load of 150 μN

and 300 μN, the decrease was not severe compared to the value at peak load of 450 μN and 600 μN. This may indicate that the size effect makes little contribution under low load and edge effect, another important factor, should be taken into account to explain the decreasing trend caused by the large indent mark.

The resin embedded in the lumen, which has a Young's modulus of 4±1GPa, serves as a second material phase making an interphase with the cell wall. Figure 4.23 shows a sketch map of the elastic heterogeneities as an interface with dissimilar material. In this case, indentation located near the interface will be affected and should be taken into consideration. Jakes demonstrated that the edge problem caused by the material's inherent properties could not be ignored, especially if the specimen possesses a high degree of heterogeneity at length scales (Jakes et al., 2007).

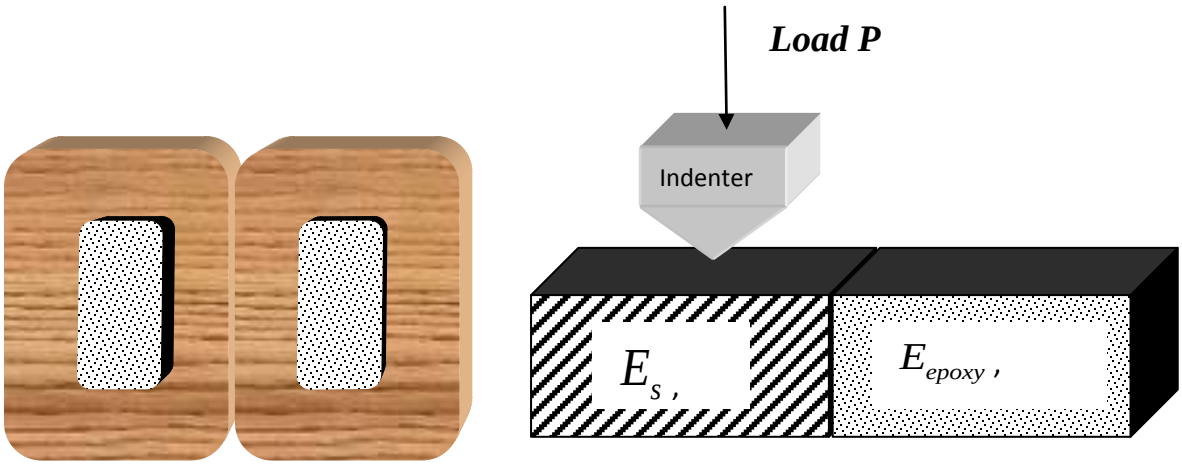

Figure 4.23 Sketch map of elastic heterogeneities as an interface with a dissimilar material like epoxy resin

To account for the decreasing trends under higher peak loads in our experiment, we referred to Jakes' results on the structural compliance effects in tracheid wall by performing an array of multiload indents up to 0.6 mN onto two adjacent tracheid walls. The sum of structural compliance and machine compliance yielded a high value, with the indents close to the empty lumen, indicating that the added structural compliance comes from the edge effects resulting from the adjacency of the lumen part. In our experiment, high peak load indents resulted in a large indent mark, which generated a big stress area. This makes it easy to cover the epoxy resin phase to decrease the final results. In addition, Lee's nanoindentation results performed on the interface between wood fiber and epoxy resin show a decrease trend when the indenter was moved from the fiber side closer to the epoxy resin side (Lee et al., 2007). His research reveals an edge effect. Thus, the edge effect proved to be a principal reason and could not be ignored during the nanoindentation test on wood material. Figure 4.24 shows a sketch image of nanoindentation's edge effect. In consequence of all the effects during the experiment, we believe that lower peak load, 150 μN in this case, is more credible and reliable for getting reasonable data, considering the cell wall's natural structure as well as the size effect and edge effect caused during the indentation procedure.

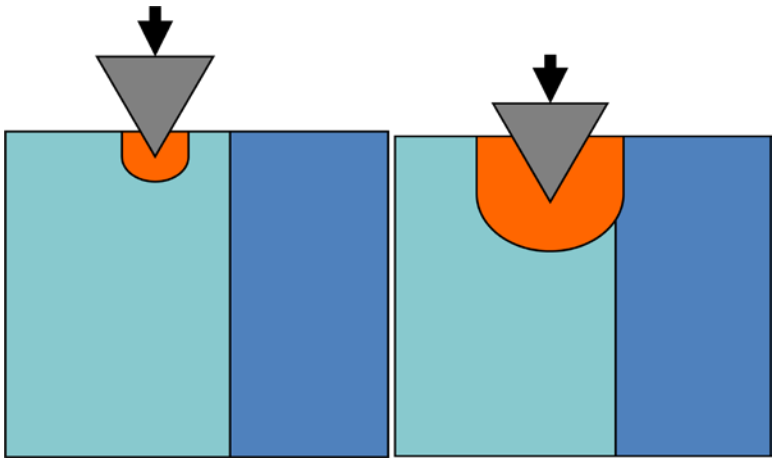

Figure 4.24 Sketch image of indentation edge effect

4.5 Conclusions

The effect of load function on the Young's modulus and hardness of wood material was explored by setting load functions with different loading rates, holding times, and unloading rates. A series of conclusions were arrived at by observing the typical load-displacement curve, analyzing the Young's modulus and hardness data, and investigating the relationship between time and displacement rate. The results showed that very low loading rates result in primary creep occurring during the holding segment and contribute to greater penetration and lower hardness. A fast loading rate causes the tip to ram into the material, generating a huge impact and decreasing hardness values. Increasing the holding time during the holding segment causes steady creep but decreases both the Young's modulus and hardness. There is no significant difference in the Young's modulus and hardness among the three loading functions with different unloading rates. The size effect of yellow pine is not significant under low peak load; however, the edge effect makes the main contribution at high peak loads such as 450 μN and 600 μN.

References

Fischer-Cripps, A.C., 2004. Nanoindentation. New York : Springer, New York.

Hainsworth, S.V., Chandler, H.W., Page, T.F., 1996. Analysis of nanoindentation load-displacement loading curves. Journal of Materials Research, 11, 1987-1995.

Hay, J.L., Pharr, G.M., 2000. Instrumented indentation testing. ASM Handbook 8, 232-243.

Jakes, J.E., Frihart, C.R., Beecher, J.F., Moon, R.J., Stone, D.S., 2008. Experimental method to account for structural compliance in nanoindentation measurements. Journal of Materials Research, 23, 1113-1127.

Jakes, J.E., Stone, D.S., Frihart, C.R., 2007. Nanoindentation size effect in wood 30th Annual Meeting of The adhesion Society, Inc. , pp. 15-17.

Lee, S.H., Wang, S., Pharr, G.M., Xu, H.T., 2007. Evaluation of interphase properties in a cellulose fiber-reinforced polypropylene composite by nanoindentation and finite element analysis. Composites Part a-Applied Science and Manufacturing, 38, 1517-1524.

Lim, Y.Y., Chaudhri, M.M., 2001. Do residual nano indentations in metals and ceramics relax with time? Journal of Physics D-Applied Physics, 34, L70-L78.

Liu, C.K., Lee, S., Sung, L.P., Nguyen, T., 2006. Load-displacement relations for nanoindentation of viscoelastic materials. Journal of Applied Physics, 100, 9.

Ngan, A.H.W., Tang, B., 2002. Viscoelastic effects during unloading in depth-sensing indentation. Journal of Materials Research, 17, 2604-2610.

Oliver, W.C., Pharr, G.M., 1992. An Improved technique for determining hardness and elastic-modulus using load and displacement sensing indentation experiments

Journal of Materials Research, 7, 1564-1583.

Oliver, W.C., Pharr, G.M., 2004. Measurement of hardness and elastic modulus by instrumented indentation: Advances in understanding and refinements to methodology. Journal of Materials Research, 19, 3-20.

Oyen, M.L., Cook, R.F., 2003. Load-displacement behavior during sharp indentation of viscous-elastic-plastic materials. Journal of Materials Research, 18, 139-150.

Tze, W.T.Y., Wang, S., Rials, T.G., Pharr, G.M., Kelley, S.S., 2007. Nanoindentation of wood cell walls: Continuous stiffness and hardness measurements. Composites Part A: Applied Science and Manufacturing, 38, 945-953.

Xing, C., Wang, S., Pharr, G., 2009. Nanoindentation of juvenile and mature loblolly pine (Pinus taeda L.) wood fibers as affected by thermomechanical refining pressure. Wood Science and Technology, 43, 615-625.

CHAPTER 5. EFFECT OF MOISTURE CONTENT ON THE MECHANICAL MEASUREMENT OF WOOD CELL WALL BY NANOINDENTATION

5.1 Abstract

Moisture content is a known factor affecting the macro-mechanical properties of wood material. In order to better understand the influence of water on the micro structure of wood cell wall, a series of nanoindentations was performed on the S2 layers of wood cell walls at varying moisture contents. Two different sample preparation methods were chosen: embedding the specimen into epoxy resin and preparing specimen without epoxy resin. Results showed a decrease of both hardness and Young's modulus for non-embedded samples under increasing moisture content. Although there was a reinforcing effect on the sample embedded in resin, results still showed that increased moisture content decreased the mechanical properties to the same extent as in the non-embedded wood cell. The moisture-content-dependent creep behavior of the wood cell wall was also investigated using Burger's model. The experimental data agree very well with Burger's model and five parameters with physical definitions were extracted from the fitting of creep curve via Burger's model. Burger's model imparts physical meaning to the constitutive wood material response in a more significant manner.

5.2 Introduction

Moisture content plays an extremely important role in the mechanical properties of wood. A wide range of studies regarding the moisture-content-related properties of wood at the macro scale is well established, and agreement has been reached regarding mechanical parameters and moisture content (Skaar, 1988). Such physical properties as elastic modulus, shrinkage, and heat conductivity are all affected by moisture content. Typically, stiffness and strength decrease with increasing moisture content. It has been

shown that moisture content also plays important roles in the bending strength and stiffness and that increased moisture content definitely decreases both properties (Arnold, 2010). To date, numerous studies have focused on the relationship between moisture content and the mechanical properties of single components in the wood cell wall from the viewpoint of the composite structure of wood cell walls. For example, Cousins conducted an measurement of the Young's and shear moduli for isolated lignin at different moisture contents and found that both Young's and shear moduli are dependent on the moisture content of lignin and that there is a linear decrease of Young's modulus and shear modulus as the moisture content of lignin increases from 3.6% to 12% (Cousins, 1976). He also investigated the effect of moisture content on the elastic modulus of hemicelluloses and proved that hemicelluloses are quite sensitive to moisture content. The same trend was observed as with lignin, that increasing the moisture content of the extracted hemicelluloses will strongly decrease the Young's modulus and shear modulus. These observations contribute to the explanation of models of the mechanical behavior of wood cell walls as a whole (Cousins, 1978). However, little research has focused on the experimental study of micro-mechanical properties of wood, primarily due to the limitations of test facilities. This chapter will investigate the effect of moisture content on the mechanical properties of wood cell wall in nano-scale.

Wood is a viscoelastic material; thus, its time-dependent properties associated with water content should be taken into account. Kojima has proposed a simulation of the creep behavior of the secondary wall as affected by the microfibril angle (MFA) and investigated the moisture content contribution to tensile creep behavior. His discussion considered the composite structure of the cell wall and concluded that tensile creep

behavior was highly dependent on both moisture content and the microfibril angle (Kojima and Yamamoto, 2004; Kojima and Yamamoto, 2005). Mukudai has proposed a viscoelastic bending model to interpret the characteristics of viscoelastic wood under moisture change cycles, based on the assumption that there is a slippage of S1 and S2 during drying (Mukudai and Yata, 1987). Padanyi conjectured that the difference between moisture accelerated creep and constant relative humidity creep reflects the amount of free volume in the fiber. In this chapter, the rheological properties of wood cell wall under different moisture contents detected by nanoindentation are presented.

5.3 Materials and Methods

5.3.1 Material and sample preparation

Loblolly pine (Pinus taeda L.) and Southern yellow pine (Pinus spp) examined in this study were obtained from southern Arkansas and Tennessee, respectively. A loblolly pine disk was cut 0.3m above the ground from a tree. The 32nd annual ring was cut into a block with radial, tangential, and longitudinal dimensions of 8mm x 8mm x 15 mm, respectively (Tze et al., 2007). The latewood portion of the 32th annual ring with a microfibril angle value of 31° was chosen and cut into a small block of 1mm x 1mm x5 mm in three dimensions. The 35th annual ring of Southern yellow pine from Georgia was picked with the latewood located in the apex of the block. The microfibril value of the Southern yellow pine was 15°. Three different specimen preparation methods were applied: embedding with epoxy resin, wood block without embedding, and wood block without resin penetration. Sample preparation methods are discussed in detail in Chapter 3.

5.3.2 Humidity generation

According to ASTM D4442, the moisture content of wood is ordinarily expressed as a percentage of the weight of the wood when oven-dry. There are four standard methods usually used for the determination of moisture content. The oven-drying method, which is most acceptable, was used in this experiment. Wood samples as mentioned above were placed in an oven heated to 101°C to 105°C and kept there until no appreciable weight change occurred in 4-h weighting intervals. The oven-dried weight was measured and the moisture content (MC) was calculated based on oven-dried weight. Two loblolly pine samples and one yellow pine sample with different preparation methods were conditioned in desiccators above desiccant glycerin solutions and immersed into water under vacuum. The specimens needed to be sealed into small desiccators to make the temperature throughout the container the same as the solution. All specimens had to be weighed immediately to the nearest 0.001 g before any re-absorption of moisture had taken place until equilibrium was reached (weight change of less than 1% from previous measurements). All glycerin solutions were maintained at a constant laboratory temperature of 23±2ºC. Table 5.2 shows the moisture content control parameters during the entire experimental procedure. The climate surrounding the sample in the Triboindentor chamber was created by desiccant and aqueous glycerin solutions according to the experimental requirements. Oven-dry weight and weight under relative humidity were used to determine the percentage of moisture content. The absolute moisture content of wood can be defined as follows:

$$W = (G_s - G_{go}) / G_{go} \times 100\% \qquad \text{Equation 5-1}$$

where G_s is the green wood's weight, and G_{go} is the weight of the oven-dry wood

Table 5.1 Summary table of parameters for moisture content control during test

Sample	Moisture content [%]	Weight before test[g]	Weight after test [g]	Relative humidity in the Chamber [%]	Test Temperature [F]
Loblolly pine wood block (A)	0	0.31613	0.31653	18	74.5
	6	0.33615	0.33658	29.9	74.5
	18	0.37652	0.37606	37	74.1
	110	0.66555	0.66385	x	74.3
Loblolly pine with epoxy treatment (B)	0	0.77050	0.77035	18	74.5
	6	0.77076	0.77076	29.4	74.2
	18	0.77261	0.77240	36	75.1
	110	x	x	x	74.2
Yellow pine without resin penetration (C)	0	0.52353	0.52358	18	74.2
	6	0.52359	0.52363	29.7	74.6
	18	0.52506	0.52457	37	74.8
	110	x	x	x	74.1

5.3.3 Nanoindentation

5.3.3.1 Measurement of wood cell wall hardness and Young's modulus by nanoindentation

A TriboIndenter® system manufactured by Hysitron, Inc. was used for all the indentation tests, and a Berkovich indenter, three-sided pyramid with an area-to-depth function was loaded for all experiments (Oliver and Pharr, 1992). All experiments were conducted with a closed-loop feedback control aimed at providing precise control of the nanoindentation probe in load-controlled modes. A drift monitor time of 40s was set up for measuring the drift of the system before any test. A single indentation procedure consisted of three parts: first, there was a 2μN set point force between the probe and sample surface. The indentation test was not started until the 2 μN pro-load force had been detected by the transducer. Second, the peak load was achieved at a loading rate of 30μm/s. Third, at this peak load, the loading was held for 5s to avoid the effect of creep

occurring in the viscous material during the unloading part (Liu et al., 2006). Finally, the unloading was executed at the same loading rate as for the loading, 5s. The scanning probe microscopy (SPM) assembly in the Triboindentor system is capable of accurately positioning the wood cell walls' S_2 layer. With a scanning size of 40µm×40µm, potential indent positions were marked on the SPM image and indents were implemented and checked by rescanning the image. Only indents in the middle of the cell wall's S_2 layer were selected as valid data. Indents performed in the embedding epoxy or at the border of cell walls were all expunged. The fluid cell tip shown in Figure 5.1, which was used for many applications that required the sample to be immersed in fluid, was chosen for the duration of the whole experiment. Its advantage is that the fluid cell probe has an extended shaft, approximately 4 mm in length, which allows the end of the probe to be completely immersed in a fluid while the probe holder and transducer remain in the air.

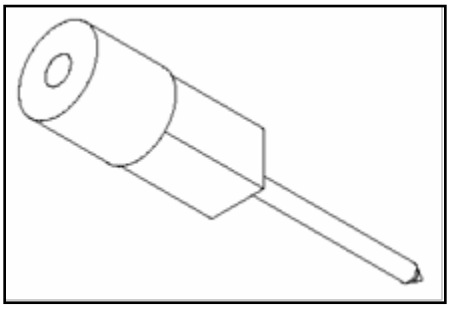

Figure 5.1 Schematic image of cell fluid tip

5.4 Rheological models

Wood material has been confirmed as being viscoelastic due to its time-dependent properties. Viscoelastic materials exhibit three behaviors: instantaneous elasticity, delayed elasticity, and viscous flow. To describe the process of creep and relaxation, several rheology theoretical models are used. Basically, a rheology model consists of a spring and a dashpot, which represent elastic and viscose properties, respectively. Maxwell and Kelvin models, made of a serial connection and parallel connection respectively, were the first models to explain the rheological properties of materials. Schiffmann summarized and compared four rheology models for nanoindentation creep and stress relaxation test to describe the rheological properties of polycarbonate (Schiffmann, 2006). The four are Burger's model, the Generalized Maxwell and Kelvin model, the Logarithmic model and the Power law model. Burger's model served as a classical rheology model which appears to be most suitable for the studies of the viscoelastic behavior of polymeric materials subjected to nanoindentation (Liu et al., 2006). Burger's model was chosen for the experimentation done in this thesis.

5.4.1 Burger's model and creep compliance

Viscoelastic materials display both viscous and elastic behavior. A viscoelastic material reacts as a spring in terms of its linear elastic properties, and when deformed will recover to its original dimensions when the stress is removed. This phenomenon is described by Hooke's Law:

$$\sigma = E \cdot \varepsilon$$ **Equation 5-2**

where E is the modulus, σ is the stress and ε is the strain. However, in the case of nanoindentation, the deformation is not a pure shear deformation but a complex superposition of compression and shear. However, the material obeys the relationship between σ and ε no matter the type of deformation.

For a creep test, the stress is held constant

$$\sigma = \sigma_0 , \quad \textbf{Equation 5-3}$$

where the creep compliance J(t) is defined by :

$$J(t) = \frac{\varepsilon(t)}{\sigma_0} \quad \textbf{Equation 5-4}$$

The load P, contact area A and indentation depth h are three important parameters in nanoindentation. The tip used in all experiments was the pyramidal indentor. (Berkovich tip) Kirsten Ingolf Schiffmann (Schiffmann, 2006) mentioned in her research that the representative stress is given by

$$\sigma = \frac{P}{A} \quad \textbf{Equation 5-5}$$

and a representative strain is defined by

$$d\varepsilon = \cot\delta \cdot \frac{dh}{h} , \quad \textbf{Equation 5-6}$$

thus, the creep compliance is given by:

$$J(t) = \frac{1}{c}\frac{A(t)}{P_0} \quad c = 2\left(1-\nu^2\right)\tan\delta \quad \textbf{Equation 5-7}$$

where ν is the Poisson ratio and δ is the half opening angle of the indentor (typically 70°in Berkovich).Load P=P (0) can be gained directly by the instrument. On the other hand, the contact area $A(t)$ has to be calculated by the area function of the tip which can be approximated by a polynomial:

$$A = C_0 h_c^2 + C_1 h_c + C_2 h_c^{1/2} + C_3 h_c^{1/4} + C_4 h_c^{1/8} + C_5 h_c^{1/16} \quad \textbf{Equation 5-8}$$

where h is the contact depth, the same as Oliver and Pharr's equation and can be related to the maximum indentation depth hmax by

$$h_c = h_{\max} - \alpha \frac{P}{S} \quad \textbf{Equation 5-9}$$

where α is the geometrical constant and S is the contact stiffness, which equals to dP/dh.

In the case of the creep test, the holding load is constant and the contact area changes with time. Thus, h_c is calculated by

$$h_c(t) = h(t) - \alpha \frac{P_0}{S_f} \quad \textbf{Equation 5-10}$$

where $h(t)$ is the actual indentation depth during the hold period

When it comes to the Burger's model, a combination of Maxwell and Kelvin's model was taken into consideration. Based on the equation that describes the stress σ and the deformation ε of viscoelastic material as mentioned above, as well as the creep compliance formula, a solution could be written for creep compliance, as follows:

$$J(t) = J_0 + J_1 \cdot t + J_2[1 - \exp(-t/\tau_0)]$$ **Equation 5-11**

where $J_0 = 1/E_e$, $J_1 = 1/\eta_1$, $J_2 = 1/E_d$ and $\tau_0 = \eta_2/E_d$ τ_0 is the retardation time which describes the retarded elastic deformation of the Kelvin model in Burger's model; this is an important parameter that reflects the viscoelastic properties of a material.

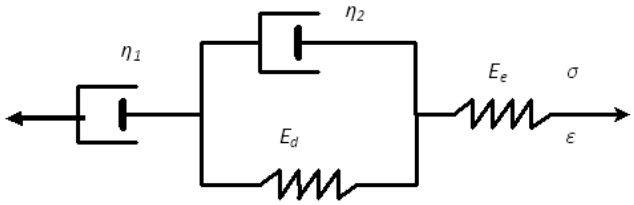

Figure 5.2 Schematic image of four-element Burgers model

5.5 Results and Discussion

The purpose of this experiment was to evaluate the effect of relative humidity treatment on the change in the cell wall structure and to correlate that effect with the change in the creep rate, elastic modulus, and hardness.

5.5.1 Cell-wall swelling

Figures 5.3 and 5.4 illustrate the interference microscope pictures taken before water absorption and after water absorption. The dimension readout function in the SPIP system makes it possible to get the profile information of the wood cell wall in three dimensions. The cursors shown in the image describe the distance between cell walls, and the values are written between the markers in the profile, as shown in Figure 5.5. The total length of a single cell was observed in both wet and air-dry conditions. An obvious dimension change (1.7143 μm) could be detected after the specimen was immersed into distilled water for 120 minutes. The overall dimension change was around 8% in width in this experiment. However, there was little dimensional change inside the cell-wall lumen. The swelling was primarily due to the dimension change of the cell wall's thickness. This is because water absorbed inside the cell wall will only come into the amorphous area of cellulose and the surface of the crystalline area. Water absorption increases the distance between molecule chains, which leads to the expansion of cellulose in the transverse direction.

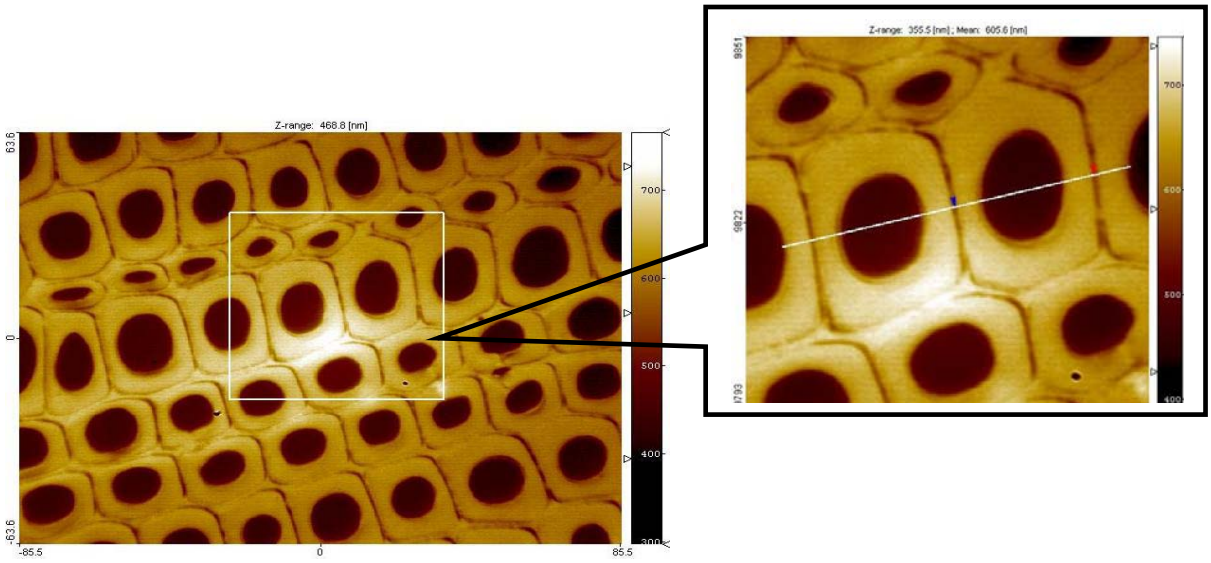

Figure 5.3 Interference microscopic picture of loblolly pine cell wall under air-dry condition

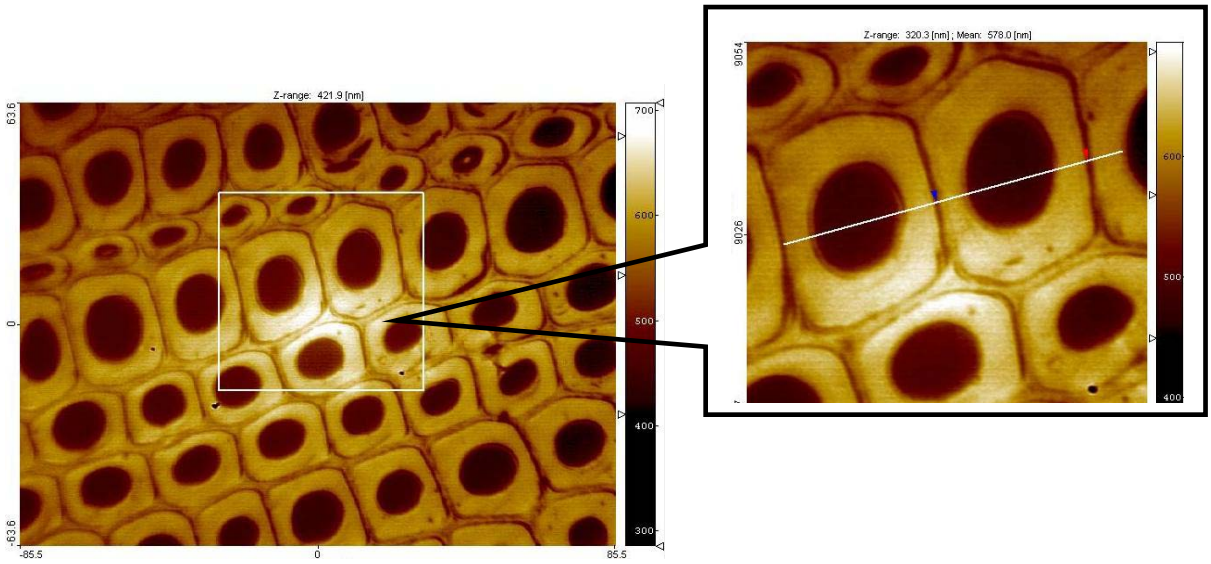

Figure 5.4 Interference microscopic picture of loblolly pine cell wall after immersed in to water for 2 hours

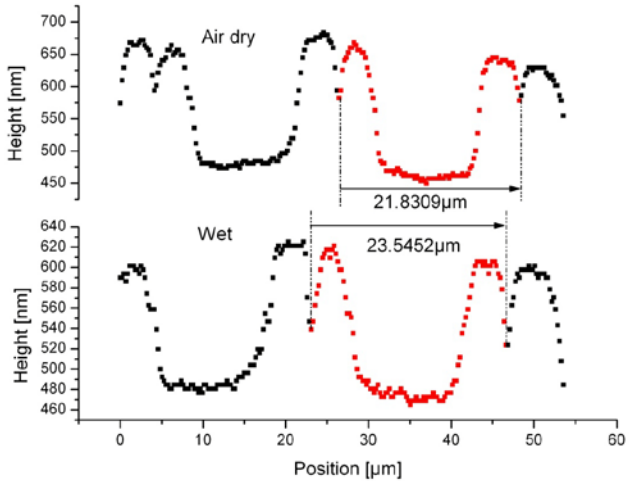

Figure 5.5 Comparison of cell wall profile before and after absorbing water

5.5.2 Effect of moisture content on Young's modulus and hardness

Figures 5.6 and 5.7 illustrate the relationship between moisture content and elastic modulus/hardness in the longitudinal direction of an unembedded wood cell wall (sample A). The trends highlighted by these two figures show that both Young's modulus and hardness tended to decrease as the moisture content increased. The percentage reduction of modulus from the oven-dried sample to the 18% moisture content sample was 32.32%. The percentage reduction of hardness from the oven-dried sample to the 18% moisture content sample was 46.93%. Those trends agree well with Kojima's results. As pointed out by previous researchers such as Kojima (Kojima and Yamamoto, 2004), the moisture-content dependent properties of wood cell wall have been verified by simulation experiments. This assumption is based on the behavior of the cell-wall structure and constituents. There is an intermediate (unstable) domain between rigid crystal and the disordered amorphous domain inside of cellulosic microfibrils. The

transition between the crystal-like and the amorphous-like state is dominated by moisture adsorption. Given this assumption, the amorphous-like domain would increase along with water absorption, resulting in a decrease of the longitudinal modulus of the wood cell wall. Moreover, Microfibrils angle has been proved to be another factor to determine the moisture dependent properties of wood cell wall, the cell wall's properties is much more dominated by micro-fibril angle because for the small microfibril angle; by contrast, it is more dominated by matrix substance when at the large microfibril angle.

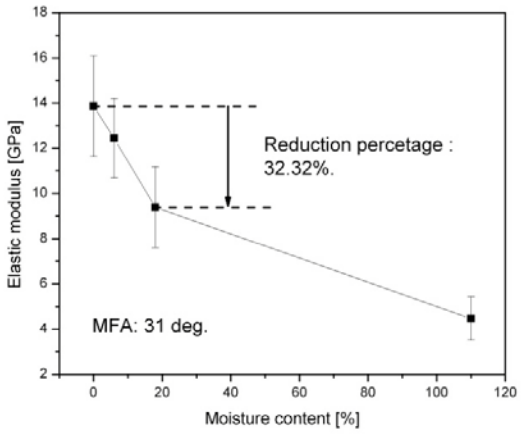

Figure 5.6 Young's modulus of cell wall without embedding under different moisture content

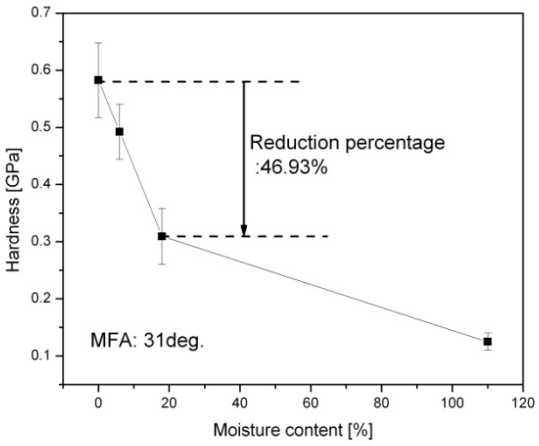

Figure 5.7 Hardness of wood cell wall without embedding under different moisture content

Figure 5.8 shows the load-displacement curves of the second layer of wood cell wall under different moisture contents. Both the maximum displacement and the residual displacement increases with the increase of moisture, which indicates that there will be a larger indentation mark on a sample with higher moisture content. As observed in the atomic force a microscope (AFM) images in Figure 5.9, there are no distinct residual mark change in the size between the oven-dried sample and the air-dried sample. However, under wet conditions, an obviously large-sized indent mark was observed (Salmen and Olsson, 1998). This softening is mainly influenced by lignin content.

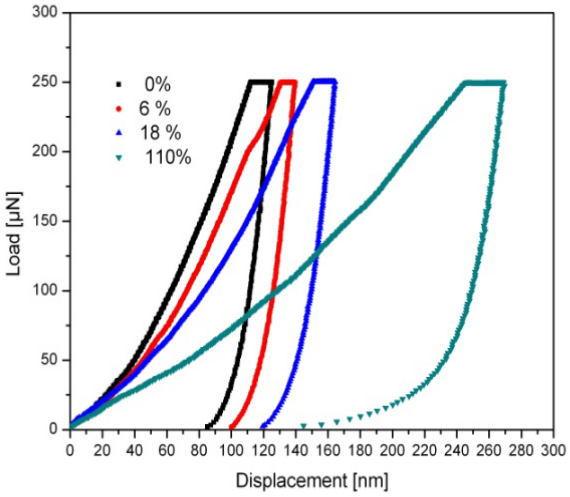

Figure 5.8 Typical indentation curves at different moisture contents with fluid cell indenter loading with a peak load of 250 µN. Five seconds holding time at maximum load for creep

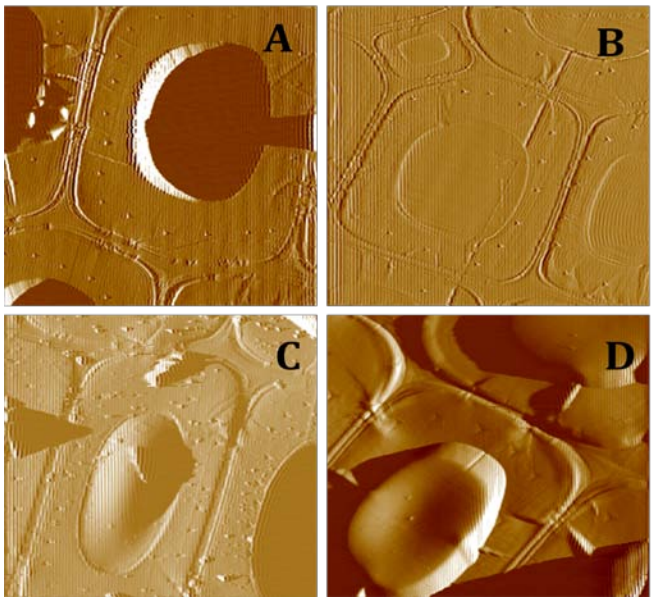

Figure 5.9 Atomic force microscope image of wood cell wall after indentation under different moisture content

The experimental results for the moisture dependency of the Young's modulus of wood cell wall treated with embedding medium are reported in Figure 5.10. The percentage reduction of the modulus from an oven-dried state to 18% moisture content is 22%. The percentage reduction of hardness from an oven-dried state to 18% moisture content state is 36.12%. Since Sample B was cut from an area adjacent to Sample A, both samples were assumed to have the same microfibril angles and chemical components. The only difference between Samples A and B was the embedding medium treatment. Both the Young's modulus and hardness values of Sample B were higher than those of sample A under the same moisture content conditions. Following previous research, referred to in Chapter 3 and conducted on the influence of embedding medium on the cell wall properties, we believe our results are due to the effect of the penetration of epoxy resin into the cell wall. Still, Sample B has the same trend observed in Sample A. The percentage of hardness reduction (Figure 5.11) which is related to the different moisture content in both samples is much higher than that of the elastic modulus. This implies that hardness is more sensitive to a change in moisture than elastic modulus. In Cousins' research (Cousins 1976; Cousins 1978), it was mentioned that the variation in the moisture content of hemicelluloses as well as that of lignin is the main reason for variation in the value of Young's modulus. Gindl et al., (2004) indicated that hardness is matrix-dominated and that MFA does not contribute to the cell wall's properties in mature wood. The results of this thesis are in agreement with previous research and the influence of moisture content on the hardness of wood cell wall.

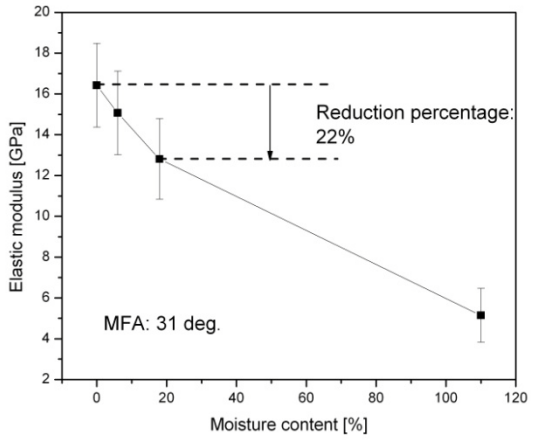

Figure 5.10 Young's modulus of embedded cell wall under different moisture content

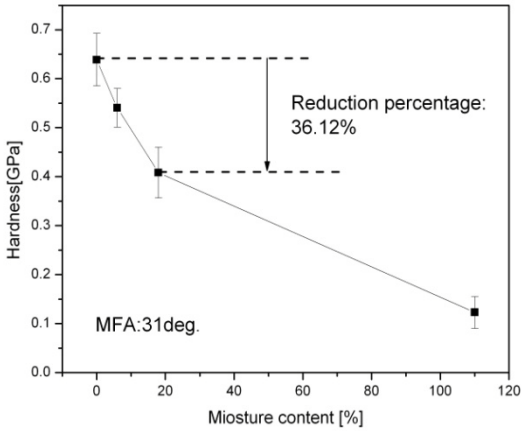

Figure 5.11 Hardness of embedded cell wall under different moisture content

Figures 5.12 and 5.13 illustrate the relationship between elastic modulus/hardness and the moisture content of wood cell wall at a small microfibril angle. Both the Young's modulus and hardness were higher than in Samples A and B even though it is without resin penetration. This is due to the contribution of the microfibril angle, the density, and the chemical components of wood cell wall. Previous research (Wu et al., 2009) (Gindl, Gupta et al. 2004) has reported on the contribution of the MFA to the Young's modulus

of wood cell wall; i.e., MFA is inversely related to elastic modulus. Research on the moisture-dependent properties of lignin and hemicelluloses has been done and has shown that these two chemical components play important roles in the response to changes in moisture content (Cousins, 1976).

According to the "interrupted lamella" model, both the elastic moduli of lignin and that of hemicelluloses will decrease with an increase in moisture content, even though hemicelluloses contribute very little to the stiffness of the matrix at high moisture contents. Meanwhile, at a high moisture content point, the cellulose fibril will decouple from the whole matrix, softening the cell wall. The percentage of reduction of the Young's modulus of Sample C decreased more notably than that of Sample A, which was also not embedded in epoxy resin. In despite of the differences in the chemical components between Sample C and Sample A, a matrix substance-dominated cell wall with a small MFA will be less sensitive to moisture content.

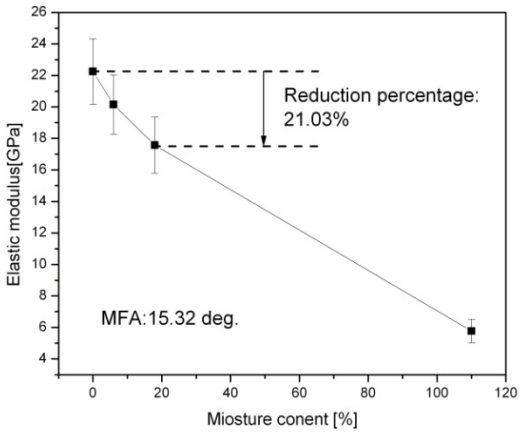

Figure 5.12 Young's modulus of wood cell wall with small MFA under different moisture content

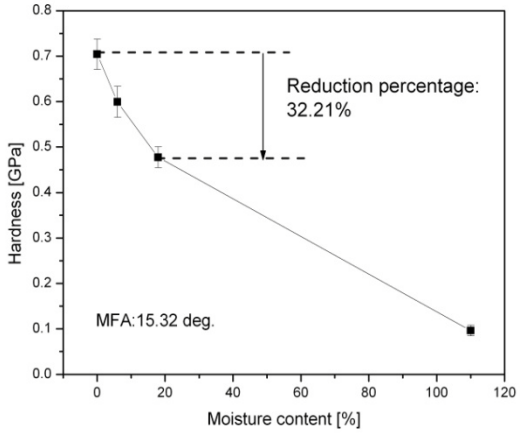

Figure 5.13 Hardness of wood cell wall with small MFA under different moisture content

5.5.3 Investigation of nanoindentation creep

Creep is the tendency of a solid material to slowly move or deform permanently under the influence of stresses. Normally, the Oliver-Pharr method is used to determine the Young's modulus and hardness; the method relies on the basic, rate-independent elastic-plastic contact and assumes the unloading curve is purely elastic. However, for polymer materials such as wood, the material's response to a rate-dependent behavior such as the contact between a tip and a semi-infinite body is viscous-elastic. The creep phenomenon will happen during the nanoindentation unloading, thus leading to an overestimation of the elastic modulus.

We introduced a 5s holding time during indentation with the purpose of eliminating a creep "nose" effect in the unloading curve. Figure 5.14 shows the relationship between displacement and time in the creep procedure under different moisture contents. Maximum displacement was obtained when the sample was fully

immersed into water. On the basis of evidence from nanoindentation data on the creep procedure of wood cell wall at different moisture contents, Figure 5.14 shows the relationship between displacement and time in the creep procedure. Since there was a 5s loading time in each experiment, the start point of displacement from the recording time was different due to the creep that occurred during the loading procedure. The displacement in the creeping period of the oven-dried cell wall was small, but it increased along with the increase in moisture content. This indicates a decrease in creep resistance with an increase in moisture content. It has been suggested that the hemicelluloses are most responsible for the time-dependent behavior wood. It has also been suggested that the distribution of hemicelluloses in typical softwood and galactoglucomannan, the main content of hemicelluloses, increases steadily from the outer parts of the cell walls in toward the lumen. There is some evidence that the addition of water influences the molecular packing in amorphous polymers for the hemicelluloses and in the amorphous areas of cellulose. Thus, water can be considered as a plasticizer that makes the cell wall softer and more ductile.

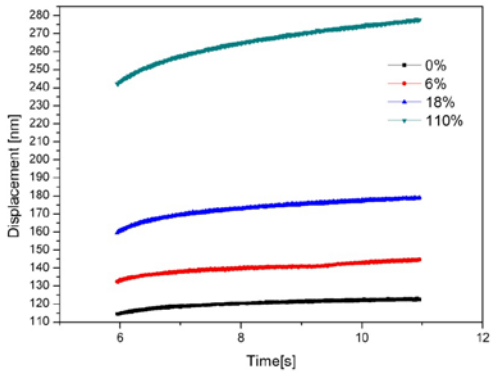

Figure 5.14 Relationship between displacement and time in the creep procedure of sample B under different moisture content

In addition to the foregoing, we focused on the relationship between moisture content in the wood cell wall and the pure creep stage which was generated by constant load. Nanoindentation creep, Ci , was defined as the change in the penetration depth divided by the constant applied load (Pmax) during the holding period (Xing et al., 2009)

$$Ci = \frac{H_2 - H_1}{P\max} \qquad \text{Equation 5-12}$$

where H_2 is the displacement at the end of creep and H_1 is the displacement at the beginning of creep

Figure 5.15 shows the relationship between the creep ratio and the moisture content of wood cell wall under three different sample preparation methods. The indentation creep ratio can be seen to have increased as the moisture content increased. The increase in the creep ratio was gradual in the three samples (wood block, embedding wood, and isolated wood) at moisture content under SFP; however, it was dramatic under wet conditions. For sample A, with a higher MFA and no embedding medium treatment, the creeping test showed the greatest increase under wet conditions. This indicates that a

cell wall with low moisture content has a better creep resistance than with high moisture content. The creep resistance of the cell wall gradually decreased as the amount of “H” bonding increased. The increase in the water content served as a plasticizer, involving a modification of the adhesion between adjacent microfibrils. The increase in the creep ratio at a high moisture content had an influence both on the hardness and the modulus, as determined from the unloading slope analysis after the hold at peak load. The increase of moisture content led to a deep penetration into the material, resulting in a large project area and a small hardness value. On the other hand, the slope of the unloading became smaller at high moisture content and led to a decrease in the elastic modulus.

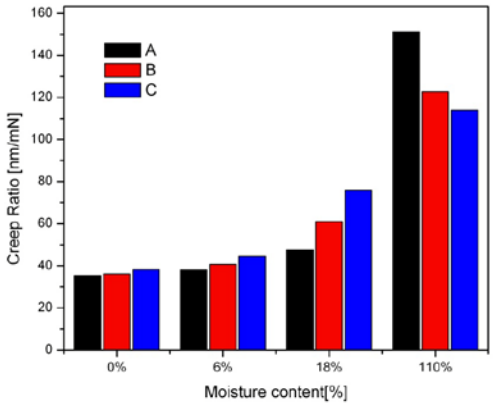

Figure 5.15 Effect of moisture content on the creep ratio of wood cell wall

5.5.4 Water absorption and its relationship with cell wall ultrastructure

Taking all possible water absorption levels into consideration and based on the chemical components existing in the S2 layers, the ability of wood to absorb water depends on the number of dissociative hydroxyl groups (Zauscher et al., 1996). In wood material, both cellulose and hemicelluloses are hydrophilic.

There are two main kinds of cross-linking between the microfibrils in a cell wall. The first is hydrogen bonding. The second is a mixture of covalent and hydrogen bonding through the ligno-hemicellulose gel. Hydrogen bonds, which in essence are interactions between molecules, exist between hydroxyl groups on adjacent microfibrils. When wood is absorbing water, it forms hydrogen bonds with other groups of atoms, which form hydroxyl groups. Such interaction accounts for wood's moisture adsorption. Lignin, hemicelluloses and crystalline cellulose surfaces make up the amorphous regions of the wood substance. According to Wangaard (1979), water is only accessible to the amorphous region, which is the reason for the limitation of mechanical properties above or at the fiber-saturation point. As the main component in the cell wall, cellulose has the water-absorption capability. Both crystalline structures and amorphous structures exist in cellulose molecules, but the amorphous cellulose absorbs water much more easily and quickly. The hydrogen bond will appear between cellulose molecules in a dry condition due to the tight structure of the crystalline area. These crystals are sometimes so tight that water cannot penetrate them. However, the hydroxyl groups in the amorphous cellulose area are responses to hygroscopicity. Dissociative hydroxyl groups in the amorphous area will attract water molecules and form the hydrogen bonds. The hygroscopic ability

depends on the amount of the amorphous area, and it will increase with the decrease of the crystalline area. Figure 5.16 shows a typical schematic diagram of a single repeated unit of cellulose molecule in a cellulose chain; there are several hydroxyl groups in the cellulose, and six of them are available for hydrogen bonding. When the cell wall absorbs water, the hydroxyl groups react with hydrogen bonds in the water. Figure 5.17 is a schematic diagram of a single repeated unit of the cellulose molecule reacting with water.

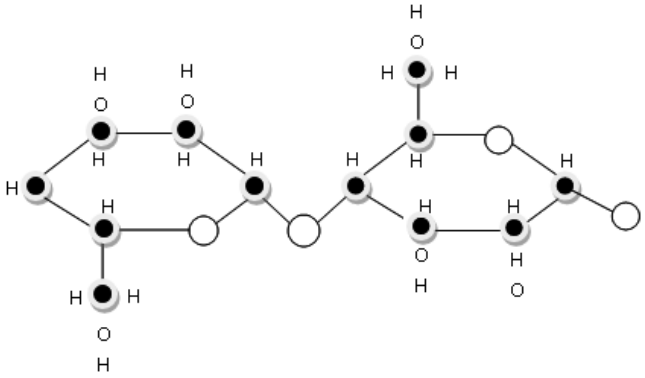

Figure 5.16 Schematic diagram of a single repeat unit of the cellulose molecule

Wood cell walls keep absorbing water when placed in a higher relative humidity environment, until reach to fiber saturation point. Water molecules, which take up the cavities of tubular cells exist as free water and does not contribute to the mechanical properties of the cell wall when above the saturation point.

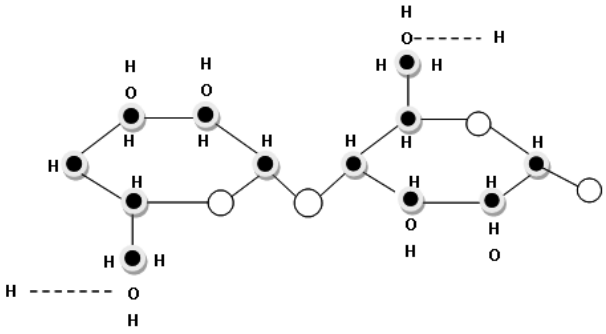

Figure 5.17 Schematic diagram of a single repeat unit of the cellulose molecule reacting with water

Similarly, hemicelluloses have the greatest ability to absorb water in the cell wall due to their structure and distribution in the natural cell wall. Hemicellulose, another important chemical component inside the S2 layer, has a random, amorphous structure with little strength. Hemicelluloses are generally found in association with cellulose in the secondary walls. They are complex, branched carbohydrate polymers formed from different monomeric sugars attached through different linkages. Substituent and noncarbodydrate components occur on hemicelluloses on either the main chain or on the carbohydrate branches. Figure 5.18 shows the schematic diagram of a single unit of the hemicellulose molecule. The potential adsorption sites are the hydroxyl groups. There are four hydroxyl groups shown in the picture, and the hydrogen bonds appear as absorbing water, as shown in Figure 5.19. Olsson (Olsson and Salm, 2004) has demonstrated that all the moisture-absorption sites (hydroxyl groups and the carboxyl groups) absorb moisture to the same relative degree, and that the rate of adsorption was the same for all these sites. Lignin has water absorption ability as well, but to a lesser degree.

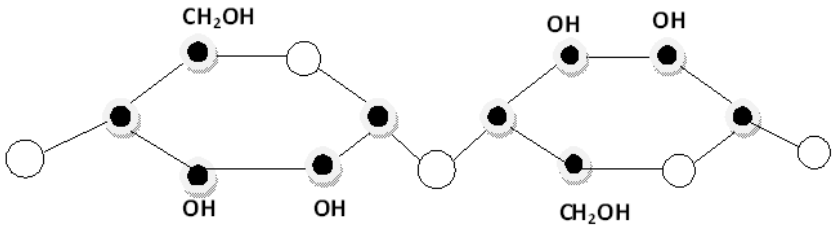

Figure 5.18 Schematic diagram of a single repeat unit of the hemicellulose molecule (galactoglucomannans)

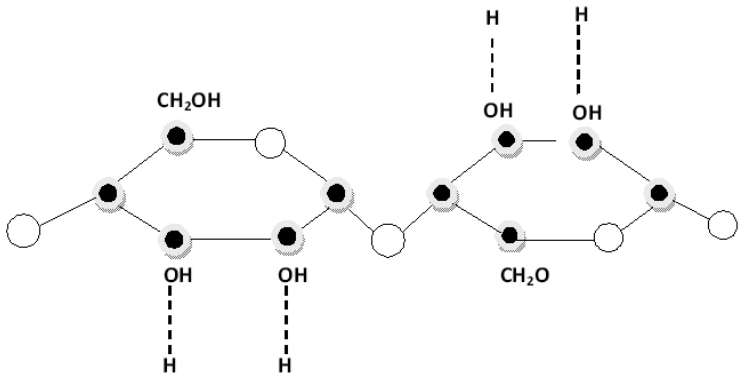

Figure 5.19 Schematic diagram of a single repeat unit of the hemicelluloses molecule (galactoglucomannans) reacting with water

5.5.5 Short-term creep of wood cell wall by nanoindentation

The creep data were modeled using the four-element Burger's model, and were found to be in excellent agreement with nanoindentation experimental creep data for holding segment. Figures 5.20 to 5.23 show the relationship between creep compliance and time. A high correlation coefficient, 0.99, was obtained. This implies that cell wall creep behavior at room temperature can be described by Burger's model and that wood cell wall is a viscoelastic material. The indentation creep procedure contains two stages: the initial stage records data from the beginning of creep to 1 s; the displacement increases rapidly with time and the creep rate decreases gradually during that period, similarly to instant creep. The second stage records data from 1s to the end of the holding period; displacement increases at a very low rate and trends toward the constant, which is the steady state region. The total deformation of the wood cell wall was separated into three parts: instantaneous elasticity, delayed elasticity, and viscous flow. Creep behavior of the wood in terms of stress and strain can be described by four parameters in Burger's

model through the observed J(t); they are Ee, Ed, η1, η2 and τ_0 representing, respectively, the modulus of elasticity, the modulus of viscoelasticity, coefficients of plasticity, viscoelasticity, and retardation time at different moisture contents. In this equation, t is the duration of the loading. Effects of moisture content on the five parameters of Burger's model were investigated. It is important to consider the value of the parameters in the simulation, which reflect intrinsic information about the composite structure of wood cell wall and its rheological properties.

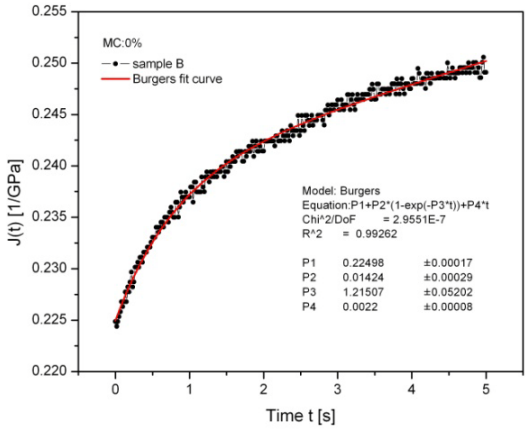

Figure 5.20 Creep Compliance J(t) of wood cell wall under oven-dry condition and Burgers model fit

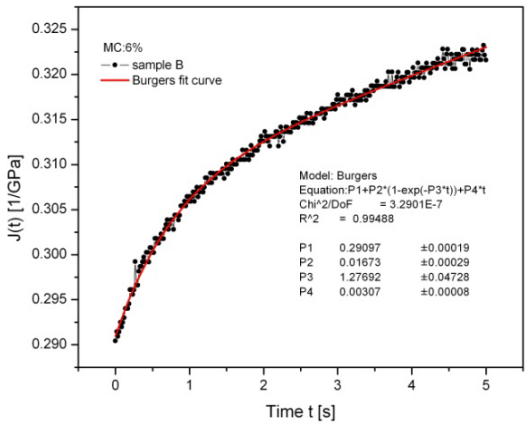

Figure 5.21 Creep Compliance J(t) of wood cell wall under air-dry condition and Burgers model fit

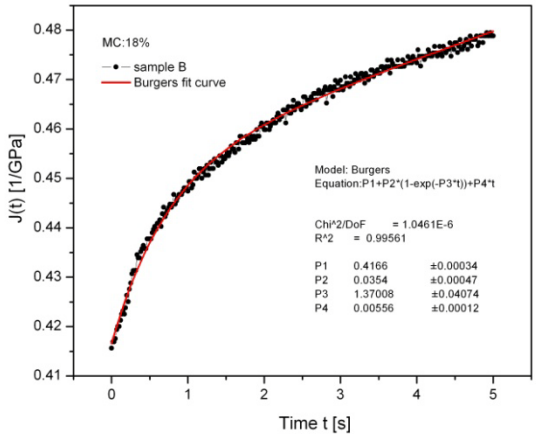

Figure 5.22 Creep Compliance J(t) of wood cell wall under 6% moisture content and Burgers model fit

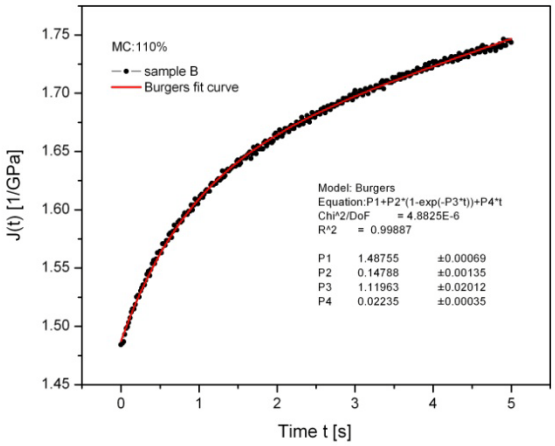

Figure 5.23 Creep Compliance J(t) of wood cell wall fully immersed into water and Burgers model fit

5.5.6 Simulated results using Burger's model

Five parameters in Burger's model were obtained by fitting the creep compliance curve during the creep procedure. Table 5.2 shows those parameters under different moisture contents. These parameters have their own physical meanings.

Table 5.2 Burgers model parameters with respect to different moisture content

Sample	*Moisture Content (%)*	E_e (Gpa)	E_d (Gpa)	η_1 (Gpa·s)	η_2 (Gpa·s)	*T ret(s)*
No.6	0	4.44	70.22	454.55	57.79	0.82
	6	3.43	59.77	325.73	46.81	0.78
	18	2.40	28.25	179.86	20.62	0.73
	110	0.67	6.76	44.74	6.04	0.89

Figure 5.24 shows the dependence of the simulated Ee on the moisture content. The trend is clear that it decreases with the increase of moisture content. This indicates that Ee, which stands for the instant elastic modulus, is highly dependent on the moisture content. As shown in Figure 5.25, the Ed, stands for the modulus of viscoelasticity, which is clearly dependent on the moisture content. By analogy, Figures 5.26 and 5.27 show the relationship between moisture content and η1, η2, which represent the coefficients of plasticity and viscoelasticity, respectively. Both η1 and η2 decrease with an increase of moisture content. The results agree very well with Kojima's research (Kojima and Yamamoto, 2005). The microfibril angle of sample B is 31. It has been suggested that creep deformation is affected by the matrix substance in the large MFA region. Kojima has verified that the longitudinal tensile creep behavior is highly dependent on both the moisture content and the MFA. However, he indicated that the reason for the moisture content's influence was not clear from the viscoelastic model. In this paper, simulation calculation on Burger's viscoelastic model by short time creep tests using nanoindentation showed the same trends as those of the tensile creep test. The only explanation for this is based on the existence and modality of the water. Bonded water as well as free water existing in the wood cell wall has been suggested to act as a

plasticizer. Bonded water will more likely to break the hydrogen bond between microfibrils, which accounts for Ee, the instant elastic modulus. The decrease of hydrogen bonds between microfibrils leads to a decrease of Ee. Besides, inter-chain distances will be increased with the addition of water, decreasing cohesion.

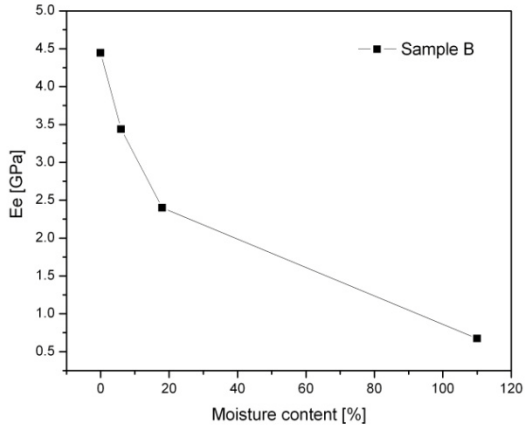

Figure 5.24 Effect of moisture content on the parameter Ee in Burger's model

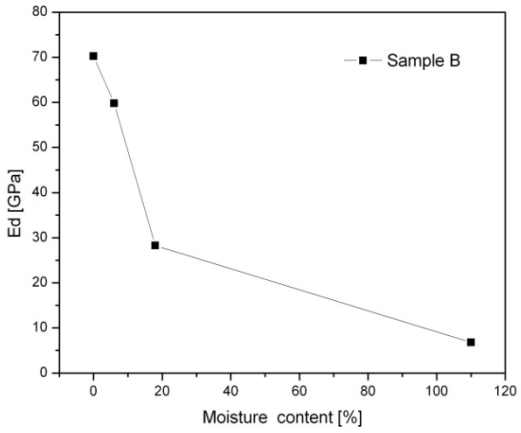

Figure 5.25 Effect of moisture content on the parameter Ed in Burger's model

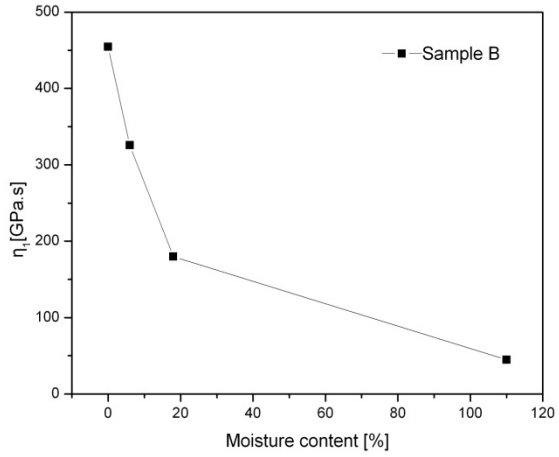

Figure 5.26 Effect of moisture content on the parameter η1 in Burger's model

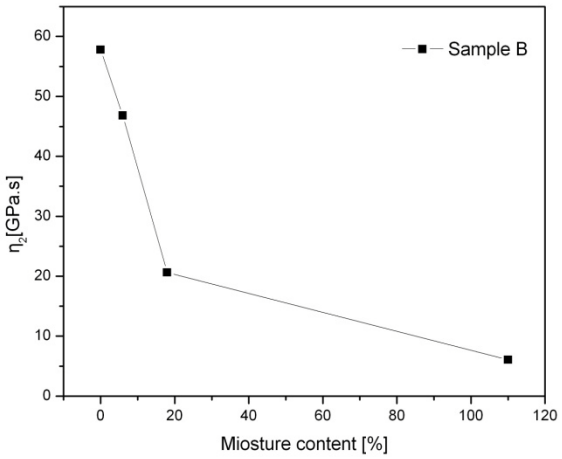

Figure 5.27 Effect of moisture content on the parameter η2 in Burger's model

Figure 5.28 shows the relationship between moisture content and retardation time. The value of retardation time is not clearly dependent on the moisture content. This is reasonable due to the way that retardation time is calculated. The value is calculated as the ratio of η2 and Ed. Both η2 and Ed have the same trend: the value increases with the

increase of moisture content. Therefore, no distinct tendency is observed as related to moisture content.

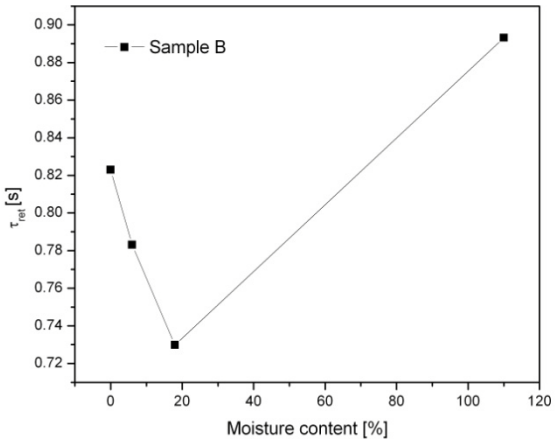

Figure 5.28 Effect of moisture content on the parameter τ_0 in Burger's model

5.6 Conclusions

This chapter focused on the mechanical properties and rheological properties of wood cell walls as influenced by moisture content. Nanoindentation was performed on cell wall under different moisture contents and results showed that both Young's modulus and hardness decrease with increase of moisture content in wood cell wall. There has been some evidence that the addition of water influences the molecular packing in amorphous polymers such as hemicelluloses and the amorphous areas of cellulose. Thus, water should be considered as a plasticizer that makes the cell wall soften and become ductile. Moreover, water inside of wood cell wall makes it easy to break the hydrogen bonds between microfibrils. Thus, the decrease of hydrogen bonds between microfibrils leads to a decrease in the cell wall's mechanical properties. Experimental data on moisture-dependent creep agree well with the simulation of Burger's model, in which five parameters are extracted to explain the rheological properties of wood cell wall. Ee, Ed, $\eta 1$ and $\eta 2$ all decrease with an increase of moisture content.

References

Arnold, M., 2010. Effect of moisture on the bending properties of thermally modified beech and spruce. Journal of Materials Science, 45, 669-680.

Barber.N.F, Meylan, B.A., 1964. The anisotropic shrinkage of wood.A theoretical model. Holzforschung, 18.

Bembey, A.K., Oyen, M.L., Bushby, A.J., Boyde, A., 2006. Viscoelastic properties of bone as a function of hydration state determined by nanoindentation. Philosophical Magazine, 86, 5691 - 5703.

Bergander, A., Salmen, L., 2002. Cell wall properties and their effects on the mechanical properties of fibers. Journal of Materials Science, 37, 151-156.

Bobji, M.S., Biswas, S.K., Pethica, J.B., 1997. Effect of roughness on the measurement of nanohardness - a computer simulation study. Applied Physics Letters, 71, 1059-1061.

Bushby, A.J., 2003. Nanoindentation of bone: Comparison of specimens tested in liquid and embedded in polymethylmethacrylate. J.Mater.Res,, 19.

Cousins, W.J., 1976. Elastic modulus of lignin as related to moisture content. Wood Science and Technology, 10, 9-17.

Cousins, W.J., 1978. Youngs modulus of hemicelluloses as related to moisture-content. Wood Science and Technology, 12, 161-167.

Dietenberger, G., Kretschmann, Hernandez, Highley, Ibach, Liu, McDonald, Miller, Moody, Rowell, Simpson, Soltis, TenWolde, Wolfe, Vick, White, Williams, Williams, Winandy, Youngquist, 1999. Wood handbook : wood as an engineering material. Madison. in: F.P.L. USDA Forest Service (Ed.).

Doerner, M.F., Nix, W.D., 1986. A method for interpreting the data from depth-sensing indentation instruments. Journal of Materials Research,, 1.

Eder, M., Jungnikl, K., Burgert, I., 2009. A close-up view of wood structure and properties across a growth ring of Norway spruce (Picea abies [L] Karst.). Trees - Structure and Function, 23, 79-84.

Eichhorn, S.J., Sirichaisit, J., Young, R.J., 2001. Deformation mechanisms in cellulose fibres, paper and wood. Journal of Materials Science, 36, 3129-3135.

Fahlen, J., Salmen, L., 2002. On the lamellar structure of the tracheid cell wall. Plant Biology, 4, 339-345.

Fengel, D., G.Wegener, 1984. Wood: chemistry,ultrastructure,reactions. Walter de Gruyter

Fischer-Cripps, A.C., 2004. Nanoindentation. New York : Springer, New York.

Franke, O., Göken, M., Hodge, A., 2008. The nanoindentation of soft tissue: Current and developing approaches. JOM Journal of the Minerals, Metals and Materials Society, 60, 49-53.

Gindl, W., Gupta, H.S., 2002. Cell-wall hardness and Young's modulus of melamine-modified spruce wood by nano-indentation. Composites Part A: Applied Science and Manufacturing, 33, 1141-1145.

Gindl, W., Gupta, H.S., Grunwald, C., 2002. Lignification of spruce tracheid secondary cell walls related to longitudinal hardness and modulus of elasticity using nano-indentation. Canadian Journal of Botany-Revue Canadienne De Botanique, 80, 1029-1033.

Gindl, W., Gupta, H.S., Schoberl, T., Lichtenegger, H.C., Fratzl, P., 2004. Mechanical properties of spruce wood cell walls by nanoindentation. Applied Physics a-Materials Science & Processing, 79, 2069-2073.

Hainsworth, S.V., Chandler, H.W., Page, T.F., 1996. Analysis of nanoindentation load-displacement loading curves. Journal of Materials Research, 11, 1987-1995.

Hay, J.L., Pharr, G.M., 2000. Instrumented indentation testing. ASM Handbook 8, 232-243.

Haygreen, J.G., Bowyer, J.L., 1996. Forest products and wood science:An introduction. Iowa State University Press, Ames,Iowa,USA.

Hepworth, D.G., Vincent, J.F.V., Jeronimidis, G., Bruce, D.M., 2000. The penetration of epoxy resin into plant fibre cell walls increases the stiffness of plant fibre composites. Composites Part A: Applied Science and Manufacturing, 31, 599-601.

Jakes, J.E., Frihart, C.R., Beecher, J.F., Moon, R.J., Stone, D.S., 2008. Experimental method to account for structural compliance in nanoindentation measurements. Journal of Materials Research, 23, 1113-1127.

Jakes, J.E., Stone, D.S., Frihart, C.R., 2007. Nanoindentation size effect in wood 30th Annual Meeting of The adhesion Society, Inc. , pp. 15-17.

Kamke, F., Lee, J., 2007. Adhesive Penetration in Wood—a Review. Wood and Fiber Science, 39, 205-220.

Kinney, J.H., Marshall, S.J., Marshall, G.W., 2003. The mechanical properties of human dentin: A critical review and re-evaluation of the dental literature. Critical Reviews in Oral Biology & Medicine, 14, 13-29.

Kojima, Y., Yamamoto, H., 2004. Properties of the cell wall constituents in relation to the longitudinal elasticity of wood - Part 2: Origin of the moisture dependency of the longitudinal elasticity of wood. Wood Science and Technology, 37, 427-434.

Kojima, Y., Yamamoto, H., 2005. Effect of moisture content on the longitudinal tensile creep behavior of wood. Journal of Wood Science, 51, 462-467.

Konnerth, J., 2009. Actual versus apparent within cell wall variability of nanoindentation results from wood cell walls related to cellulose microfibril angle. J Mater Sci, 44.

Konnerth, J., Harper, D., Lee, S.-H., Rials, T.G., Gindl, W., 2007. Adhesive penetration of wood cell walls investigated by scanning thermal microscopy (SThM). Holzforschung, 62, 91-98.

Konnerth, J., Valla, A., Gindl, W., 2007. Nanoindentation mapping of a wood-adhesive bond. Applied Physics a-Materials Science & Processing, 88, 371-375.

Koponen, S., Toratti, T., Kanerva, P., 1989. Modeling longitudinal elastic and shrinkage properties of wood

Wood Science and Technology, 23, 55-63.

Larnøy, E., Eikenes, M., Militz, H., 2010. Detection of chlorine-labelled chitosan in Scots pine by energy-dispersive X-ray spectroscopy. Wood Science and Technology.

Lee, S.H., Wang, S.Q., Pharr, G.M., Kant, M., Penumadu, D., 2007. Mechanical properties and creep behavior of lyocell fibers by nanoindentation and nano-tensile testing. Holzforschung, 61, 254-260.

Lee, S.H., Wang, S.Q., Pharr, G.M., Xu, H.T., 2007. Evaluation of interphase properties in a cellulose fiber-reinforced polypropylene composite by nanoindentation and finite element analysis. Composites Part a-Applied Science and Manufacturing, 38, 1517-1524.

Li, W.H., Shin, K., Lee, C.G., Wei, B.C., Zhang, T.H., He, Y.Z., 2008. The characterization of creep and time-dependent properties of bulk metallic glasses using nanoindentation. Materials Science and Engineering: A, 478, 371-375.

Lim, Y.Y., Chaudhri, M.M., 2001. Do residual nano indentations in metals and ceramics relax with time? Journal of Physics D-Applied Physics, 34, L70-L78.

Liu, C.K., Lee, S., Sung, L.P., Nguyen, T., 2006. Load-displacement relations for nanoindentation of viscoelastic materials. Journal of Applied Physics, 100, 9.

Ma, Z., Long, S., Pan, Y., Zhou, Y., 2008. Loading rate sensitivity of nanoindentation creep in polycrystalline Ni films. Journal of Materials Science, 43, 5952-5955.

Megraw, R.A., 1986. Wood quality factors in loblolly pine

Mittra, E., Akella, S., Qin, Y.-x., 2006. The effects of embedding material, loading rate and magnitude, and penetration depth in nanoindentation of trabecular bone. Journal of Biomedical Materials Research Part A, 79.

Mukudai, J., Yata, S., 1987. Further modeling and simulation of viscoelastic behavior (bending deflection) of wood under moisture change. Wood Science and Technology, 21, 49-63.

Nakano, T., 2003. Effects of cell structure on water sorption for wood. Holzforschung, 57, 213-218.

Nakano, T., 2008. Analysis of cell wall swelling on the basis of a cylindrical model. Holzforschung, 62, 352-356.

Nakano, T., Yamamoto, S., Norimoto, M., Nakai, T., Ishikura, Y., 2006. Effects of ultrastructure on water adsorption of bamboo. Mokuzai Gakkaishi, 52, 352-357.

Ngan, A.H.W., Tang, B., 2002. Viscoelastic effects during unloading in depth-sensing indentation. Journal of Materials Research, 17, 2604-2610.

Olesiak, S., Oyen, M., Ferguson, V., 2010. Viscous-elastic-plastic behavior of bone using Berkovich nanoindentation. Mechanics of Time-Dependent Materials, 14, 111-124.

Oliver, W.C., Pharr, G.M., 1992. An Improved technique for determining hardness and elastic-modulus using load and displacement sensing indentation experiments

Journal of Materials Research, 7, 1564-1583.

Oliver, W.C., Pharr, G.M., 2004. Measurement of hardness and elastic modulus by instrumented indentation: Advances in understanding and refinements to methodology. Journal of Materials Research, 19, 3-20.

Olsson, A.-M., Salm, L., 2004. The association of water to cellulose and hemicellulose in paper examined by FTIR spectroscopy. Carbohydrate Research, 339, 813-818.

Oyen, M.L., Cook, R.F., 2003. Load-displacement behavior during sharp indentation of viscous-elastic-plastic materials. Journal of Materials Research, 18, 139-150.

Qing, H., Mishnaevsky, L., 2009. Moisture-related mechanical properties of softwood: 3D micromechanical modeling. Computational Materials Science, 46, 310-320.

Salmen, L., Burgert, I., 2009. Cell wall features with regard to mechanical performance. A review COST Action E35 2004-2008: Wood machining - micromechanics and fracture. Holzforschung, 63, 121-129.

Salmen, L., Olsson, A.M., 1998. Interaction between hemicelluloses, lignin and cellulose: Structure-property relationships. Journal of Pulp and Paper Science, 24, 99-103.

Scallan, A.M., Tigerstrom, A.C., 1992. Swelling and elasticity of the cell-walls of pulp fibers

Journal of Pulp and Paper Science, 18, J188-J193.

Schiffmann, K.I., 2006. Nanoindentation creep and stress relaxation tests of polycarbonate: Analysis of viscoelastic properties by different rheological models. International Journal of Materials Research, 97, 1199-1211.

Skaar, C., 1988. Wood-water relations

Spurr, A.R., 1969. A low-viscosity epoxy resin embedding medium for electron microscopy. Journal of Ultrastructure Research, 26, 31-43.

Tze, W.T.Y., Wang, S., Rials, T.G., Pharr, G.M., Kelley, S.S., 2007. Nanoindentation of wood cell walls: Continuous stiffness and hardness measurements. Composites Part A: Applied Science and Manufacturing, 38, 945-953.

Wangaard, F.F., 1979. Wood: its structure and properties. Journal of Educational Modules for Materials Science and Engineerin 1.

Wimmer, R., Lucas, B.N., Oliver, W.C., Tsui, T.Y., 1997. Longitudinal hardness and Young's modulus of spruce tracheid secondary walls using nanoindentation technique. Wood Science and Technology, 31, 131-141.

Wu, Y., Wang, S., Zhou, D., Xing, C., Zhang, Y., 2009. Use of nanoindentation and silviscan to determine the mechanical properties of 10 hardwood species

Wood and Fiber Science, 41, 64-73.

Wu, Y., Wang, S., Zhou, D., Xing, C., Zhang, Y., Cai, Z., 2010. Evaluation of elastic modulus and hardness of crop stalks cell walls by nano-indentation. Bioresource Technology, 101, 2867-2871.

Xie, Z.H., Swain, M.V., Swadener, G., Munroe, P., Hoffman, M., 2009. Effect of microstructure upon elastic behaviour of human tooth enamel. Journal of Biomechanics, 42, 1075-1080.

Xing, C., Riedl, B., Cloutier, A., Shaler, S., 2005. Characterization of urea–formaldehyde resin penetration into medium density fiberboard fibers. Wood Science and Technology, 39, 374-384.

Xing, C., Wang, S., Pharr, G., 2009. Nanoindentation of juvenile and mature loblolly pine (Pinus taeda L.) wood fibers as affected by thermomechanical refining pressure. Wood Science and Technology, 43, 615-625.

Yamamoto, H., Kojima, Y., 2002. Properties of cell wall constituents in relation to longitudinal elasticity of wood. Wood Science and Technology, 36, 55-74.

Yu, Y., Fei, B., Zhang, B., Yu, X., 2007. Cell-wall mechanical properties of bamboo investigated by in-situ imaging nanoindentation. Wood and Fiber Science, 39, 527-535.

Zauscher, S., Caulfield, D.F., Nissan, A.H., 1996. The influence of water on the elastic modulus of paper .1. Extension of the H-bond theory. Tappi Journal, 79, 178-182.

Zou, L., Jin, H., Lu, W.-Y., Li, X., 2009. Nanoscale structural and mechanical characterization of the cell wall of bamboo fibers. Materials Science and Engineering: C, 29, 1375-1379.

CHAPTER 6. CONCLUSIONS AND FUTURE WORKS

6.1 Conclusions

6.1.1 Effect of epoxy embedding medium on the measurement of mechanical properties of lignocellulosic materials

Nanoindentation has proved itself to be a valuable tool for characterizing the mechanical properties of wood cell wall in recent years. However, this technique is still not been fully matured due to facility and wood sample preparation limitations. Many efforts have been made to improve the estimation of wood cell wall properties by nanoindentation. A better understanding of the effect of the role of the embedding medium is crucial for insight into the interaction between epoxy resin and cell wall structure. A series of contrast experiments was made to verify that embedding medium enhances both the Young's modulus and the hardness of the wood cell wall. Typically, the modulus of loblolly pine embedded in epoxy resin increased by 14% and the hardness by 32% compared to unembedded wood cell, at a confidence level of 95%. Similarly, there was a 15.5% increase for the Young's modulus and 11.3% for the hardness of red oak at the confidence level of 95%. Moreover, vacuum time affects neither reduced modulus nor the hardness of wood cell wall, which indicates that resin penetration is a fast procedure and occurs through several avenues, including pits, lumen, and nano-penetration. Finally, a new embedding method was developed to prevent resin from penetrating into wood cell wall. This method is reasonable for small specimens, such as a single fiber, wood chip, wood remains, and so forth.

6.1.2 Effect of load function on the nanoindentation measurement of wood cell wall

Effect of load function on the Young's modulus and hardness of wood material is explored by setting load functions with different loading rates, holding time and unloading rates. A series of conclusions were achieved by observing the typical load-displacement curve, analyzing the Young's modulus and hardness data and investigating the relationship between time and displacement rate. Results show that: 1) Very low loading rates result in primary creep occurring during holding segment and contribute to greater penetration and lower hardness. A fast loading rate causes the tip to ram into material, which generates a huge impact and decreases hardness values. 2) Increasing the holding time during the holding segment leads to steady creep but decreases both the Young's modulus and hardness. 3) There is no significant difference in the Young's modulus and hardness among the three loading functions with different unloading rates. 4) The size effect is not significant under small peak loads for yellow pine; however, edge effect makes the main contribution at high peak loads, such as 450 μN and 600 μN.

6.1.3 Effect of moisture content on the mechanical measurement of wood cell wall by nanoindentation

Mechanical properties and rheology properties of wood cell walls as influenced by moisture content were studied. Nanoindentation was performed on cell wall under different moisture contents and results showed that both Young's modulus and hardness decrease with increase of moisture content in wood cell wall. There has been some evidence that the addition of water influences the molecular packing in amorphous polymer such as hemicelluloses and amorphous area of cellulose. Thus, water will be considered as a plasticizer, which makes the cell wall soften and ductile. Moreover, water inside of wood cell wall makes it easy to break the hydrogen bonds between microfibrils.

Therefore, the decrease of hydrogen bond between microfibrils leads to a decrease in the cell wall's mechanical properties. Experimental data on the moisture dependent creep agree well with the simulation of Burgers model, in which five parameters are extracted to explain the rheology properties of wood cell wall. Ee, Ed, η1 and η2 all decrease with an increase of moisture content.

6.2 Future Works

6.2.1 Temperature-dependent properties of wood cell wall via nanoindentation

Wood and other biomass materials are sensitive to both moisture and temperature. High-temperature nanoindentation is a useful tool for exploring the mechanical properties of materials at high temperature. Thermal drift is the biggest challenge for high temperature indentation, especially in areas under 100nm in size. Methods for wood cell sample to be attached with hot stage and techniques to reduce the thermal drift problem will be studied. By varying both temperature and moisture, the Young's modulus, hardness, and time-dependent properties will be studied. Some models will be built to explain the difference of mechanical properties in wood cell under different temperature and moisture levels.

6.2.2 Dynamic mechanical properties analysis (Nano DMA) of wood cell wall at small scale and modulus mapping technique

The dynamic mechanical analysis method has long been used to characterize the time-dependent properties of materials on the macro scale. Moreover, along with the development of modern experimental technology, investment in smaller-scale investigation has attracted more attention. However, the dynamic viscoelastic

characterization of materials through nanoindentation has not been studied in detail. Recently more attention has been given to dynamic indentation and the models applied in the evaluation of the results. For both time- and temperature-dependent behavior, dynamic viscoelastic testing based on nanoindentation provides the advantage of dramatically decreasing the testing time by getting the data over a certain range of frequencies rather than increasing the testing time.

Multiple issues regarding the application of nano DMA should be considered. From the perspective of soft tissue, nano DMA offers a unique library of approaches for the improvement of structural and engineering materials. The majority of soft tissues have fine structures that need to investigated, especially at the small scale. Nano DMA will serve as a powerful tool to describe the properties of these fine structures. In addition, in the wood products research area, especially for wood fiber and wood-adhesive bonding, dynamic nanoindentation presents itself as a possible method for testing viscoelastic properties in order to account for the time-dependent phenomenon. We expect more work on this area because it is believed to be a useful method to get as much information as possible about the properties of wood-based composites as well as cellulose fiber.

Vita

Yujie Meng was born in Shanxi, China and she is a Masters candidate at University of Tennessee. In 2007, she graduated from Nanjing Forestry University with a Bachelor of Packaging Engineering concentrated in Wood-based packaging material. She designed an undergraduate research thesis evaluating the sound absorption properties of Wood-Plastic Composite. She started to work as a research assistant in Forest Products Center at University of Tennessee in 2008 to pursue her Master's Degree. She is currently pursuing a PhD degree in Natural Resources in the College of Agricultural Sciences and Natural Resources under the advising of Dr. Siqun Wang and Dr. Timothy M. Young. Her research was mainly focused on the characterizations of nano-mechanics on bio-materials.